DOCTORAL (PHD) DISSERTATION

NGUYEN HUU HUONG DUYEN

Debrecen

2026

UNIVERSITY OF DEBRECEN

DOCTORAL SCHOOL OF FOOD SCIENCES

Head of the Doctoral School:

Prof. Dr. Béla Kovács, PhD

professor

Supervisor:

Prof. Dr. Prokisch József, PhD

professor

CARBON NANODOTS IN FOOD: FROM FORMATION TO APPLICATION

Prepared by:

Nguyen Huu Huong Duyen

PhD candidate

DEBRECEN

2026

CARBON NANODOTS IN FOOD: FROM FORMATION TO APPLICATION

Dissertation submitted in partial fulfilment of the requirements for the doctoral (PhD) degree in **Food Sciences**

Written by **Nguyen Huu Huong Duyen** certified Food Engineer, M.Eng

Prepared in the framework of the Food Sciences Doctoral school of

the University of Debrecen

Dissertation supervisor: **Dr. Prokisch József, full professor, PhD**

The official opponents of the dissertation:

…….

…….

The evaluation board:

Chairperson:……

Members: ……

…….

…….

…….

The date and venue of the dissertation defense:…….

TABLE OF CONTENTS

ABBREVIATIONS *1*

1. INTRODUCTION *3*

1.1. Justification for the study and problem context **3**

1.2. Research objectives **5**

1.3. Research questions **6**

1.3.1. Foundations of CND Formation in Food Systems 6

1.3.2. Implications for Food Safety and Mechanistic Understanding 6

1.3.3. Applications in Detection and Sustainable Food Technology 6

2. LITERATURE REVIEW *8*

2.1. Fundamentals of carbon nanodots (CNDs) **8**

2.1.1. What are carbon nanodots (CNDs)? 8

2.1.2. Properties of CNDs 11

2.1.3. Characterization of CNDs 12

2.2. CNDs in Thermally Processed Foods **17**

2.2.1. Detection and Occurrence of CNDs in Food 17

2.2.2. Potential Formation Mechanisms in Food Matrices 18

2.2.3. Factors Influencing CND Formation in Processed Foods (RQ1) 22

2.2.4. Methods for quanlitative and quantitative CNDs in food products 23

2.3. Green Synthesis Methods for CNDs and Their Effects on Properties (RQ2) **26**

2.3.1. Fundamental Synthetic Approaches: Top-Down vs. Bottom-Up 26

2.3.2. Definition and Scope of Green Synthesis of CNDs 26

2.3.3. Green Bottom-Up Synthesis from Food and Bio-Based Sources 27

2.3.4. Common Green Synthesis Techniques 27

2.3.5. Machine Learning for Predictive Optimization of Green CND Synthesis 28

2.4. Detection Methods for Food-derived CNDs (RQ3) **30**

2.4.1. Fluorescence-Based Approaches 30

2.4.2. Electron Microscopy and Particle Sizing 30

2.4.3. Surface Chemistry Spectroscopy 30

2.4.4. Chromatographic Separation with Fluorescence Detection 31

2.4.5. Matrix Effects and Multi-Modal Strategies 31

2.5. Food Safety and Toxicological Considerations (RQ4 – RQ6) **32**

2.5.1. Cytotoxicity 32

2.5.2. Genotoxicity 33
2.5.3. Bioaccumulation and Biodistribution 33
2.6 Functional Applications in Food Systems (RQ7 - RQ8) 35
2.6.1. Probes and Sensors for Food Contaminants 36
2.6.2. CNDs in Smart and Active Packaging 37
2.6.3. Nutrient Monitoring and Quality Control 37
2.6.4. Toward Safe and Sustainable Use 38
2.6.5. Environmental Implications of Large-Scale CNDs Synthesis 39
3. MATERIAL AND METHODS 40
3.1. Objective 1: Synthesis and characterize CNDs using the Maillard reaction model (addessing RQ1 – RQ3) 40
3.1.1. Materials 40
3.1.2. Method 40
3.1.3. Characterize the synthesized CNDs from Maillard reaction model 42
3.2. Objective 2: Develop an analytical method to detect CNDs in food products (addessing RQ3) 43
3.2.1. Quantitative Measurement of CNDs Using Fluorescence Spectroscopy 43
3.2.2. Quantitative Measurement of CNDs Using HPLC-SEC-FD 44
3.3. Objective 3: Detection of CNDs and understand formation mechanisms in food products (addessing RQ4 - RQ5) 46
3.3.1. Detection of CNDs in different types of food products 46
3.3.2. Understanding Formation Mechanisms in Food Products: Case study of coffee brewing 48
3.4. Objective 4: Applications of CNDs in food industry (addessing RQ6 - RQ8) 50
3.4.1. Develop rapid method to detect caffeine in beverages using CNDs. 50
3.4.2. Sustainable valorization of food waste into CNDs 51
3.5. Analytical methods to study the properties of CNDs in foods. 56
3.5.1. Fluorescence Spectroscopy 56
3.5.2. UV-Visible Spectroscopy 56
3.5.3. Transmission Electron Microscopy (TEM) 56
3.5.4. X-ray Diffraction (XRD) 56
3.5.5. Raman Spectroscopy 57
3.5.6. Fourier-Transform Infrared Spectroscopy (FTIR) 57

3.5.7. Elemental (C/N) analysis and carbon quantification. 57
3.5.8. High-Performance Liquid Chromatography with Fluorescence Detection (HPLC-SEC-FD) 57
3.5.9. High-Performance Liquid Chromatography for the determination of caffeine 57
3.5.10. Quantum yield determination 58
3.5.11. Other methods 58
3.6. Statistical analysis 58
4.1. Results related to Objective 1: Synthesis and characterization of carbon nanodots (CNDs) using Maillard reaction model (addessing RQ1 – RQ3) 59
4.1.1. Synthesis of green carbon nanodots (CNDs) using the Maillard reaction model 59
4.1.2. Characterization of synthesized Carbon nanodots derived from glycine and sucrose (Gly-S-CNDs) 62
4.1.3. Stability of synthesized Carbon nanodots derived from glycine and sucrose (Gly-S-CNDs) 63
4.2. Results related to Objective 2: Development of methods to detect and quantify carbon nanodots (CNDs) in food matrices (addressing RQ3) 66
4.2.1. Quantitative measurement of CNDs using fluorescence spectroscopy 66
4.2.2. Quantitative Measurement of CNDs using high-performance liquid chromatography with size exclusion and fluorescence detection (HPLC-SEC-FD) 68
4.3. Results related to Objective 3: Detection of carbon nanodots (CNDs) and elucidation of their formation mechanisms in food products (addressing RQ4–RQ5) 75
4.3.1. Detection of CNDs in food products 75
4.3.2. Characterization of food-derived carbon nanodots (F-CNDs) 78
4.3.3. Understanding the formation mechanisms of carbon nanodots (CNDs) in food products 83
4.4. Results related to Objective 4: Applications of carbon nanodots in the food and agricultural industry (addressing RQ7–RQ8) 88
4.4.1. Develop a Rapid Detection method to detect Caffeine in Beverages using glycine-sucrose derived carbon nanodots (Gly-S-CNDs) 88
5. CONCLUSION AND RECOMMENDATIONS 110

5.1. Research contribution 110
5.2. Limitations and Future Research 110
5.3. Conclusion 112
5.3.1. Synthesis and Characterization of Green Carbon Nanodots (CNDs) 112
5.3.2. Development of Detection Methods for Carbon Nanodots (CNDs) in Foods 112
5.3.3. Detection and Formation Mechanisms of CNDs in Food Products 112
5.3.4. Applications in Food and Agriculture 112
6. NEW SCIENTIFIC RESULTS 114
7. PRACTICAL RESULTS 116
8. SUMMARY 117
REFERENCES 119
PUBLICATIONS IN THE FIELD OF RESEARCH 134
STATEMENT 140
ACKNOWLEGMENT 141

ABBREVIATIONS

AE-HPLC	Anion-exchange high-performance liquid chromatography
ANN	Artificial neutral networks
ANN	Artificial neutral network
ANOVA	Analysis of variance
Arg-CNDs	Arginine-derived carbon nanodots
BP-CNDs	Banana peel-derived carbon nanodots
C-CNDs	Coffee-derived carbon nanodots
CCD	Central composite design
CNDs	Carbon nanodots
CQDs	Carbon quantum dots
DI water	Deionized water
DLS	Dynamic Light Scattering
EEM	Excitation-emission matrix
F-CNDs	Food-derived carbon nanodots
FTIR	Fourier Transform Infrared spectroscopy
Gln-CNDs	Glutamine-derived carbon nanodots
Gly-C-CNDs	glycine-citric acid-derived carbon nanodots
Gly-CNDs	Glycine-derived carbon nanodots
Gly-S-CNDs	glycine-sucrose-derived carbon nanodots
GQDs	Graphene quantum dots
HPLC-SEC-FD	High-performance liquid chromatography with size-exclusion column and fluorescent detector
KNN	K-Nearest neighbors
LC-MS	Liquid Chromatography-Mass Spectrometry
LOD	Limit of detection
LOQ	Limit of quantification
Lys-C-CNDs	lysine-citric acid-derived carbon nanodots
M-CNDs	Maillard reaction-derived carbon nanodots
ML	Machine learning
Phe-CNDs	Phenylalanine-derived carbon nanodots
PL	Fluorescent spectra

Pro-CNDs	Proline-derived carbon nanodots
QY	Quantum yield
R^2	Coefficient of determination
RMSE	Root Mean Square Error
RP-HPLC	Reverse-phase high-performance liquid chromatography
RSD	Relative standard deviation
RT	Retention time
SD	Standard deviation
SEM	Scanning electron microscopy
SVR	Support vector regression
TDS	Total dissolved solid
TEM	Transmission electron microcopy
Tyr-CNDs	Tyrosine-derived carbon nanodots
U-C-CNDs	urea-citric acid-derived carbon nanodots
XGBoost	Extreme gradient boositng
XPS	X-ray Photoelectron spectroscopy
XRD	X-ray diffraction

1. INTRODUCTION

1.1. Justification for the study and problem context

Carbon-based nanomaterials have gained major scientific attention for their unique structural and functional properties. The 2023 Nobel Prize in Chemistry was awarded for the discovery and development of quantum dots – a unique nanoscale luminescent carbon-based material (Nobel-Prize 2023). Carbon Nanodots (CNDs) represent an emerging branch of the quantum dots family, sharing characteristics like strong luminescence and small size with traditional quantum dots while offering superior water dispersibility and biocompatibility (Chahal et al., 2024). Furthermore, CNDs share similar size-dependent fluorescence properties and have rapidly found relevance in emerging fields such as food safety, smart packaging, and nutrient delivery (Gao et al., 2024; D. Nguyen, El-Ramady, et al., 2024; D. H. H. Nguyen, Muthu, et al., 2025; Rossini et al., 2019).

CNDs are small, quasi-spherical fluorescent particles typically less than 10 nm - are particularly notable due to their photoluminescence, aqueous solubility, low toxicity, and biocompatibility (Kang et al. 2020)(Shi et al. 2019). The discovery of CNDs dates back to Xu et al. (2004, p. 2), who first reported fluorescent carbon nanoparticles produced during the purification of single-walled carbon nanotubes introduced a new category of photoluminescent carbon-based nanomaterials.

Notably, CNDs are not only synthetically produced under controlled laboratory conditions but are also formed naturally during common food processing methods, such as roasting, baking, grilling, and caramelization (Y. Li et al., 2017; D. Nguyen, Muthu, El-Ramady, Béni, et al., 2024; Semsey et al., 2024; Sk et al., 2012a). These thermally driven reactions, particularly the Maillard reaction between amino acids and reducing sugars, can result in the *in situ* formation of fluorescent nanoparticles within the food matrix (D. Li, Xie, et al., 2019; D. Nguyen, Muthu, El-Ramady, Daróczi, et al., 2024; D. H. H. Nguyen, El-Ramady, Törős, et al., 2025). Foods like coffee, roasted meat, bread crusts, and fried spices have been shown to contain measurable amounts of CND-like structures (D. Nguyen, Muthu, El-Ramady, Béni, et al., 2024; Semsey et al., 2025; Sk et al., 2012a). Recently, there is growing interest in the green synthesis of CNDs from food waste and other edible or biocompatible precursors offered sustainability advantages (Pajewska-Szmyt et al., 2020; Wu et al., 2024). However, the resulting nanomaterials

may exhibit batch variability and matrix-dependent behaviour, complicating their integration into food industry workflows (D. Nguyen, El-Ramady, et al., 2024).

The presence of CNDs in food products spans three critical contexts, including (1) their unintentional formation during thermal food processing, (2) their intentional green synthesis from food-derived precursors, and (3) their incorporated application in food and agricultural systems, such as contaminant detection and intelligent packaging. This leads to three notable and relatively unexamined challenges. First, there is a limited understanding of the physicochemical mechanisms that govern the formation of CNDs in real food systems, particularly under varying conditions of temperature, time, moisture content, and food matrix composition (X. Shi et al., 2019; P. Zhao et al., 2021). Second, the implications for food safety, human exposure, and regulatory oversight remain unclear. While numerous studies report that lab-synthesized CNDs exhibit biocompatibility and low toxicity (J. Liao et al., 2021; Yang et al., 2009), others have shown that cytotoxicity may be influenced by particle size, surface functional groups, dosage, and light-induced degradation (Havrdová et al., 2022; Y.-Y. Liu et al., 2021; D. Nguyen, El-Ramady, et al., 2024). Third, the application of food-derived CNDs - whether in sensors, packaging, or nutrient delivery systems - poses unresolved questions related to material stability, consistency, and performance under real-world conditions (Bhatlawande et al., 2024; D. H. H. Nguyen, Muthu, et al., 2025).

As outlined above, these contexts give rise to three major challenges: limited understanding of formation mechanisms of CNDs, unclear toxicological and regulatory implications, and practical barriers to applications and scale-up. This PhD research is therefore designed to bridge these critical knowledge gaps by investigating how CNDs form in real food systems, developing and validating analytical detection methods, and exploring both the risks and potential applications of CNDs across the food production, consumption, and regulatory ecosystem.

1.2. Research objectives

The overarching aim of this PhD research is to investigate the formation, detection, and application of carbon nanodots (CNDs) in processed food systems, with a particular emphasis on green synthesis, analytical detection, sustainability, and food safety considerations.

Specific objectives are as follows:

- **Objective 1:** To optimize the synthesis of CNDs using Maillard-reaction model systems under various reaction conditions, and to characterize their properties via spectroscopic, microscopic, and chromatographic methods, aligning with sustainability and circular-economy principles.
- **Objective 2:** To establish and validate analytical methods for detecting CNDs in real food matrices.
- **Objective 3:** To determine the occurrence of CNDs in six categories of food products (bakery, roasted cereals, beverages, chocolate products, spices, and black foods) and to elucidate their formation mechanisms through case studies.
- **Objective 4:** To develop applications of synthesized CNDs for the food industry, including (i) a rapid sensing method using CNDs, and (ii) valorization techniques for producing CNDs from food wastes.

1.3. Research questions

To address the knowledge gaps outlined above, this PhD thesis is guided by the following eight research questions, organized into three thematic categories: (1) Foundations of Formation, (2) Implications for Safety and Understanding, and (3) Applications in Food Industry. Research questions for each category were listed in **Figure 1**.

1.3.1. Foundations of CND Formation in Food Systems

- **RQ1**: What are the key physicochemical and processing factors (e.g., temperature, matrix composition, time, pH) that influence the formation of CNDs in thermally processed foods?
- **RQ2**: How do different green synthesis methods, using food-based precursors, affect the size, structure, fluorescence, and surface functionality of CNDs?
- **RQ3**: What analytical and spectroscopic techniques are most effective for detecting and characterizing CNDs within complex food matrices?

1.3.2. Implications for Food Safety and Mechanistic Understanding

- **RQ4**: What are the proposed mechanistic pathways for the formation of CNDs during thermal food processing, particularly those involving Maillard-type reactions?
- **RQ5**: How do food-derived CNDs interact with food components (e.g., caffeine, Maillard products)?
- **RQ6**: Based on the current literature, what are the key toxicological considerations and regulatory concerns associated with the presence or use of CNDs in food systems?

1.3.3. Applications in Detection and Sustainable Food Technology

- **RQ7:** How can food-derived or synthetically produced CNDs be applied in the rapid detection of specific compounds (e.g., caffeine) in food products?
- **RQ8**: What are the practical and technological challenges in scaling up green synthesis and applying CNDs in food safety, packaging, or agricultural applications?

These questions form the conceptual backbone of the thesis and are addressed through a combination of experimental studies, synthesis trials, analytical method development, and critical review of the scientific literature.

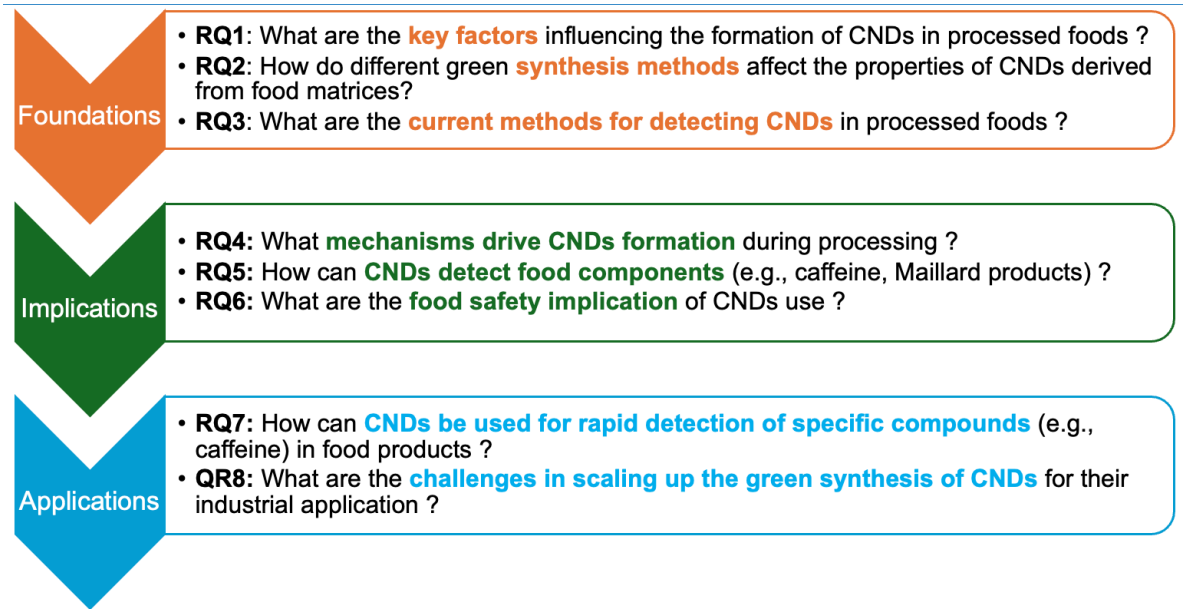


Figure 1. Logical structure of research questions

2. LITERATURE REVIEW

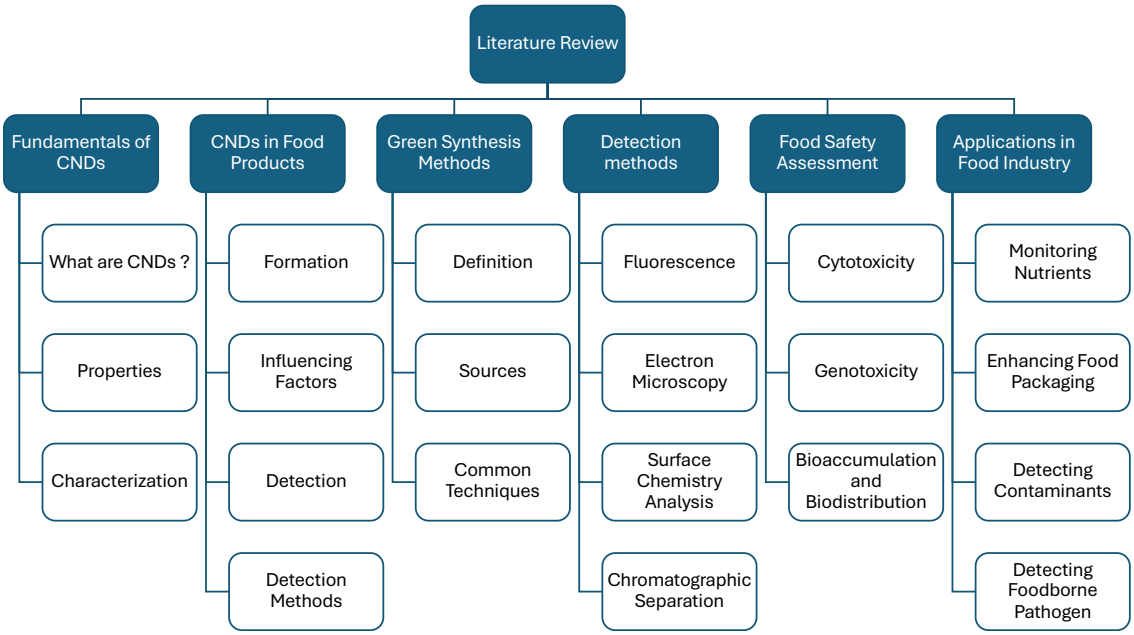


Figure 2. Outline of literature review

2.1. Fundamentals of carbon nanodots (CNDs)

2.1.1. What are carbon nanodots (CNDs)?

Carbon nanodots (CNDs), also referred to in the literature as carbon dots (CDs), are a class of photoluminescent, carbon-based nanomaterials typically less than 10 nm in size. Structurally, they consist of amorphous to graphitic carbon cores surrounded by oxygen-, nitrogen-, or hydrogen-containing functional groups, which confer high aqueous solubility and surface reactivity (Mintz et al., 2021; H. Wang et al., 2020). Initially discovered during carbon nanotube purification (Xu et al. 2004), CNDs have since become recognized for their excitation-dependent fluorescence, aqueous stability, and ease of synthesis from a variety of carbon-rich sources.

Terminology and scope. In the literature, "CDs" is an umbrella term that may include several sub-classes with partially overlapping features. CNDs typically denote dots with an amorphous or partly graphitic core and dominant surface-stateemission; carbon quantum dots (CQDs) tend to have more ordered, quantum-confined cores; and graphene quantum dots (GQDs) are few-layer graphene fragments exhibiting edge and quantum-confinement effects. These categories are not always used consistently across studies. Raphaël de Boëver et al. (2022) explicitly states "no definitive consensus exists to date on several key aspects such as the actual definition of CDs," while A. Cayuela et al.

(2016) proposed "a new set of abbreviations and definitions for them to avoid contradictions found in literature." The structural distinctions are experimentally validated: M. Liu et al. (2017) demonstrated clear separation of amorphous CNDs (green-emissive) from crystalline GQDs (yellow-emissive) with different oxidation degrees and photostability. Xue-Tao Tian et al. (2019) confirms the general separation into GQDs and CNDs, though notes that "it is their structures rather than their precursors and preparation strategy that govern whether C-dots are GQDs or CNDs." In this dissertation, CNDs refers to sub-10 nm, colloidally stable, carbon-based nanoparticles produced via top-down or bottom-up routes from, possessing a carbonized core with abundant surface functionalities and measurable photoluminescence. Where necessary, CQDs and GQDs are named explicitly to avoid ambiguity.

Structural motifs and surface chemistry. The carbon cores of CNDs typically contain small sp^2 islands embedded within an sp^3-rich matrix (Margraf et al., 2015). The sp^2 domains can foster π–π transitions and delocalized electronic states, while the surrounding amorphous regions and abundant edge/defect sites host functional groups such as –OH, –COOH, –C=O, and $–NH_2$ (Mintz et al., 2021; Sciortino et al., 2017). Heteroatom doping effects are extensively documented showing N/S/Se doping modulates electronic structure and optical responses (Geng et al., 2020). The density and identity of surface groups also govern zeta potential, solubility in high-ionic-strength media, and the ability to bind metal ions, biomolecules, or food-matrix components, features that later enable sensing and packaging applications (Y. Park et al., 2016a). The proposed structure of CNDs was illustrated in **Figure 3** (Zhu et al., 2015).

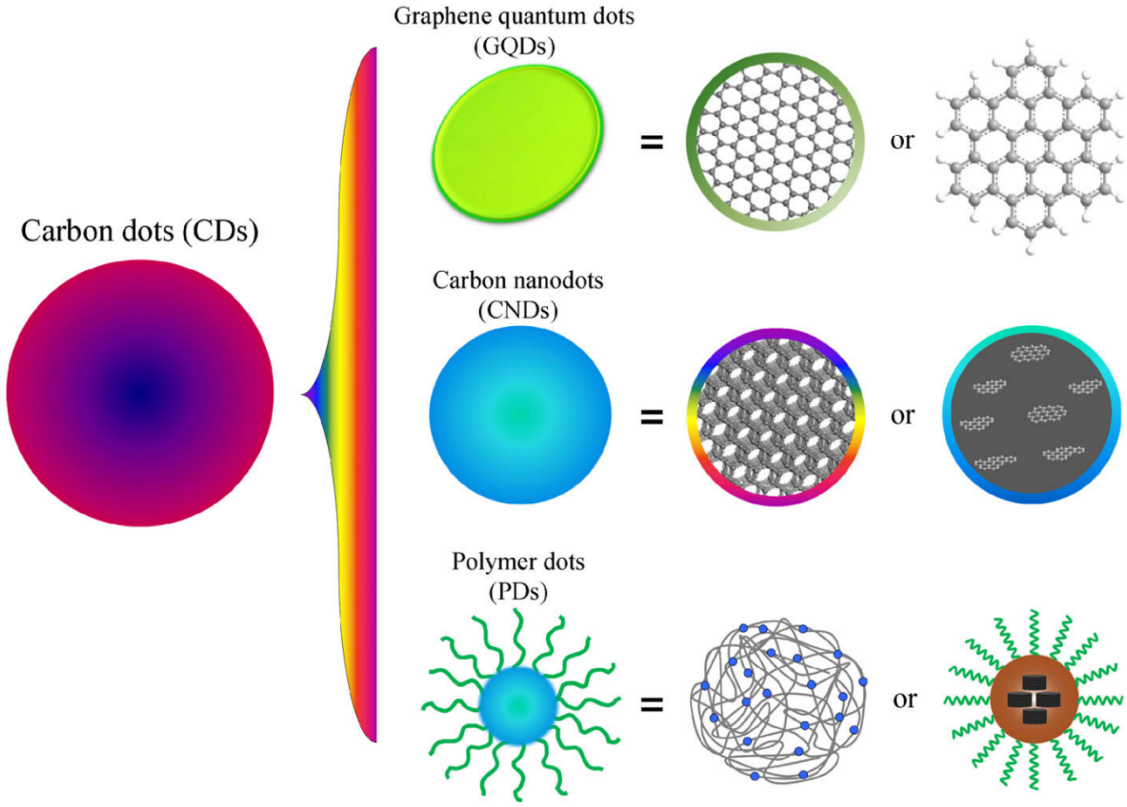


Figure 3. The proposed strucure of carbon nanodots (CNDs) (Zhu et al., 2015)

Photoluminescence at a glance. CNDs are best known for bright, often excitation-dependent emission spanning the visible range (Mintz et al., 2021). Several complementary models are invoked to explain this behavior: (i) core-state emission associated with quantum-confined sp^2 domains (Tepliakov et al., 2019); (ii) surface-state/defect emission arising from diverse functional groups and edge sites (Meiling et al., 2018a); and (iii) molecular/fluorophore-state emission, where fluorescent molecular species formed during synthesis contribute to the spectra (Soni et al., 2021). The relative contributions of these pathways depend strongly on precursor chemistry, carbonization temperature/time, and post-synthetic purification. This complexity explains why CNDs can display broad emission bands, large Stokes shifts, and variable lifetimes. A quantum yield, lifetime analyses, and excitation–emission matrices is provided in **Section 2.1.2**.

Origins and synthesis. Since the initial observations in 2004 (Xu et al., 2004), CNDs have been produced via top-down methods (oxidative cutting, electrochemical or laser ablation of bulk carbon) (Wang et al. 2023) and bottom-up routes (hydro/solvothermal, microwave, or thermal carbonization of small molecules such as citric acid and urea, as well as complex biomass) (Etefa et al., 2024). Bottom-up syntheses typically proceed

through dehydration, polymerization, aromatization, and carbonization; in amine-rich systems, Maillard-type chemistry can yield N-doped structures with stabilized surface states (D. Li, Xie, et al., 2019). These strategies are attractive because they are low-cost, water-based, and compatible with renewable precursors - an advantage for sustainability-oriented applications, including those in food systems. Detailed synthetic conditions and precursor choices are discussed in **Section 2.3**.

Why CNDs matter. Compared with traditional semiconductor quantum dots, CNDs are widely reported to exhibit relatively low cytotoxicity, strong resistance to photobleaching in aqueous media, and facile functionalization without expensive or air-sensitive reagents. Consequently, they have been deployed across biosensing (Buiculescu et al., 2016), environmental monitoring (Bosu et al., 2023), bioimaging (Hui et al., 2019), drug delivery (Z. Wang et al., 2022), anti-counterfeiting inks (Kalytchuk et al., 2018), semiconductor photocatalysis (Yu et al., 2016), and light-emitting devices (Y. Shi et al., 2023). Their increasing relevance to food science stems from exactly these features: bright and tunable fluorescence for contamination/freshness sensing, rich chemistry for immobilization in coatings or films, and the possibility of deriving them from edible or food-grade precursors (D. H. H. Nguyen, Muthu, et al., 2025). Applications specific to the food industry, including monitoring nutrients, enhancing packaging, and detecting contaminants and pathogens, are reviewed in **Section 2.6**.

Current challenges. Despite rapid progress, two conceptual issues frame the field. First, nomenclature and standardization: the same material may be labeled CNDs, CDs, CQDs, or GQDs across papers, and reporting practices vary for size distributions, purification protocols, and the presence of molecular fluorophores. Second, structure–property correlations remain under active debate, particularly the extent to which emission arises from core versus surface versus molecular states under different syntheses. These topics, together with safety and regulatory aspects relevant to food contact and ingestion, are discussed in later sections.

2.1.2. Properties of CNDs

Carbon nanodots (CNDs) display a wide range of physicochemical and optical characteristics that distinguish them from other nanomaterials, making them useful in many different fields. One notable trait is their tunable fluorescence, which arises due to quantum confinement effects, surface defect states, and molecular fluorophores found on their surfaces (Cao et al., 2013; Fu et al., 2015). This fluorescence can be modulated by

changing the core composition, doping elements, or surface functional groups, enabling their use in bioimaging, optical sensing, and intracellular labeling (Bao et al., 2015; Fu et al., 2015; Hoan et al., 2018).

CNDs also exhibit strong photoluminescence, often comparable to that of semiconductor quantum dots, but with significantly reduced cytotoxicity and making them suitable for applications in bioimaging and fluorescence imaging *in vivo* (Rodríguez-Varillas et al., 2022; Yang et al., 2009). Their excitation-dependent emission behavior allows for multiplexed detection in optical devices, while their photochemical and physicochemical stability ensures performance reliability in various environments, including *in vitro* and *in vivo* (Ali et al. 2020; Fu et al. 2015; Hoan et al. 2018; Omer et al. 2022).

Surface functionalization is a key property of CNDs that enables fine-tuning of their chemical, optical, and electronic characteristics (M. Han et al., 2017). By introducing functional groups such as amino, carboxy, and hydroxy moieties through covalent modifications like amidation and silylation, or non-covalent approaches such as π–π stacking and electrostatic interactions (Yan et al., 2018), researchers can enhance fluorescence quantum yields, improve solubility, and increase complexation capacity (Yan et al., 2018). This versatility allows CNDs to be tailored for making surface engineering a central strategy in advancing their multifunctional potential (Y. Park et al., 2016b).

Otherwise, these nanoparticles exhibit excellent biocompatibility, low cytotoxicity, and chemical inertness, making them superior to conventional fluorescent dyes and semiconductor quantum dots for *in vivo* imaging (Jaleel & Pramod, 2018; Qu et al., 2012).

2.1.3. Characterization of CNDs

To fully understand CNDs, they must be characterized in terms of their optical properties, structure, surface chemistry, and colloidal behavior. **Figure 4** shows four main groups of techniques: (A) Optical properties; (B) Morphology and structure; (C) Surface chemistry; and (D) Surface charge and colloidal stability.

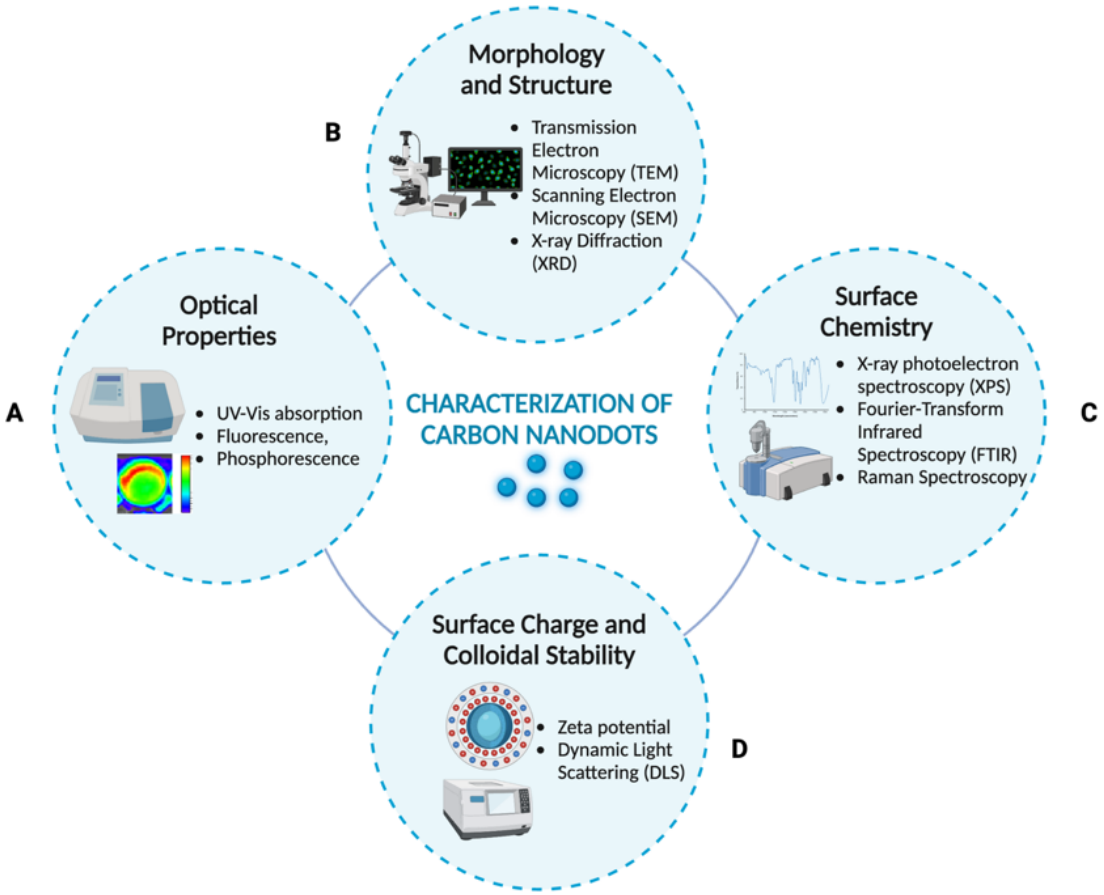


Figure 4. Characterization of CNDs includes four primary groups: **A**, optical properties; **B**, morphology and structure; **C**, surface chemistry; D, surface charge and colloidal stability.

2.1.3.1. Optical Properties

CNDs are well known for their optical properties, especially in fluorescence; therefore, understanding the optical mechanisms of CNDs is crucial for developing tailored materials with specific functional purposes (M. Liu, 2020), such as bioimaging, sensing, catalysis, and environmental monitoring (Lin et al., 2012; Q. Zhao et al., 2020; Y. Zhao et al., 2015). There are two main techniques for fully understanding these properties: (1) UV-Vis absorption, and (2) fluorescence measurement (**Figure 4A**).

Optical characterization is fundamental to understanding the photophysical behavior of CNDs. Typically, CNDs exhibit absorption peaks in the ultraviolet to visible range, primarily due to π–π* transitions in aromatic carbon bonds and n–π* transitions involving oxygenated functional groups (Lin et al., 2012). These peaks often appear around 280–360 nm, confirming the presence of conjugated sp^2 domains and surface functionalities.

One of the most defining characteristics of CNDs is their fluorescence, which can be either excitation-dependent or excitation-independent. This emission behavior is influenced by surface defects, quantum confinement, band-edge states, and multiple emissive centers (M. Liu, 2020; Y. Zhao et al., 2015). Fluorescence intensity and emission wavelength can be further modulated by altering synthesis conditions, applying chemical doping, or introducing post-synthetic treatments such as UV irradiation (Y. Zhao et al., 2015). CNDs fluorescence is also environmentally responsive, meaning it can be enhanced or quenched by ions, biomolecules, or pH, making CNDs highly adaptable as sensing elements in analytical systems (Fu et al., 2015, p. 20; Lin et al., 2012). For example, changes in photoluminescence are used to detect heavy metals, toxins, or spoilage in food products.

2.1.3.2. Morphology and Core Structure

Morphological and structural characterization of CNDs is essential for linking size, shape, and crystallinity to their fluorescence, reactivity, and dispersion stability. Techniques such as Transmission Electron Microscopy (TEM), Scanning Electron Microscopy (SEM), and X-ray Diffraction (XRD) provide complementary insights into nanostructure and surface architecture, enabling prediction and tuning of CNDs performance in food, biomedical, and sensing applications (**Figure 4B**).

TEM is one of the most widely used techniques for visualizing CNDs at the single-particle level, offering direct insight into particle shape, diameter, and aggregation state (Jurkiewicz et al., 2018). TEM can resolve features in the 1–10 nm range, often revealing quasi-spherical shapes and lattice fringes that indicate graphitic or amorphous domains. SEM complements TEM by providing surface topography and particle clustering information, particularly useful for aggregated samples or freeze-dried CNDs (Abinaya et al., 2022; Mintz et al., 2021).

XRD is used to determine the crystallinity, core structure and phase composition of bulk CNDs material. Most CNDs show a broad diffraction peak around 20–30° (2θ), corresponding to disordered carbon core structures. However, graphitic features, planar defects, and partial ordering can be observed depending on the synthesis method (Jurkiewicz et al., 2018; Neumann et al., 2020). XRD is especially useful for evaluating the degree of carbonization and identifying differences between materials such as black CNDs, yellow CNDs, and carbon nitride dots (Mintz et al., 2021).

The combination of TEM and XRD can reveal detailed information about complex microstructures in CNDs, including size, shape, and core structure (Neumann et al., 2020).

2.1.3.3. Surface Chemistry

The surface chemistry of CNDs is a key determinant of their optical properties, solubility, and biological interactions. As shown in **Figure 4C**, various characterization techniques, such as Fourier Transform Infrared Spectroscopy (FTIR), X-ray Photoelectron Spectroscopy (XPS), and Raman spectroscopy, are employed to analyze surface functionalities.

FTIR spectroscopy is commonly used to identify surface functional groups such as carboxyl (-COOH), hydroxyl (-OH), and amine ($-NH_2$), which originate from precursor decomposition or post-synthesis treatments (Fawaz et al., 2023; Ren et al., 2019). These groups contribute to hydrophilicity, colloidal stability, and photoluminescence intensity.

XPS reveals the elemental composition and oxidation state of CNDs, with the O/C atomic ratio serving as a key indicator of surface oxidation (Tan et al., 2013). A thorough understanding of surface chemistry is essential for tuning functional properties and ensuring batch-to-batch consistency, particularly in complex systems such as food matrices (Fawaz et al., 2023; Zhou et al., 2019).

Raman spectroscopy can provide valuable insights into the carbon-carbon bonds that make up CNDs, revealing even slight structural changes (Mintz et al., 2021). Studies have shown that CNDs are inherently heterogeneous systems, with carbon cores containing both sp^2 and sp^3 domains (Righetto et al., 2017). However, the nature of CNDs fluorescence remains controversial, with some research suggesting it may originate from free molecules rather than the carbon cores themselves (Righetto et al., 2017).

2.1.3.4. Surface Charge and Colloidal Stability

Surface charge and colloidal stability are critical factors influencing the dispersion, reactivity, and biological compatibility of CNDs, particularly in aqueous and biological environments. As summarized in **Figure 4D**, two primary techniques are employed for evaluating these parameters: Dynamic Light Scattering (DLS) and zeta potential measurements. These measurements are particularly important when CNDs are dispersed in complex media such as cell culture solutions, food matrices, or serum-containing environments, where interactions with proteins, salts, and other solutes can alter surface behavior (Murdock et al., 2008). Variables such as sonication, dilution, and media

composition can also significantly influence colloidal properties and downstream biological or toxicological effects.

DLS is used to assess the hydrodynamic diameter of CNDs and monitor their stability over time under varying conditions of pH, ionic strength, and temperature (Carvalho et al., 2018). This is essential for determining aggregation behavior and storage performance in formulations.

Zeta potential analysis provides insight into surface charge, which directly affects electrostatic interactions, colloidal dispersion, and the tendency to agglomerate. Higher absolute zeta potential values (positive or negative) generally indicate greater stability (Carvalho et al., 2018).

2.2. CNDs in Thermally Processed Foods

2.2.1. Detection and Occurrence of CNDs in Food

Although CNDs were initially studied as laboratory-synthesized nanomaterials, they were later identified as naturally forming byproducts in thermally processed foods. Their presence was first reported in caramelized sugars and baked bread (Sk et al., 2012a), where the high-temperature conditions formed the fluorescent nanoscale particles. Since then, growing research has confirmed that common cooking methods, such as roasting (X. Song, Wang, et al., 2018), baking (Sk et al., 2012a), grilling (Y. Li et al., 2017), and frying (Dwandaru et al., 2019), can generate CNDs as a result of complex thermal reactions, particularly the Maillard reaction, caramelization, and lipid or protein degradation (H. Wang et al., 2020). These reactions, long known for enhancing food's sensory qualities, are now recognized as routes for CNDs formation. The formation of CNDs has been reported in a diverse set of food products, listed in **Table 1,** representatively:

- In grilled and roasted meats, CNDs form through thermal breakdown of proteins and fats, particularly in surface regions exposed to charring. Their particle size and fluorescence vary with temperature and exposure time (Cong et al., 2018; Y. Li et al., 2017; X. Song, Wang, et al., 2018).
- In baked goods, CNDs have been detected in crust regions of bread, with characteristics dependent on the sugar type and baking temperature (Sk et al., 2012a).

Across these studies, CNDs have shown a consistent nanoscale size (typically 1–10 nm) and amorphous or partially graphitized carbon structure, as listed in **Table 1**, with surfaces enriched in oxygen- and nitrogen-containing functional groups. Fluorescence is one of the most identifiable features of these particles, often used for detection in food extracts.

Importantly, the physical and optical properties of CNDs are highly variable, depending on the food matrix and processing conditions. For instance, bread-derived CNDs had sizes around 27.5 nm, while jaggery (a traditional unrefined sugar made from concentrated sugarcane juice) and biscuits produced significantly smaller particles (down to 3.9 nm), with quantum yields ranging from 0.55% to over 6% (Sk et al., 2012a). In roasted meats, increasing the temperature from 200 °C to 300 °C reduced particle size and increased fluorescence quantum yield by more than double (X. Song, Wang, et al., 2018).

These findings suggest that temperature acts as both a driver of carbonization and a modulator of nanostructure development.

Detection of these particles in real food systems is primarily based on fluorescence spectroscopy, coupled with electron microscopy and surface chemical analysis (Mintz et al., 2021). Their strong emission, often excitation-dependent, distinguishes them from other food components and allows for targeted analysis, although quantification remains challenging due to interference from native fluorophores and matrix complexity. These observations demonstrate that CNDs are relatively common in modern diets, forming unintentionally during routine cooking processes. Their occurrence depends on the thermal exposure, composition, and structure of foods, indicating that controlling or predicting their formation could be possible under specific processing conditions. These findings highlight the need for further research into how they form and raise important questions about their biological fate and safety, which are discussed in the upcoming sections.

2.2.2. Potential Formation Mechanisms in Food Matrices

The formation of CNDs in thermally processed foods arises from the breakdown and rearrangement of major food components-including carbohydrates, proteins, and lipids-under high-temperature conditions. These transformations involve a complex series of dehydration, polymerization, and carbonization reactions, ultimately leading to the creation of fluorescent, carbon-rich nanostructures (Q.-Q. Shi et al., 2014; H. Wang et al., 2020). The presence of heteroatoms, such as nitrogen, can further enhance the optical properties and yield of the CNDs (Q.-Q. Shi et al., 2014). Three primary reaction pathways have been implicated in the *in-situ* formation of CNDs in food:

- **Maillard reaction:** The Maillard reaction is one of the most widely studied mechanisms in food chemistry, involving a condensation reaction between reducing sugars and amino acids. While it is known for producing flavor compounds and the characteristic browning of cooked foods, recent studies have shown that Maillard reaction products (MRPs) can form into carbon nanostructures under sufficient thermal conditions (D. Li et al., 2018). Melanoidins, the high-molecular-weight brown polymers formed in the later stages of Maillard chemistry, have been suggested as key intermediates in the formation of food-derived CNDs (D. Li, Xie, et al., 2019). Their rich carbon and

nitrogen content, combined with structural conjugation, supports nucleation, carbon core development, and surface passivation of resulting nanodots.

- **Caramelization:** Caramelization refers to the thermal decomposition of sugars in the absence of amino acids. The reaction generates complex aromatic compounds and brown pigments, and was the first food-related pathway shown to produce CNDs, as reported by Sk et al. (2012a). The efficiency of CNDs formation via caramelization depends on several variables, including temperature, sugar type, and pH of the matrix.
- **Pyrolysis:** Under more extreme thermal conditions-typically above 200–300 °C-pyrolysis occurs, leading to the anaerobic degradation of organic matter into carbonaceous residues. This mechanism is particularly relevant in heavily roasted, grilled, or charred foods, where proteins and lipids contribute carbon and nitrogen frameworks that condense into CNDs structures (Y. Li et al., 2017; X. Song, Wang, et al., 2018; H. Wang et al., 2020). CNDs formed through pyrolysis generally exhibit smaller particle sizes and stronger photoluminescence, although the lack of control over conditions can introduce variability in composition and morphology.

Although CND formation has been mainly linked to dry-heat processing, the potential for wet-heat food processes and specific chemical pretreatments to induce or modulate CND formation remains insufficiently explored. A proposed mechanism described by Wang et al. (2020) outlines a stepwise formation process (**Figure 5**): (**1**) decomposition of food macromolecules through pyrolysis or dehydration, (**2**) polymerization into conjugated chains, and (**3**) carbon core formation and surface passivation, resulting in fluorescent CNDs. The resulting nanodots vary in size, yield, and fluorescence depending on both precursor composition and processing intensity.

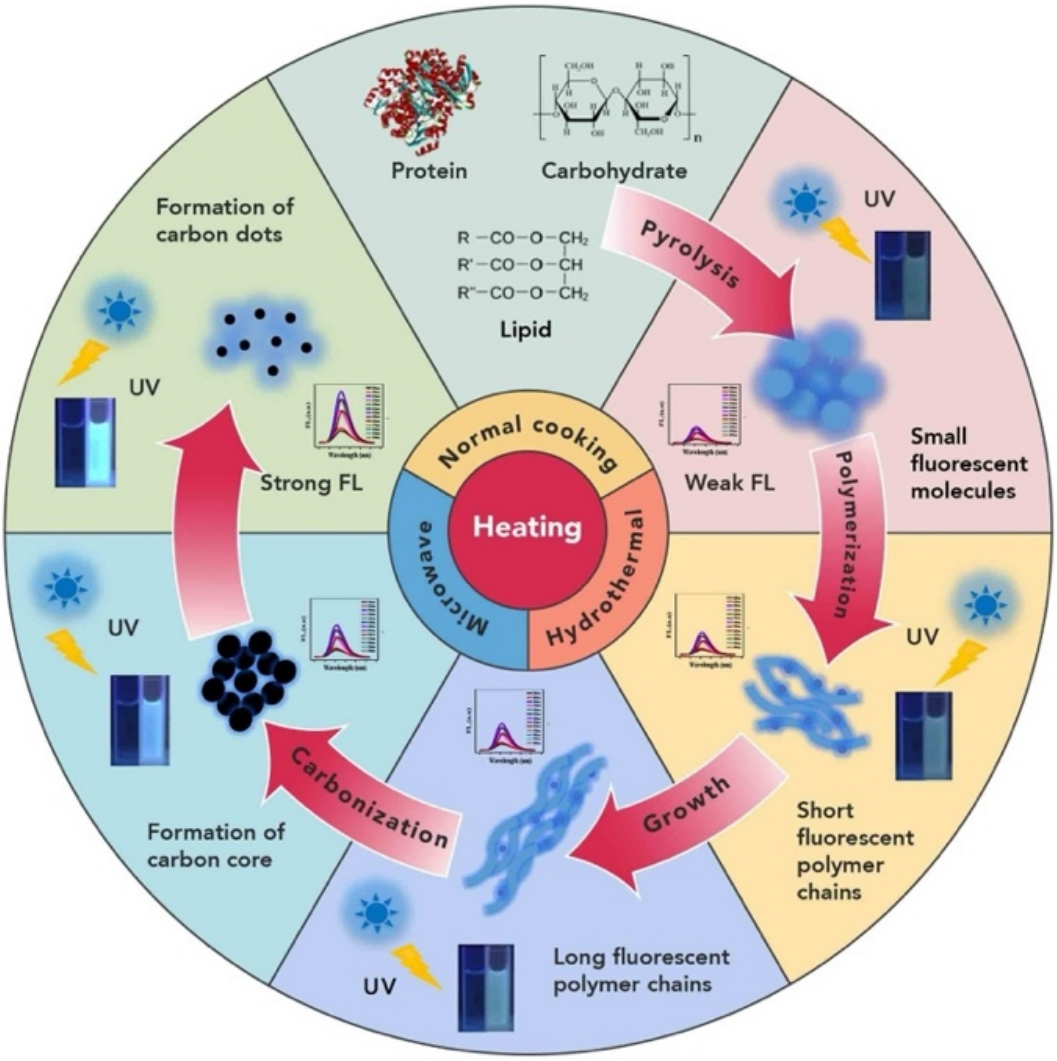


Figure 5. Schematic representation of CNDs formation pathways in processed foods (H. Wang et al., 2020).

Table 1. Reported carbon nandots (CNDs) in processed foods.

Food Source	Processing Method	Temperature Range	Particle Size Range	Fluorescence Properties	Chemical structure	Refs
Sandwich leftover	Hydrothermal	-	-	Temperature depends	Pyridinic N and graphitic N	(Ahn et al., 2019)
Kangkung (*Ipomoea aquatica*)	Frying and roasting	250°C, 88°C	1- 10 nm	Red (674–677 nm), Green (500–519 nm)	C=C, C=O, C-H, O-H	(Dwandaru et al., 2019)
Hamburger	Grilling	220–300°C	Decreased with temp	QY: 23.25% at 260°C	-	(Y. Li et al., 2017)
Bread, jaggery, caramel	Caramelization	180°C, 200°C	4 - 30 nm	QY: 1.2–0.63%	Carbohydrate coating	(Sk et al., 2012a)
Chicken	Roasting	200–300°C	17.1- 2.1 nm	QY: 6.71–17.46%	-	(X. Song, Wang, et al., 2018)
Lamb	Baking	200–350°C	-	QY increased	Temp-dependent surface groups	(H. Wang et al., 2019)
Breadcrumbs	Frying	180°C	-	-	-	(Yin et al., 2024)
Calamansi & ineapple waste	Hydrothermal	-	-	Ex: 365 nm	-C-N	(De Yro et al., 2019)
Mature vinegar	Fermentation	-	0.5 - 2.5 nm	QY: 5.71 %	-OH;C=O; –COOH	(Cao et al., 2017)
Pizza	Grilling	-	~3.33 nm	QY:2.14 %	C=O; –OH; –NH2; COOH	(Cong et al., 2019)
Yellow croaker	Canning	-	1.8- 5.8 nm	QY: 9.7%	C–O–C; C=O; –OH;CO–NH	(D. Li, Na, et al., 2019)
Pike Eel	Grilling	160–300°C	1.75- 4.2 nm	QY:12.86 - 80.16%	C=O; C=C; C-O; –OH	(Bi et al., 2018)
Roasted salmon	Roasting	200°C	2.7 ± 0.5 nm	-	-	(Y. Song et al., 2019)
Roasted duck	Roasting	170°C	1.3 nm	QY: 4.4%	-OH;C=O; –COOH	(Cong et al., 2018)
Beer	Fermentation	-	2.5 nm	QY: 7.39%	-	(Z. Wang et al., 2015)

2.2.3. Factors Influencing CND Formation in Processed Foods (RQ1)

The formation of CNDs in thermally processed foods is influenced by a complex of matrix composition, process conditions, and external modifiers, which can potentially influence CNDs formation efficiency, size, fluorescence, and chemical characteristics as observed across various food systems, including:

- **Temperature**: Temperature is the most critical factor in the CNDs formation. Studies consistently show that higher processing temperatures promote the carbonization of sugars, amino acids, and lipids, thereby increasing CNDs yield and enhancing fluorescence intensity (Y. Li et al., 2017; X. Song, Wang, et al., 2018). For instance, in roasted chicken, particle sizes decreased from 17.1 nm to 2.1 nm as roasting temperature increased from 200 °C to 300 °C, accompanied by a significant increase in quantum yield (X. Song, Cao, et al., 2018).
- **Time and Duration of Thermal Exposure**: Extended heating allows for further dehydration and carbonization, leading to smaller, brighter fluorescence, and more uniform CNDs (Papaioannou et al., 2019; Santos et al., 2025). A systematic understanding of how time–temperature conditions affect CND size, aggregation, and fluorescence is still lacking.
- **Precursors and Food Matrix Composition:** The type and ratio of macronutrients-particularly carbohydrates and proteins-influence both the formation pathway and the surface chemistry of resulting CNDs. For example, high sugar content favors caramelization-driven formation (Sk et al., 2012a). Protein-rich matrices enable nitrogen doping, which improves fluorescence efficiency, high quantum yields, and alters surface charge (Meiling et al., 2018b; Q.-Q. Shi et al., 2014). Polyphenols and antioxidants can act as stabilizers or dopants, modifying particle behavior. Bread crusts, jaggery, and coffee grounds produce CNDs with widely different particle sizes and emission profiles, attributable to differences in their chemical precursors (Sk et al., 2012a). Chemical agents present in the matrix-or introduced intentionally-can significantly influence the formation route and product characteristics. The presence of nitrogen-rich compounds (e.g., tetraethylenepentamine, TEPA) has been shown to increase C–N bonding and improve optical properties (De Yro et al., 2019).

- **pH and Buffering Conditions**: Both Maillard and caramelization reactions are pH-sensitive. However, the effects of pH and alkaline pretreatments commonly used in food processing on CNDs formation mechanisms and optical properties remain unclear.
- **Processing Method (Pyrolysis - Dry vs. Hydrothermal – Wet)**: CNDs can form under both dry-heat and wet-heat food processing conditions; however, how differences in thermal intensity and reaction environment influence particle size, structural order, and optical properties has not yet been systematically clarified.

2.2.4. Methods for quanlitative and quantitative CNDs in food products

A range of tools has been used to detect or quantify CNDs-UV–Vis/fluorescence spectroscopy, Raman spectroscopy, TEM, and several chromatography methods. Each method has their advantages, but their shortcomings become pronounced in complex, multi-component food matrices, as listed in **Table 2**.

UV–Vis and fluorescence spectroscopy. UV–Vis and fluorescence spectroscopy are commonly used for rapid screening and characterization of CNDs. However, their lack of molecular separation leads to signal overlap and matrix interference, significantly reducing specificity in complex samples (Astefanei et al., 2015; John et al., 2022; Kumar & Rhim, 2024). This restricts their utility in quantitative applications, especially when precision and selectivity are critical.

Raman spectroscopy. Raman spectroscopy, although useful for structural fingerprinting, is compromised by the intrinsic fluorescence of CNDs and food components, which often overwhelms the Raman signal. These fluorescence interferences, combined with low quantification reliability, limit Raman's effectiveness in CND analysis (Astefanei et al., 2015; John et al., 2022)

Transmission electron microscopy (TEM). TEM provides high-resolution imagery for assessing particle morphology and size distribution, making it valuable for fundamental characterization. However, TEM is qualitative, low-throughput, and requires extensive sample preparation, rendering it impractical for routine analysis in food matrices (Gong et al., 2014; Q. Hu et al., 2014; Vinci & Colon, 2012).

Chromatographic method. Other chromatographic methods, including reverse-phase HPLC (RP-HPLC) and anion-exchange HPLC (AE-HPLC), offer better resolution than spectroscopic techniques but still fall short in complex food systems. These approaches often necessitate intensive sample cleanup and lack broad validation for food-based

quantification (Q. Hu et al., 2014; Vinci & Colon, 2012). Quantitative performance metrics such as reproducibility and detection limits are also rarely reported.

HPLC-SEC-FLD. In contrast, the HPLC-SEC-FLD method developed in this study provides a robust and highly sensitive platform tailored for the quantification of CNDs in complex food matrices. It enables both size-based separation and fluorescence-based detection, mitigating matrix interference while allowing for precise nanoparticle quantification. This method demonstrates high reproducibility (≤3% deviation) and effectively isolates CNDs fractions from non-fluorescent and low-molecular-weight impurities (Trubetskaya et al., 2021). These characteristics make it especially well-suited for processed food applications where matrix complexity is a significant analytical barrier.

In summary, while traditional methods serve important roles in characterizing CNDs, HPLC-SEC-FLD offers the most practical balance of specificity, sensitivity, and reproducibility for quantitative analysis in food systems. Its adaptability, coupled with the ability to analyze multiple CNDs types simultaneously, underscores its potential as a standard method for CNDs monitoring in food safety, nanotoxicology, and regulatory frameworks.

Table 2. Comparative Analysis of Analytical Methods for Carbon Nanodots (CNDs) Quantification

Method	LOD/LOQ	Advantages	Disadvantages	Ref.
UV–Vis / Fluorescence Spectroscopy	Not consistently reported	Rapid screening, accessible instrumentation	Low specificity, overlapping signals in complex samples	(Astefanei et al., 2015; John et al., 2022; Kumar & Rhim, 2024)
Raman Spectroscopy	Not applicable	Structural fingerprinting, non-destructive	Fluorescence interference, low quantification reliability	(Astefanei et al., 2015; John et al., 2022)
Transmission Electron Microscopy (TEM)	Not applicable	High-resolution imaging, particle morphology	Qualitative only, low throughput, complex prep	(Gong et al., 2014; Q. Hu et al., 2014) (Vinci & Colon, 2012)

RP-HPLC	Not reported	Some separation capability, applicable to synthetic CNDs	Limited data in food matrices, requires secondary validation	(Q. Hu et al., 2014) (Gong et al., 2014)
AE-HPLC	Not reported	Selective for charged species, some environmental applications	Matrix complexity requires extensive prep	(Vinci & Colon, 2012).
LC-MS	LOD: 0.002–0.005% w/w (LC-UV); 0.04–1.1 µg/g (LC-APCI-MS); 0.4 pg/L–1.6 ng/L (LC-APPI-MS)	Ultra-sensitive, detailed molecular info	High cost, requires standards, complex operation	(Astefanei et al., 2015)

2.3. Green Synthesis Methods for CNDs and Their Effects on Properties (RQ2)

In addition to their unintentional formation during thermal food processing, CNDs can also be intentionally synthesized for functional use in food systems. Their small size, tunable fluorescence, biocompatibility, and stability make them highly attractive for applications such as contaminant detection, smart packaging, nutrient sensing, and antimicrobial coatings (Moradi et al., 2023; X. Shi et al., 2019; L. Zhao et al., 2023). From a mechanistic perspective, CND synthesis is generally classified into two fundamental strategies: top-down and bottom-up. Within these strategies, green synthesis does not constitute an independent third route, but rather refers to environmentally benign implementations—predominantly of bottom-up approaches—using renewable or food-derived precursors, low-toxicity solvents, and reduced energy input. This conceptual relationship between synthesis strategies and precursor sources is illustrated in **Figure 6**.

2.3.1. Fundamental Synthetic Approaches: Top-Down vs. Bottom-Up

CNDs can be synthesized via two overarching strategies:

- **Top-down methods**, which involve breaking down bulk carbon structures (e.g., graphite, soot, carbon fibers) using physical, chemical, or electrochemical techniques such as laser ablation, arc discharge, or oxidation (Wang et al. 2017)(Wang et al. 2023). While these methods can produce narrow particle sizes, they often suffer from low control over surface functionality and require harsh conditions.
- **Bottom-up methods**, in contrast, build CNDs from molecular precursors such as citric acid, sucrose, amino acids, or plant extracts via thermal decomposition, microwave irradiation, or hydrothermal treatment. These approaches offer greater control over size, fluorescence, and heteroatom doping, and are thus more suited for food-related and biocompatible applications (Shin et al. 2015; Wang et al. 2019; Wang et al. 2015).

2.3.2. Definition and Scope of Green Synthesis of CNDs

In this thesis, the term “green synthesis” refers to the use of renewable or food-based precursors, aqueous or low-toxicity solvents, and synthesis conditions designed to minimize environmental impact and safety risks. Accordingly, “green CNDs” denote carbon nanodots produced via such environmentally benign routes, with emphasis on biocompatibility and suitability for food systems.

Importantly, green synthesis does not represent a separate synthesis mechanism, but rather a context-dependent classification based on precursor selection and processing conditions. In practice, green CNDs are most commonly produced via bottom-up methods, although rare top-down implementations using benign reagents have also been reported. Thus, the distinction between conventional and green synthesis lies not in the fundamental reaction pathway, but in the choice of precursors, solvents, and energy input, as summarized in **Figure 6**.

2.3.3. Green Bottom-Up Synthesis from Food and Bio-Based Sources

Recent studies highlight the feasibility of synthesizing CNDs from natural food wastes, edible plant parts, or agro-byproducts, offering low-cost, environmentally friendly pathways (De Yro et al., 2019). These sources provide inherent carbon, nitrogen, and oxygen-rich precursors that contribute to both the core structure and surface functionality of the resulting CNDs. For examples, orange juice, banana juice, and lemon juice, which have been used to produce fluorescent CNDs via microwave and hydrothermal methods, often showing pH-dependent fluorescence and antimicrobial activity (De & Karak, 2013; MoziOğlu, 2022; Sahu et al., 2012). In another case, Guava leaves (Ramanarayanan & Swaminathan, 2020), *Trapa bispinosa* peels (Mewada et al., 2013), and *Lawsonia inermis* leaves (Mary Alex et al., 2020)have also served as biomass for producing nanoscale CNDs with antioxidant, anti-inflammatory, and UV-absorbing properti**es**, relevant to both food safety and cosmetic applications.

2.3.4. Common Green Synthesis Techniques

Several green synthesis techniques are well-established for producing CNDs suitable for food and biomedical applications:

- **Hydrothermal synthesis**: Involves heating natural precursors (e.g., sugars, acids, peels) in sealed aqueous environments. It allows fine control over size and quantum yield (Sa et al., 2017; Tomskaya et al., 2018).
- **Microwave-assisted synthesis**: Enables rapid carbonization under high-energy microwaves. Precursors such as lemon juice, egg membranes, and denatured proteins yield CNDs with diverse optical and antimicrobial functions (MoziOğlu, 2022; X. Wang et al., 2011).
- **Solvothermal synthesis**: Similar to hydrothermal, but employs organic solvents to fine-tune hydrophobicity or other physicochemical properties.

Examples include food waste-derived CNDs with high biocompatibility and strong fluorescence (S. Y. Park et al., 2014).

Each method offers different trade-offs in terms of scalability, uniformity, energy demand, and fluorescence performance. Hydrothermal treatment is cost-effective but yields can be modest; microwave synthesis is fast and scalable but may require optimization to avoid aggregation (Wu et al. 2021). The development of green, scalable, and tunable methods for CNDs synthesis is key to their safe and effective integration in food systems. Each synthesis route influences critical properties such as particle size, stability, fluorescence intensity, and biocompatibility, which in turn affect their performance as sensors, preservatives, or labeling agents.

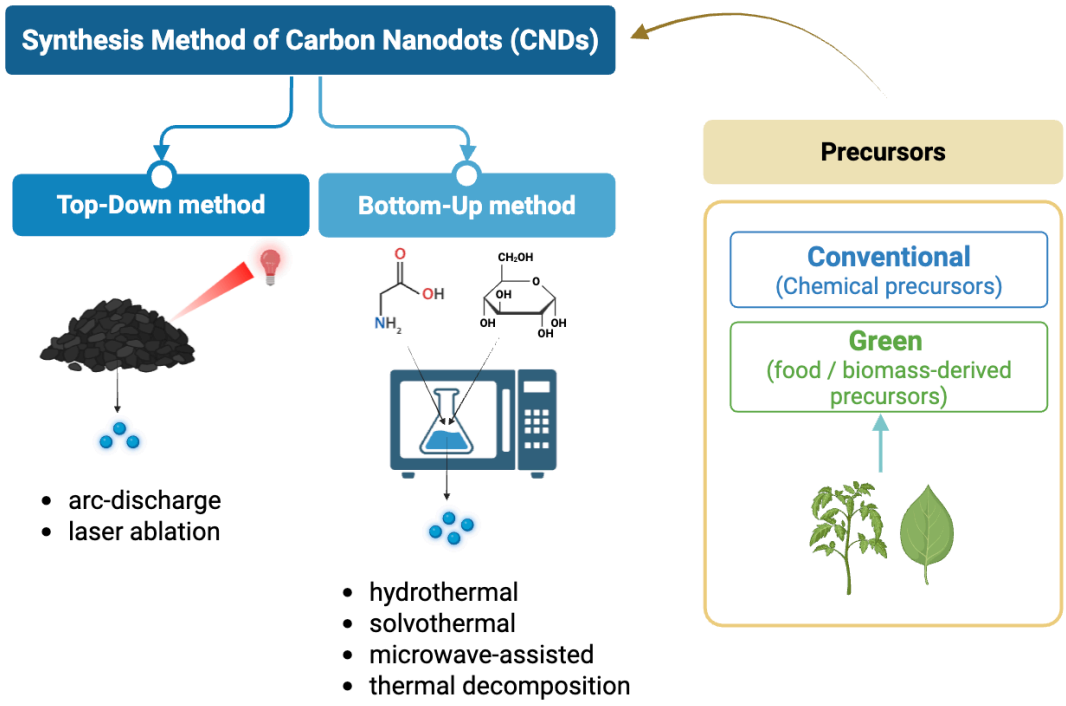


Figure 6. Schematic overview of CND synthesis methods and precursor sources (chemical vs biomass-derived).

2.3.5. Machine Learning for Predictive Optimization of Green CND Synthesis

Machine learning (ML) techniques have been successfully applied to predict and optimize the optical properties of CNDs and synthesis conditions, leading to CNDs with enhanced quantum yields and improved corrosion inhibition properties (Y. Han et al., 2020). Artificial neural networks (ANNs) have been used to predict emission color and wavelength with high accuracy, revealing that reaction method, purification, and solvent

choice are crucial factors (Senanayake et al., 2022). Regression models have guided the synthesis of CNDs with enhanced quantum yields, identifying precursor mass and alkaline catalyst volume as key parameters (Y. Han et al., 2020). Multiple linear regression has been employed to predict spectral characteristics of red and near-infrared emitting CNDs, providing an open-source code for researchers (Tuchin et al., 2024). The extreme gradient boosting (XGBoost) model has shown excellent performance in predicting CNDs optical properties, enabling the design of CNDs with specific fluorescence intensities and emission centers (Hong et al., 2022).

ML algorithms have demonstrated the ability to model complex relationships between synthesis parameters and material properties, reducing reliance on trial-and-error approaches (Mondal et al., 2025). The integration of ML with traditional experimental methods has accelerated the discovery of novel carbon nanomaterials with enhanced functional properties, opening new avenues for applications in photocatalysis, energy storage, sensing, and corrosion inhibition (Y. Han et al., 2020; Mondal et al., 2025).

2.4. Detection Methods for Food-derived CNDs (RQ3)

Detecting carbon nanodots (CNDs) formed during food processing remains analytically demanding due to their nanoscale size, structural heterogeneity, and coexistence with chemically similar fluorophores in food matrices. Although their photoluminescence offers a useful analytical handle, matrix-derived signals from Maillard products or caramelization compounds frequently overlap with CND-specific emissions, complicating reliable identification and quantification.

2.4.1. Fluorescence-Based Approaches

Fluorescence spectroscopy is the most widely applied tool for detecting CNDs in food systems, owing to its high sensitivity and operational simplicity (Lin et al., 2012; Y. Zhao et al., 2015). Excitation-dependent emission is often used to distinguish CNDs from background signals, though this becomes problematic in complex foods such as coffee, caramel, or baked products, where multiple fluorophores co-exist. Advanced methods, including fluorescence lifetime imaging or spectral deconvolution, can improve specificity but require more specialized setups (Fu et al., 2015, p. 20; M. Liu, 2020).

2.4.2. Electron Microscopy and Particle Sizing

Transmission electron microscopy (TEM) remains the gold standard for confirming CNDs presence and morphology, directly visualizing nanoscale features such as quasi-spherical shapes and lattice fringes (Jurkiewicz et al., 2018). Scanning electron microscopy (SEM) provides complementary surface topography (Abinaya et al., 2022; Mintz et al., 2021), while X-ray diffraction (XRD) reveals crystallinity and degree of graphitization (Neumann et al., 2020). To assess colloidal behavior, dynamic light scattering (DLS) and zeta potential analyses are often employed, offering insights into hydrodynamic size and electrostatic stability (Carvalho et al., 2018; Murdock et al., 2008). While informative, these methods are labor-intensive and low-throughput.

2.4.3. Surface Chemistry Spectroscopy

Spectroscopic tools such as Fourier-transform infrared (FTIR), Raman spectroscopy, and X-ray photoelectron spectroscopy (XPS) provide critical insights into the chemical functionalities of food-derived CNDs. FTIR detects hydroxyl, carbonyl, and amine groups originating from precursor decomposition (Fawaz et al., 2023; Ren et al., 2019), while XPS determines elemental composition and oxidation states (Tan et al., 2013; C. Zhao et al., 2019). Raman spectroscopy complements these analyses by resolving sp^2/sp^3 domains and subtle carbon structural changes (Mintz et al., 2021; Righetto et al., 2017).

Together, these techniques help explain how surface chemistry governs solubility, fluorescence behavior, and reactivity, though their utility in raw food extracts is limited by background signals from complex mixtures.

2.4.4. Chromatographic Separation with Fluorescence Detection

High-performance liquid chromatography coupled with fluorescence detection (HPLC-FD) provides enhanced selectivity by physically separating nanoscale particles from small-molecule fluorophores. Size-exclusion chromatography with fluorescence detection (HPLC-SEC-FD) is particularly promising, enabling the isolation of nanoparticle fractions and confirmation of their emission properties (D. H. H. Nguyen, El-Ramady, & Prokisch, 2025; Törős et al., 2025). This technique has successfully distinguished CNDs from melanoidins and other Maillard products in processed foods. However, challenges such as co-elution, lack of standardized reference materials, and sample-dependent matrix effects remain.

2.4.5. Matrix Effects and Multi-Modal Strategies

Food-derived CNDs often interact with proteins, lipids, and polysaccharides, modifying their fluorescence intensity, solubility, and recovery efficiency (Carvalho et al., 2018; Murdock et al., 2008). Many particles remain trapped within insoluble fractions, necessitating optimized extraction protocols, such as solvent-assisted dispersion, ultrasonication, or centrifugation-though these treatments may themselves alter particle characteristics. Increasingly, researchers adopt multi-modal workflows that integrate optical, spectroscopic, and electron microscopy techniques to strengthen detection confidence. While effective, these combined strategies require specialized expertise and remain limited to research laboratories.

2.5. Food Safety and Toxicological Considerations (RQ4 – RQ6)

While CNDs have shown tremendous potential in food-related applications, ranging from sensing and packaging to antimicrobial protection, their toxicological profile and food safety implications remain underexplored. As nanomaterials increasingly find roles in direct and indirect food contact systems, it is critical to assess the cytotoxic, genotoxic, and biodistributional behavior of CNDs across biological systems. **Figure 7** summarizes the principal domains of safety assessment.

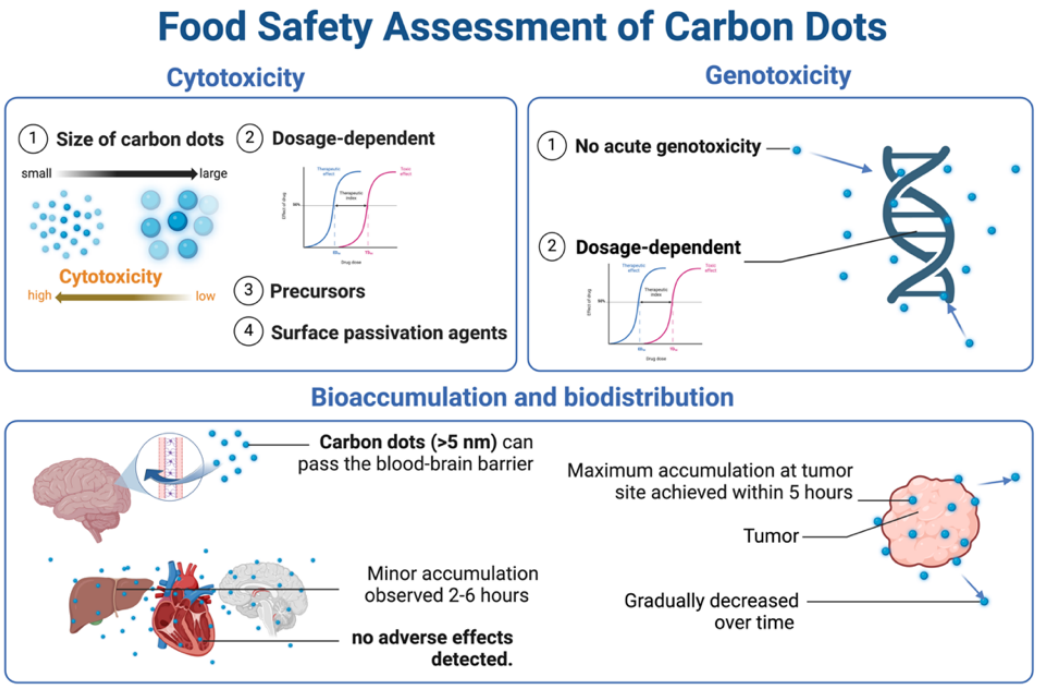


Figure 7. Key aspects of CNDs food safety assessment consist of (**1**) Cytotoxicity, (**2**) Genotoxicity, and (**3**) Bioaccumulation and biodistribution (D. Nguyen, El-Ramady, et al., 2024).

2.5.1. Cytotoxicity

CNDs are generally regarded as having lower cytotoxicity compared to traditional semiconductor quantum dots, largely due to their carbon-based composition and biocompatible nature. However, experimental findings suggest that their cytotoxicity is not negligible and varies depending on synthesis parameters. Wang et al. (2011) and (Hola et al. 2014) reported that the cytotoxic potential of CNDs is closely linked to precursor materials, surface passivation agents, concentration, and particle size. For example, (Sahu et al., 2012) demonstrated that CNDs synthesized from common precursors like glucose or citric acid can retain residual impurities affecting

biocompatibility. Conversely, CNDs derived from natural materials such as orange juice displayed low cytotoxicity and high cellular tolerance.

The dose–response relationship is particularly significant. (Li et al. 2018a) showed that while 80% of cells survived exposure at 1 mg/mL, up to 90% cell death was observed at 10 mg/mL. Liao et al. (2015) reported no toxicity for CNDs derived from Kvass up to 20 mg/mL, further suggesting that both precursor type and concentration modulate cytotoxic outcomes. Surface functionalization also plays a critical role: biocompatible coatings such as PEG, carboxyl, or amino groups have been shown to reduce toxicity by enhancing stability and reducing reactive interactions. Mukherjee et al. (2022) emphasized that the inclusion of heteroatoms like N, S, or O can improve photophysical properties while enhancing biological tolerance. Furthermore, smaller CNDs tend to be more readily internalized by cells, potentially inducing higher cytotoxic effects-consistent with findings in other quantum dot systems (Derfus et al. 2004)(Nygård et al. 2000).

2.5.2. Genotoxicity

Genotoxicity refers to the ability of a compound to damage genetic material, potentially leading to mutations, chromosomal instability, or carcinogenesis. In the case of CNDs, current evidence suggests a low genotoxic profile, especially at doses commonly used in food and biomedical research. Pelaz et al. (2017) reported no observable genotoxic effects or organ abnormalities in animals exposed to CNDs at 51 mg/kg body weight. Similarly, Zaidi et al. (2022) demonstrated the biosafety of photoluminescent CNDs generated by nitric acid oxidation, observing no acute genotoxicity or toxicity in murine models. In vitro assessments have supported these findings: Havrdová et al. (2021) found no significant DNA damage in cells exposed to CNDs at concentrations up to 400 μg/mL. However, at higher concentrations, alterations in cell morphology and increased mortality were reported, suggesting that dosage remains a limiting safety factor. These results suggest that CNDs do not cause acute genotoxic effects at relevant concentrations, but long-term genomic stability and low-dose chronic exposure remain open questions requiring further investigation.

2.5.3. Bioaccumulation and Biodistribution

Understanding how CNDs distribute, accumulate, and clear within biological systems is central to predicting their safety, especially under dietary or chronic exposure conditions. Initial studies suggest that CNDs exhibit low systemic accumulation and are efficiently cleared, but the difference based on particle size, surface chemistry, and exposure route.

Yang et al. (2009a) reported limited *in vivo* accumulation of CNDs and no overt organ toxicity, supporting their general biocompatibility. However, other studies revealed organ-specific distribution, especially in the brain, liver, and heart. Song et al. (2018) observed that ultra-small CNDs (<5 nm) could cross the blood-brain barrier within two hours of oral administration in mice. (Shabbir et al. 2022) further confirmed that CNDs may localize in both cytoplasm and nucleus, leading to apoptosis in L929 cells. Similarly, Li et al. (2018a) demonstrated rapid intracellular transport in both plant and animal models, with particles localizing in cytoplasmic regions and occasionally within nuclei. The ability of CNDs to penetrate biological barriers raises important considerations for neurotoxicity and unintended tissue accumulation.

In vitro digestion studies by Li et al. (2018a) also revealed that CNDs can be quenched or degraded by saliva, gastric juice, and bile, potentially reducing bioavailability during digestion. However, follow-up biodistribution studies in animals found fluorescence signals in key organs 2–6 hours after administration, underscoring the need to assess longer-term accumulation and clearance kinetics. Liao et al. (2021) demonstrated delayed clearance in tumor-bearing mice, suggesting that retention may be enhanced in pathological or inflamed tissues.

2.6 Functional Applications in Food Systems (RQ7 - RQ8)

CNDs have gained widespread attention in food science due to their unique structural and optical properties, including fluorescence, biocompatibility, tunable surface chemistry, and antimicrobial activity. Because the structure and surface functionalization of CNDs can be tailored, their interactions with specific analytes can be optimized, enabling application designs that match the target substance and intended food system. The primary application of CNDs in food systems, structured under four subsections (**Figure 8**), including (**1**) CNDs-based sensors enable monitoring of key nutrients, (**2**) detect contaminants, (**3**) identify foodborne pathogens directly or indirectly, and (**4**) are integrated into smart packaging for quality and freshness control.

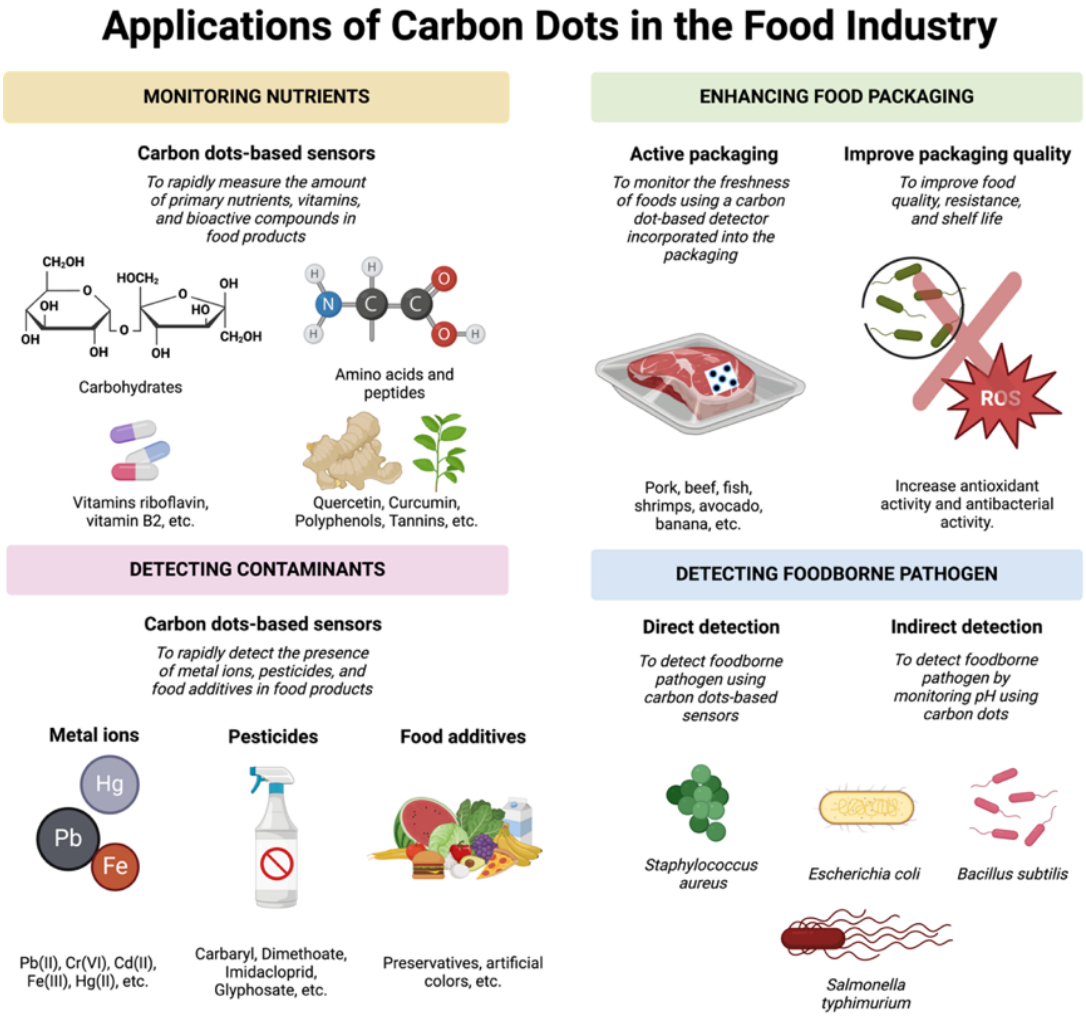


Figure 8. Application of Carbon Nanodots (CNDs) in the food sector (D. Nguyen, El-Ramady, et al., 2024).

2.6.1. Probes and Sensors for Food Contaminants

The application of CNDs in detecting food contaminants represents one of their most actively explored and promising functionalities in food-related research. Owing to their intrinsic photoluminescence and highly tunable surface chemistry, CNDs can be engineered as sensitive probes for specific classes of analytes through tailored synthesis and functionalization. Importantly, CNDs-based sensing is target-specific: different analytes require CNDs with distinct sizes, surface functional groups, or heteroatom doping, rather than a single universal nanodot system.

- **Detection of Metal Ions:** CNDs have demonstrated high sensitivity in detecting trace metal ions such as Pb(II), Cd(II), Hg(II), and Fe(III). These ions, prevalent in contaminated water and foods, pose significant health risks. Functionalized CNDs bind selectively to these ions, leading to fluorescence quenching or enhancement, which serves as a detection signal. Detection limits often fall within the nanomolar range, outperforming conventional sensors (P. Zhao et al., 2021)(Hoang et al. 2023). CNDs-based fluorescent probes have been reported to have high sensitivity for detecting heavy metal contaminants in water, achieving very low detection thresholds. Reported limits include 2.3 nM for Cr(VI), 0.08 ppb for Pb(II), 0.29 nM for Cd(II), 0.07 μM for Fe(III), and 63 nM for other ions (Du et al. 2023; Pandey et al. 2020; Sahu and Khan 2020; Zhang et al. 2020; Zhao et al. 2021b).
- **Pesticide Residue Detection:** CNDs-based fluorescence sensors operate via "off-on-off" mechanisms that rely on either direct molecular binding or enzymatic inhibition pathways. These systems have been employed to detect organophosphates, carbamates, and herbicides, achieving detection limits as low as 2 pM for glyphosate (Bera and Mohapatra 2020)Cao and Guo (2024) developed CNDs sensors to detect imidacloprid in vegetables based on Förster Resonance Energy Transfer (FRET) principle.
- **Food Additives and Artificial Colorants:** Sensors based on CNDs can quantify illegal or excessive levels of food additives such as nitrites, sulfites, and formaldehyde, as well as artificial dyes like Tartrazine (Yang et al. 2020) and Sudan Red II (Ramoğlu et al. 2021). Detection is achieved through fluorescence changes upon interaction with target molecules, enabling high specificity even in complex food matrices (Su et al., 2022)(Yang et al. 2020). Unlike preservatives, which are harder to trace, CND-based sensors can effectively detect most common synthetic food colorants. These include yellow dyes such as tartrazine and sunset yellow, red

dyes such as Sudan I and Sudan II, and the blue dye indigo carmine (Albalawi et al. 2023; Ali et al. 2021; Ramoğlu et al. 2021; Su et al. 2022; Yang et al. 2020; Zhao et al. 2021a).

- **Foodborne Pathogen Detection:** Foodborne pathogens represent a significant food safety concern. Recent studies have shown that CNDs can be effectively used for the detection of bacterial and fungal pathogens. Their high surface area, modifiable surfaces, and fluorescence properties allow them to bind or interact with specific microbial targets, triggering detectable fluorescence signals. CNDs have been applied to detect *Staphylococcus aureus* (Gao et al. 2024; John et al. 2020; Zhao et al. 2021a), *Escherichia coli* (John et al. 2020; Zhao et al. 2021a) and toxins such as aflatoxin B1 (Li et al. 2024). Incorporating nanohybrids like magnetic nanoparticles, enzyme complexes, or silver nanoshells can significantly enhance the sensitivity and speed of CNDs-based sensors (Abu et al. 2020). Immunomagnetic separation techniques using CNDs-labeled probes have enabled real-time detection of *E. coli* and *Salmonella* in complex matrices such as milk and fruit juices (Zhao et al. 2009). Additionally, pH-sensitive CNDs have been used to detect shifts in food environments caused by microbial growth, further supporting their role in food pathogen detection (Pathak et al. 2020).

2.6.2. CNDs in Smart and Active Packaging

CNDs enhance the functionality of packaging systems through their pH-sensitive fluorescence and antimicrobial properties. By integrating CNDs into biopolymer matrices such as chitosan, alginate, and gelatin, active packaging materials are created that not only protect the food but also provide real-time information on spoilage or contamination. These CNDs-based films have extended shelf lives of avocados (Ezati et al. 2022), tomatoes (Bao et al. 2023), blueberries (Chen et al. 2023), and meats (Lin et al. 2022) by several days to weeks, while also inhibiting bacterial and fungal growth. Additionally, CNDs impart UV-blocking and antioxidant capabilities to packaging films, protecting light-sensitive nutrients and improving product stability Khan et al. (2024).

2.6.3. Nutrient Monitoring and Quality Control

CNDs-based sensors have been employed for the detection of essential food nutrients. These sensors offer advantages over traditional methods, including low detection limits, rapid response, and compatibility with small devices. For instance, glucose sensors incorporating enzyme-functionalized CNDs detect concentrations as low as 11.3 μM in

saliva or urine (Haiyang et al., 2024), while vitamin B_2 detection using doped CNDs achieves limits of 12.5 ng/mL (Meng & Wu, 2024). Such capabilities pave the way for personalized nutrition tracking and real-time quality assurance in food processing lines. CNDs have been used to develop novel nanosensors and nano biosensors for food quality control including glucose, amino acids, and vitamins B_2 (Jurkiewicz et al., 2018).

2.6.4. Toward Safe and Sustainable Use

While the functional potential of CNDs in food systems is vast, ensuring safety and sustainability remains a critical priority. Multiple risk mitigation strategies have been developed to address cytotoxicity, genotoxicity, and environmental concerns associated with CNDs. These strategies are illustrated in **Figure 9** and represent essential guidelines for minimizing risks associated with food-grade CNDs.

- **Selecting Appropriate Precursors**: The choice of carbon sources greatly affects the biocompatibility and size of CNDs. Natural precursors, such as fruits, vegetables, and biomass, typically yield smaller CNDs (1–8 nm) with lower cytotoxicity, compared to synthetic compounds which may lead to larger and m,ore toxic particles (Yao et al. 2019)(Hola et al., 2014).
- **Optimizing Synthesis Methods**: Synthesis conditions, including temperature, solvent choice, and method, influence the surface chemistry, size, and optical properties of CNDs (Atabaev 2018; De and Karak 2013; Wang et al. 2014). Lower synthesis temperatures or solvent-assisted methods may help reduce toxicity while preserving fluorescence (D. Nguyen, El-Ramady, et al., 2024).
- **Surface Modification and Functionalization:** Surface passivation using agents like ethylenediamine or citric acid improves water dispersibility and biocompatibility. Doping with nitrogen, phosphorus, or sulfur enhances luminescence and reduces cytotoxic interactions (Yao et al. 2019)(Park et al. 2016)(Wang et al. 2014).
- **Developing Detection Protocols:** Robust analytical techniques such as fluorescence spectroscopy, HPLC, and UV-Vis absorbance must be standardized for quantifying CNDs in food matrices. The amount of CNDs can be determined by comparing the absorbance of a sample to a calibration curve (Churchill et al. 2009).

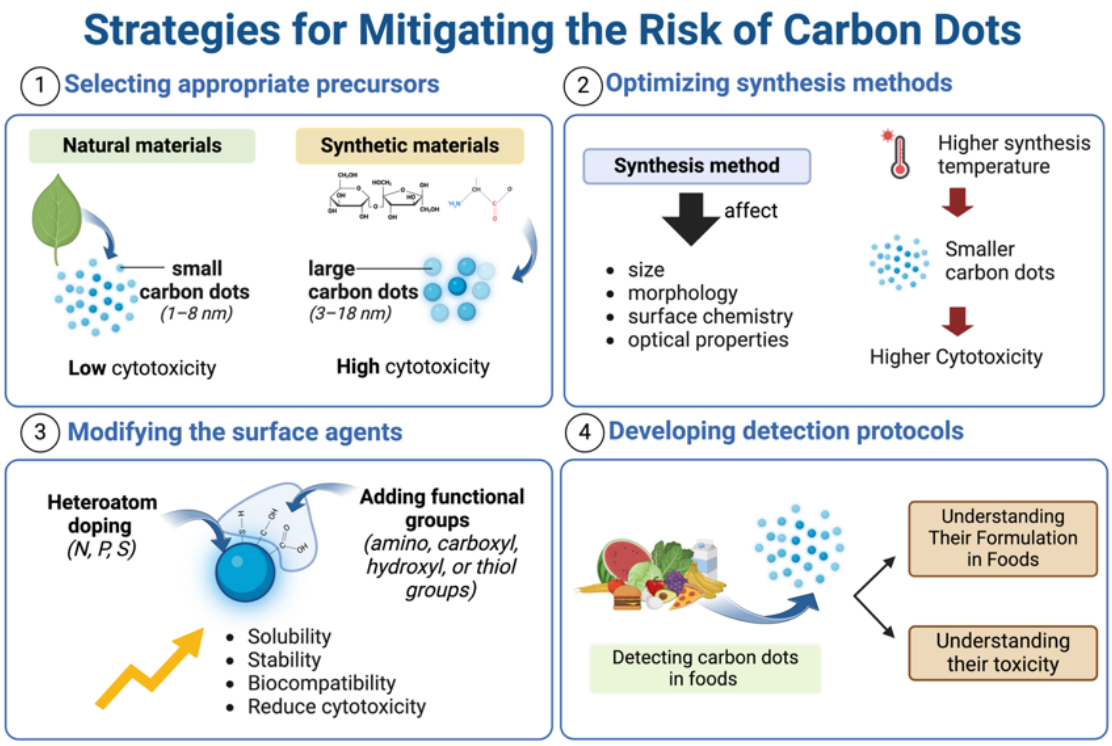


Figure 9. Approaches to minimizing potential risks of CNDs (D. Nguyen, El-Ramady, et al., 2024).

2.6.5. Environmental Implications of Large-Scale CNDs Synthesis

The environmental impact of large-scale CNDs synthesis depends strongly on precursor selection, solvent use, and energy demand. Recent reviews emphasize that future studies should explicitly evaluate the environmental effects of starting materials, solvents, and generated byproducts (Ren et al., 2024). In this context, food-waste valorization offers clear sustainability advantages: Park et al. (2014) reported the production of approximately 120 g of carbon dots from 100 kg of food waste using simple, environmentally friendly methods. espite these promising examples, large-scale implementation remains challenging. Current synthesis approaches are often considered resource-inefficient, with concerns regarding waste generation, energy consumption, and batch-to-batch variability (Huang & Ren, 2025; Ren et al., 2024). Moreover, comprehensive life-cycle assessments are largely absent, highlighting the need for systematic evaluation of scalability, environmental footprint, and quality control strategies before widespread industrial adoption.

3. MATERIAL AND METHODS

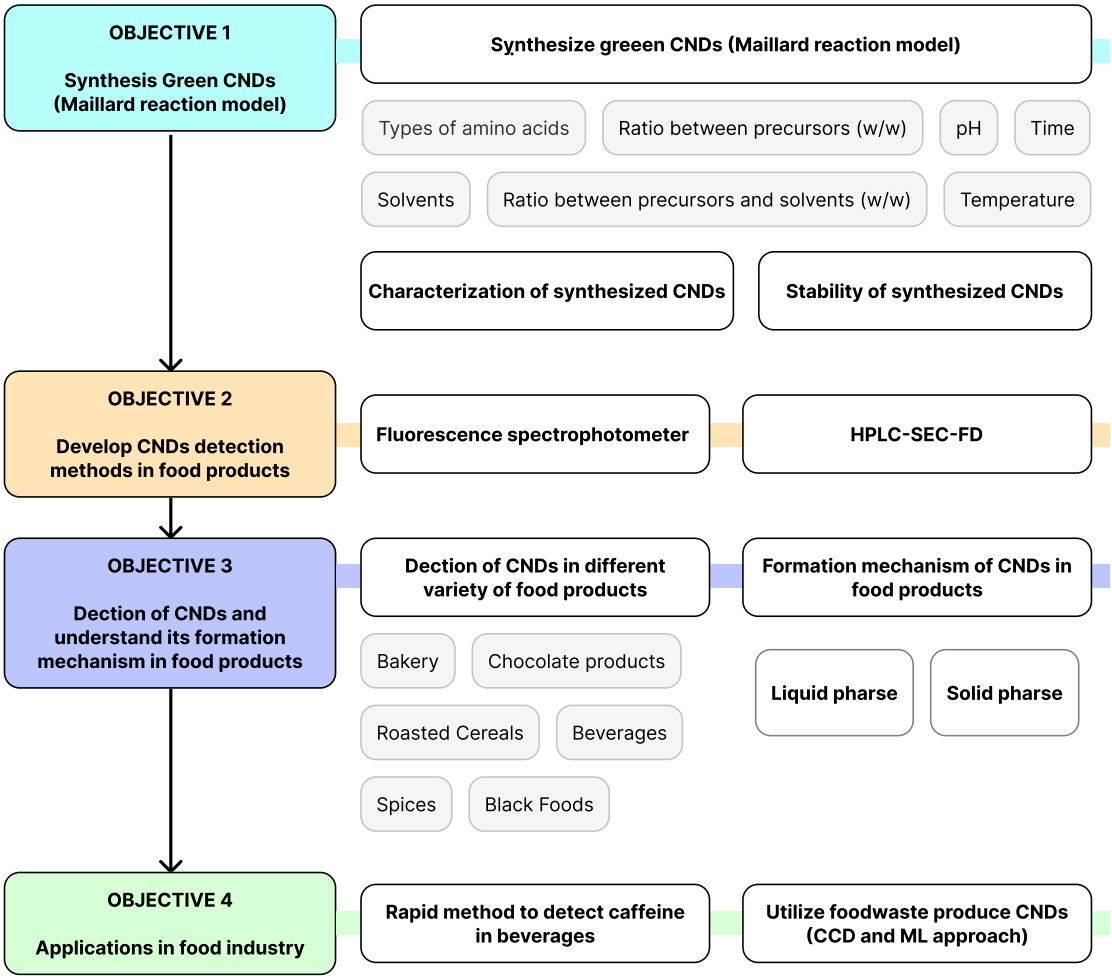


Figure 10. The overall experimental design of this PhD dissertation.

3.1. Objective 1: Synthesis and characterize CNDs using the Maillard reaction model (addessing RQ1 – RQ3)

3.1.1. Materials

L-arginine, glycine, L-tyrosine, L-proline, L-glutamine, L-phenylalanine, and sucrose were obtained from Vital-Trend Ltd. (Budapest, Hungary). Hydrochloric acid (1.0 M), sodium hydroxide (0.01 M), and ethanol (≥ 99.5%) were purchased from VWR International Ltd. (Pennsylvania, USA) and used as received without additional purification. All experiments were conducted using ultrapure water.

3.1.2. Method

The synthesis of CNDs via the Maillard reaction was designed in three stages, including: (1) optimization of conditions to synthesize CNDs via the Maillard reaction model, (2) characterization of synthesized CNDs, and (3) evaluation of the stability of synthesized

CNDs. The Maillard reaction was chosen as a model for these experiments with amino acids and sugars as the precursors; therefore, all parameters were kept constant during the synthesis process. Amino acids (1 mmol) and sucrose (1 mmol) were dissolved in deionized water (20 mL) and heated at 120 °C for 12 h. After cooling to ambient temperature, an equal volume of pre-chilled ethanol was added to precipitate and remove unreacted amino acids. The mixture was incubated at −20 °C for 30 min and centrifuged at 10,000 rpm for 30 min. The supernatant, containing the soluble CND fraction, was collected and purified by sequential treatment with a cellulose-packed column followed by filtration through a 0.22 μm membrane. The purified solution was freeze-dried to obtain CND powder, which was stored until further use.

In the first experiment, to obtain CNDs exhibiting strong fluorescence and small particle size, three sequential experimental phases were conducted, as outlined in **Figure 11**. First, six amino acids-namely L-arginine, glycine, L-tyrosine, L-proline, L-glutamine, and L-phenylalanine-were reacted with sucrose to identify the most suitable precursor for CNDs production (**Figure 11A**). Second, once the optimal amino acid was identified, its molar ratio with sucrose was varied across nine combinations (ranging from 2:0 to 0:2 mmol) to optimize synthesis yield and quality (**Figure 11B**). Third, nine solvent systems were tested for their efficacy in extracting CNDs, including deionized (DI) water pH 6.0 as control, pH-adjusted DI water (pH 2.0 and pH 9.0), and ethanol solutions ranging from 20% to 100% (**Figure 11C**). Fluorescence intensity was used as the primary criterion to determine optimal conditions, and all experiments were conducted in triplicate.

Finally, the stability of synthesized CNDs was evaluated under different environmental conditions to simulate real-world food and biological systems. For ionic strength testing, CNDs were diluted in NaCl solutions ranging from 0.1 M to 1.0 M, and fluorescence intensity was measured after equilibration. Temporal stability was assessed by recording fluorescence intensity at fixed intervals over a 60-minute period at room temperature. pH stability was examined by adjusting CND suspensions to pH values ranging from 4.0 to 11.0 using HCl and NaOH, followed by fluorescence analysis at an excitation wavelength of 360 nm. All measurements were performed in triplicate, and emission spectra were recorded to monitor peak position and intensity variation across treatments.

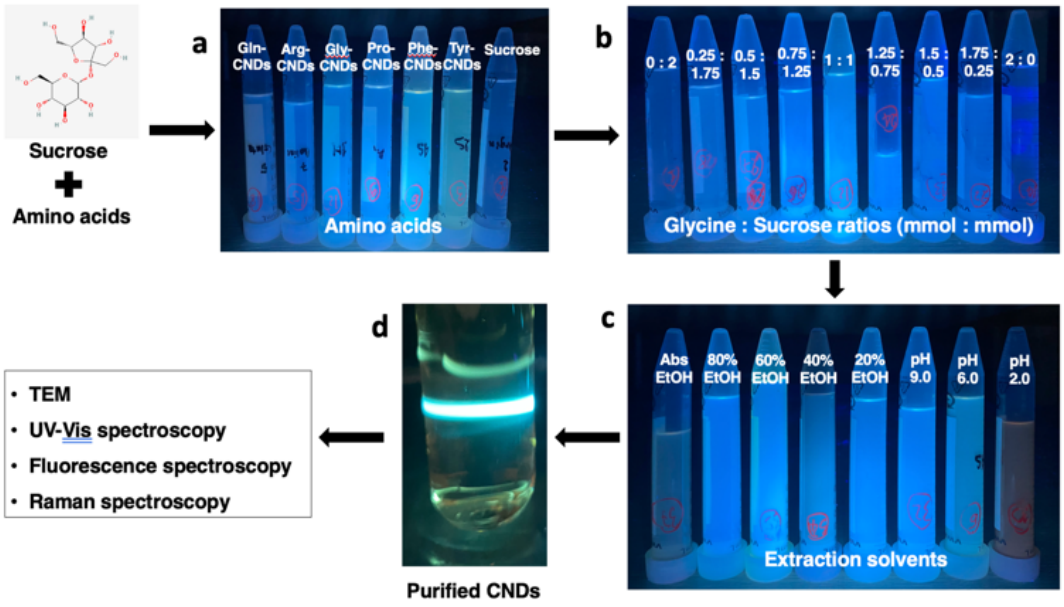


Figure 11. Experimental workflow illustrating for synthesis of CNDs using Maillard reaction as studied model, with UV-lamp images of the final product, starting from (a) fluorescence comparison of CNDs synthesized from six amino acids (Arg, Gly, Tyr, Pro, Gln, Phe); (b) influence of glycine-to-sucrose ratios (mmol/mmol) on CND fluorescence; (c) effects of different extraction solvents (DI water, pH-adjusted water, and various ethanol concentrations); and (d) characterization of purified CNDs by TEM, UV-Vis, fluorescence, and Raman spectroscopy (D. Nguyen, Muthu, El-Ramady, Daróczi, et al., 2024).

3.1.3. Characterize the synthesized CNDs from Maillard reaction model

The synthesized carbon nanodots derived from the Maillard reaction model (glycine–sucrose CNDs; Gly-S-CNDs) were systematically characterized to evaluate their morphology, size distribution, optical properties, structure, and surface chemistry. Morphology and particle size were analyzed by transmission electron microscopy (TEM). Optical properties were assessed using fluorescence spectroscopy and UV–visible spectrophotometry. Structural features were examined by Raman spectroscopy and X-ray diffraction (XRD), while surface functional groups were identified by Fourier-transform infrared spectroscopy (FTIR). In addition, high-performance liquid chromatography with size-exclusion chromatography and fluorescence detection (HPLC-SEC-FD) was used to confirm the nanodot fraction and collect purified Gly-S-CNDs for subsequent experiments. Detailed instrumental settings and analytical procedures are provided in **Section 3.5 (Analytical methods).**

3.2. Objective 2: Develop an analytical method to detect CNDs in food products (addessing RQ3)

3.2.1. Quantitative Measurement of CNDs Using Fluorescence Spectroscopy

3.2.1.1. Materials

All experiments were conducted using ultrapure water. Food samples included raw dough (prior to any thermal treatment), bread crumb, and bread crust. Raw dough refers to the unbaked mixture prepared before oven heating. Bread crumb and bread crust denote the inner soft portion and the outer browned layer of baked bread, respectively, which were separated manually after baking. In addition, commercially available fresh bread was purchased from an ALDI supermarket on the same day of use and used as a representative real food sample.

3.2.1.2. Methods

A quantitative fluorescence-based method was developed to measure the concentration of CNDs in food matrices. Purified Maillard reaction-derived carbon nanodots (Gly-S-CNDs)**,** synthesized from glycine and sucrose at a 4:1 (w/w) ratio as described in **Objective 1,** were used to prepare a stock standard solution, with the carbon content determined using an elemental analyzer. Full-scan fluorescent measurement was run to detect the optimum excitation wavelength and emission wavelength of Gly-S-CNDs. Standard curves were generated by recording the fluorescence intensity of serially diluted Gly-S-CNDs solutions (0–3200 mg dm^{-3}) at an excitation wavelength of 360 nm (optimum excitation wavelength of Gly-S-CNDs) using an FP-8500 fluorescence spectrophotometer (Jasco Co., Oklahoma, USA). Calibration curves were freshly prepared on each measurement day, and method performance was validated in terms of reproducibility, detection limit, and inter-day variation using the standard addition method.

For food samples, 1 g of sample (e.g., dough, bread crust, bread crumb) was mixed with 10 mL of distilled water and sonicated for 30 minutes. The mixture was centrifuged at 10000 rpm for 10 minutes, and the supernatant was combined with an equal volume of cold ethanol (40% v/v) and incubated at 4 °C for 30 minutes. After centrifugation (10000 rpm, 30 minutes), the resulting supernatant was filtered through a 0.22 µm membrane and analyzed using fluorescence spectroscopy at 360 nm excitation.

3.2.2. Quantitative Measurement of CNDs Using HPLC-SEC-FD

3.2.2.1. Materials

All chemicals were of analytical grade. HPLC-grade deionized water and acetonitrile were purchased from VWR (Debrecen, Hungary). Standard carbon nanodots (CNDs), including glycine-citric acid-derived carbon nanodots (Gly-C-CNDs), glycine-sucrose-derived carbon nandots (Gly-S-CNDs), urea-citric acid-derived carbon nanodots (U-C-CNDs), and lysine-citric acid-derived carbon nanodots (Lys-C-CNDs), were synthesized at Nanofood Laboratory, University of Debrecen and used as calibration materials. For each formulation, precursor 1 (glycine/lysine/urea) and precursor 2 (citric acid or glucose) were mixed at a 4:1 (w/w) ratio and heated by pyrolysis at 180 °C for 2 h in an oven under a closed system. The obtained powders were ground and dispersed in ultrapure water. The water-soluble fractions were collected, dialyzed overnight using a dialysis membrane (DEGASA Co., Heidelberg, Germany), freeze-dried, ground into fine powders, and stored for future use.

3.2.2.2. *Methods*

Quantification of carbon nanodots (CNDs) in food matrices was performed using high-performance liquid chromatography with size-exclusion chromatography and fluorescence detection (HPLC-SEC-FD). The system (Ecom Spol. s.r.o., Prague, Czech Republic) was operated under isocratic conditions with a flow rate of 0.7 mL/min and an injection volume of 5 µL. Fluorescence detection was set at 380 nm excitation and 460 nm emission.

Four types of water-soluble CNDs synthesized as described in Section 3.2.2.1—glycine–citric acid-derived CNDs (Gly-C-CNDs), glycine–sucrose-derived CNDs (Gly-S-CNDs), urea–citric acid-derived CNDs (U-C-CNDs), and lysine–citric acid-derived CNDs (Lys-C-CNDs)—were evaluated during method development. Based on fluorescence stability, chromatographic behavior, and reproducibility, glycine–sucrose-derived CNDs (Gly-S-CNDs), synthesized via the Maillard reaction using a defined glycine-to-sucrose molar ratio (as specified in Objective 1), were selected as the standard reference material. Calibration curves were established over a concentration range of 0.1–10 mg/L and results were expressed as Gly-S-CND equivalents.

The method was applied to four representative food matrices subjected to prolonged thermal treatment: (1) coffee brew, (2) black apple, (3) black banana, and (4) black pearl. These samples were selected to represent food systems with extensive heat-induced

reactions. Food samples were homogenized, extracted with deionized water (1 g in 100 mL), and filtered sequentially through coarse, fine, and 0.2 μm syringe filters prior to analysis. CNDs were identified based on retention time (<10 min), corresponding to nanoparticle-sized species. Quantification was based on peak area. Method performance was evaluated through precision, recovery, and inter-laboratory comparison.

3.3. Objective 3: Detection of CNDs and understand formation mechanisms in food products (addessing RQ4 - RQ5)

3.3.1. Detection of CNDs in different types of food products

3.3.1.1. Materials

A range of thermally processed food products was analyzed to investigate the occurrence of carbon nanodots (CNDs) and their potential formation mechanisms. Six major food categories were examined: bakery products, chocolates, beverages, black foods, spices, and roasted cereals. For each food category, products from three different commercial brands or suppliers were selected to improve data robustness and minimize brand-specific bias.

Bakery products (bread, biscuits, and pretzels) were purchased fresh on the day of analysis from ALDI Süd (Essen, Germany), Spar Magyarország Kft. (Bicske, Hungary), and Coop Hungary Zrt. (Budapest, Hungary). Raw dough refers to the unbaked mixture prepared before oven heating. Bread crumb and bread crust denote the inner soft portion and the outer browned layer of baked bread, respectively, which were separated manually after baking

Chocolates (milk, dark, and white) were obtained from Lindt & Sprüngli AG (Kilchberg, Switzerland), Nestlé S.A. (Vevey, Switzerland), and Ludwig Schokolade GmbH & Co. KG – Schogetten brand (Berlin, Germany).

Beverages included coffee, tea, and cola.

Coffee brews were prepared in the laboratory from roasted coffee beans using a water-to-coffee ratio of 1:10 (w/v). Three coffee types were used: (1) 100% Arabica (Coffea arabica L.) purchased from ALDI Süd (Essen, Germany), medium–dark roast (8/10), origin Peru; (2) 100% Robusta (Coffea canephora L.) sourced from Laviet Coffee Factory (Da Lat, Vietnam), roast level 8/10; and (3) a 50:50 Arabica–Robusta blend from the same supplier (Laviet Coffee Factory, Da Lat, Vietnam).

Tea infusions – brewed tea- were prepared from dried black, oolong, and green tea leaves purchased from Cau Dat Farm Tea Joint Stock Company (Da Lat, Vietnam) using a water-to-tea ratio of 1:10 (w/v). Cola beverages were purchased from Coca-Cola HBC Hungary Ltd. (Budapest, Hungary) and analyzed as supplied.

Black foods (black garlic, black apple, and black banana) were purchased from Ebonfare Kft. (Budapest, Hungary). These products are commercially manufactured via prolonged thermal treatment under controlled temperature and humidity, resulting in extensive

Maillard reactions and dark coloration. No additional heat treatment was applied in the laboratory.

Spices (ground clove, red chili, turmeric, and ginger) were purchased from Alpaka Kft. (Szeged, Hungary) and analyzed as supplied.

Roasted cereals (rice, oats, peanuts, soybeans, lentils, and beans) were purchased from Auchan Magyarország Kft. (Budaörs, Hungary). These products were commercially roasted by the supplier, and no further roasting was performed in this study.

All samples were analyzed within one week of purchase to minimize storage-related changes. All experiments were conducted using ultrapure water, ethanol (≥99.5%), and other analytical-grade reagents supplied by VWR International Ltd. (Radnor, PA, USA).

3.3.1.2. Methods

CNDs were extracted from each food sample following a standardized procedure adapted from **methods of Objective 1: Synthesis and characterize green CNDs using the Maillard reaction model (addessing RQ1 – RQ3)** (D. Nguyen, Muthu, El-Ramady, Daróczi, et al., 2024). Approximately 1 g of each homogenized sample was mixed with 10 mL of ultrapure water and sonicated for 30 minutes. The liquid samples were lyophilized before extracting CNDs, like other solid samples. The suspension was centrifuged at 10000 rpm for 10 minutes, and the supernatant was combined with cold ethanol (40%, v/v) in a 1:1 ratio. After 30 minutes of incubation at 4 °C, the mixture was centrifuged again at 10000 rpm for 30 minutes. The resulting supernatant was filtered through a 0.22 μm syringe filter to obtain a clear extract containing the CNDs.

The fluorescence properties of the extracted CNDs were measured using an FP-8500 fluorescence spectrophotometer from Jasco company, located in Oklahoma, USA at an excitation wavelength of 360 nm. Standard calibration curves, prepared from Gly-S-CNDs synthesized in Objective 1, were used for quantification. UV-Vis spectrophotometry (Lambda 35, PerkinElmer, USA) was performed to confirm characteristic absorbance features of CNDs. For selected samples, CND morphology and size distribution were characterized using TEM (JEM-2000FXII) produced by JEOL Ltd. In Tokyo, Japan.

To understand the formation mechanisms, the concentration of CNDs was compared across different food matrices and processing conditions (e.g., roasting, baking, brewing). Differences in CND levels among bread crust, bread crumb, and dough were used to assess the influence of direct heat exposure. Similar comparisons were made across

beverages, black foods, and roasted cereals to correlate thermal treatments with CND generation.

3.3.2. Understanding Formation Mechanisms in Food Products: Case study of coffee brewing

3.3.2.1. Materials

Three varieties of roasted coffee beans were selected to study the formation of CNDs in liquid systems: (1) 100% Arabica (*Coffea arabica* L.) purchased from ALDI supermarket (Essen, Germany), roasted at level 8/10 and originating from Peru; (2) 100% Robusta (*Coffea canephora* L.) roasted at level 8/10 and sourced from Laviet Coffee factory (Da Lat, Vietnam); and (3) a 50:50 blend of Arabica and Robusta from the same supplier. All samples were analyzed within one month of purchase. Ultrapure water (18.2 MΩ·cm), ethanol (≥ 99.5%), hydrochloric acid (0.01 M), sodium hydroxide (0.01 M), and HPLC-grade acetonitrile (≥ 99.5%) were supplied by VWR International Ltd. (Pennsylvania, USA).

3.3.2.2. Methods

The extraction of carbon nanodots from coffee brews (C-CNDs) followed a procedure adapted from Nguyen et al. (2024) with modifications. Coffee beans were ground using a Timemore Chestnut C2 grinder (fine: 0.3 mm, medium: 0.7 mm, coarse: 1.1 mm). A standard brewing protocol was applied using 100% Arabica coffee beans ground to medium size (0.7 mm). Briefly, 10 g of ground coffee was brewed with 150 mL of deionized water at 100 °C for 180 s using a V60 coffee dripper (HARIO Co., Ltd., Japan) and 0.45 μm filter paper. To isolate C-CNDs, the coffee brews were precipitated with cold ethanol (96%, 1:1 v/v), centrifuged at 4032 × g for 15 min, and further purified using a macroporous cellulose column followed by filtration through a 0.22 μm syringe filter. The purified extracts were subsequently lyophilized, and the resulting solids were used for morphological and particle size analysis by transmission electron microscopy (TEM). Four experiments were conducted to investigate the formation of C-CNDs: (1) effect of coffee bean type (Arabica, Robusta, and Arabica–Robusta blend), (2) effect of grinding size, (3) effect of sample-to-water ratio, and (4) effect of brewing conditions (time and temperature). Experiments (2)–(4) were performed using 100% Arabica coffee beans to isolate the influence of individual brewing parameters, while the effect of bean type was evaluated separately. **Figure 12** illustrates the experimental workflow to understand the formation of C-CNDs. First, after detecting C-CNDs in coffee brews, C-CNDs was

characterized with TEM, UV-Vis, and fluorescence spectroscopy (**Figure 12A**). Then, four experiments were established to further understand the formation of C-CNDs including (1) effect of types of coffee beans, (2) effect of grinding size, (3) effect of sample-to-water ratio, and (4) effect of brewing conditions (**Figure 12B**). Finally, the correlation between the formation of C-CNDs and other compositions were studied (**Figure 12C**).

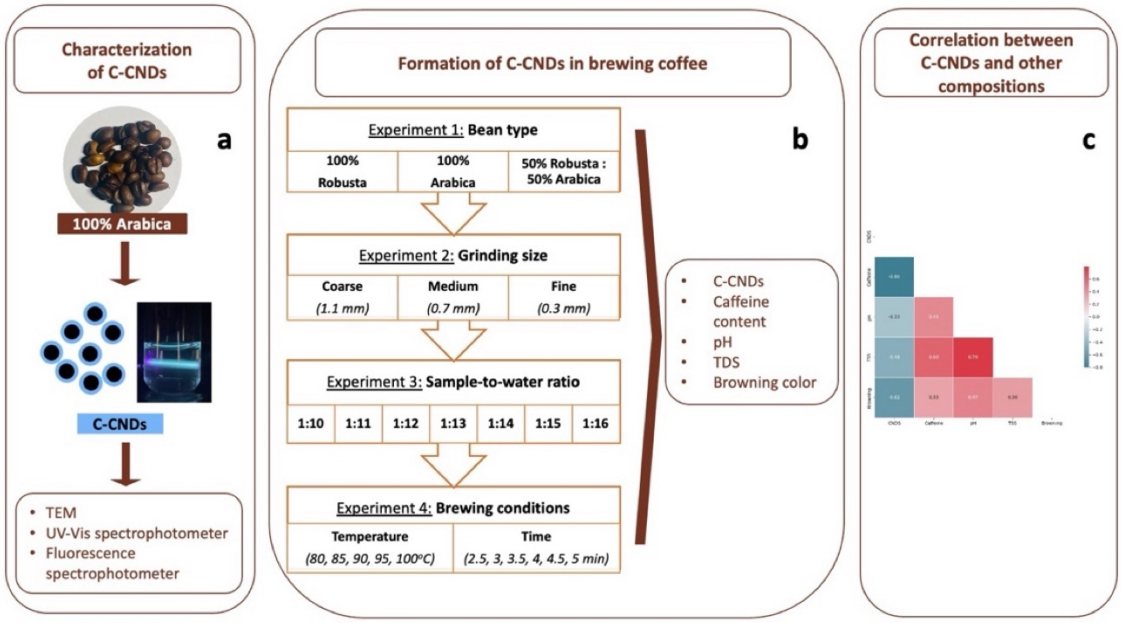


Figure 12. Experimental workflow illustrating coffee-derived carbon nanodots (C-CNDs) formation in coffee: (a) isolation and characterization (TEM, fluorescence, UV–Vis); (b) four experiments to understand C-CNDs formation in coffee brews including (1) types of coffee beans, (2) grinding size, (3) coffee: water, and (4) coffee making conditions; (c) correlation analyses with coffee constituents (D. Nguyen, Muthu, El-Ramady, Béni, et al., 2024).

3.4. Objective 4: Applications of CNDs in food industry (addessing RQ6 - RQ8)

3.4.1. Develop rapid method to detect caffeine in beverages using CNDs.

3.4.1.1. Material

Roasted *Coffea arabica* L. beans (Peru origin; roast level 8/10) were purchased from ALDI (Essen, Germany). Commercial energy drinks were obtained from HELL ENERGY Magyarország Ltd. (Szikszó, Hungary), XIXO Company Ltd. (Szentkirályszabadja, Hungary), and Hansen Natural Company (Corona, CA, USA). Tea beverages included green tea (Taiwan), black tea (Taiwan), and oolong tea (Vietnam), all purchased as commercial products. In addition, an adulterated sample (sample 7) was prepared as a "fake coffee" mixture containing burnt corn (Vietnam).

Ultrapure water was used in all experiments. Analytical-grade caffeine standard was supplied by Sigma-Aldrich (St. Louis, MO, USA). Potential interfering substances used for selectivity evaluation included glucose, fructose, ascorbic acid, citric acid, benzoic acid (E210), acrylamide, 5-hydroxymethylfurfural (5-HMF), and inorganic salts (NaCl, KCl, $CaCl_2$, $MgCl_2$), all purchased from VWR International (Radnor, PA, USA).

3.4.1.2. Method

The experimental workflow for developing and validating a Gly-S-CND–based fluorescence assay for caffeine detection is illustrated in **Figure 13** and summarized as follows:

(1) Preparation of Gly-S-CNDs (fluorescent probe): Glycine–sucrose–derived carbon nanodots (Gly-S-CNDs), synthesized under Objective 1 of this dissertation, were used as fluorescent probes. Glycine and sucrose were mixed at a 4:1 (w/w) ratio and subjected to a Maillard reaction via thermal treatment at 180 °C for 2 h in a closed system. The resulting solid products were ground, dispersed in ultrapure water, purified, lyophilized, and stored for subsequent measurements.

(2) Establishment of fluorescence sensing conditions: Fluorescence measurements were performed using an excitation wavelength of 360 nm, and emission spectra were recorded in the range of 400–600 nm. The fluorescence response of Gly-S-CNDs was measured in the absence and presence of caffeine to confirm signal enhancement.

(3) Selectivity (interference) evaluation: To assess selectivity, Gly-S-CNDs were incubated with caffeine and with individual potential interferents commonly present in beverages. Tested interferents included glucose, fructose, ascorbic acid, citric acid,

benzoic acid (E210), acrylamide, 5-HMF, Na^+, K^+, Ca^{2+}, and Mg^{2+}, each at a final concentration of 500 µM. Relative fluorescence intensity (I/I_0) was calculated to evaluate interference effects.

(**4) Calibration and analytical performance**: Calibration curves were constructed using caffeine standards over the concentration range of 0–2060 nM (triplicate). Linearity was assessed, and LOD/LOQ values were calculated. Precision and accuracy were evaluated by recovery tests using spiked beverage samples.

(5) Reference validation using HPLC: Caffeine quantification was independently performed using high-performance liquid chromatography (HPLC) following ISO 20481:2008. An ECS05 gradient HPLC system (ECOM, Prague, Czech Republic) equipped with a UV–Vis PDA detector (ECDA2800) and a Nucleosil C18 column (150 × 4.6 mm, 5 µm) was used. Separation was conducted at 25 °C using a 90:10 (v/v) acetonitrile/0.01 M phosphate buffer (pH 6.4) mobile phase at 2 mL min^{-1} for 8 min. Caffeine was detected at 272 nm and eluted between 5.3 and 5.6 min. Fluorescence-based caffeine results were compared against HPLC values to validate the rapid method.

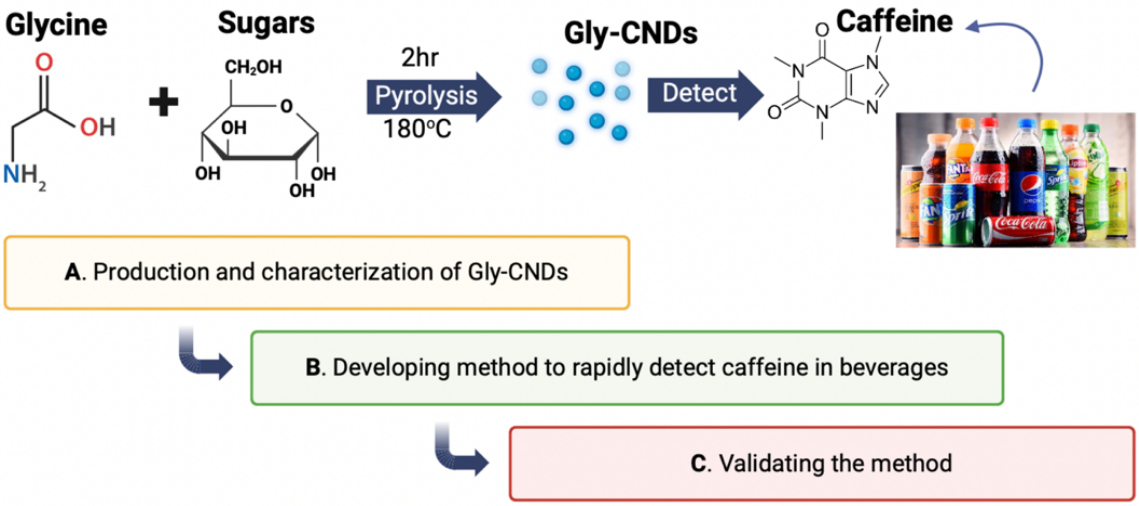


Figure 13. Three-stage design for Gly-S-CND enabled caffeine measurement. (A) Gly-S-CNDs production and characterization; (B) rapid detection method tailored to beverage and food samples; (C) validation of analytical performance.

3.4.2. Sustainable valorization of food waste into CNDs

3.4.2.1. Screening of Food Waste Precursors for CND Production

3.4.2.1.1. Material

Food waste samples were grouped into six compositional categories and used as carbon precursors for CND synthesis: (1) Polyphenol-rich wastes: extracted black tea leaves,

extracted green tea leaves, extracted oolong tea leaves, extracted coffee grounds, onion skins; (2) Mineral-rich wastes: eggshells; (3) Protein-rich wastes: leftover cheese; (4) Acid-rich wastes: lemon peels; (5) Lipid-rich wastes: used cooking oil; (6) Fiber-rich wastes: banana peels. All solid food wastes were collected from local food-processing or household sources in Hungary. Each waste type was collected from three independent batches (n = 3) to account for natural variability. Solid samples were washed thoroughly with distilled water, freeze-dried, and ground into fine powders prior to use. Liquid waste (used oil) was filtered to remove suspended solids.

3.4.2.1.2. Method

The overall workflow, from pyrolysis to purification and characterization, is outlined in **Figure 14**. Food waste powders (or filtered oil residues) were subjected to pyrolysis at 200 °C for 2 h. Where applicable, citric acid or sucrose was added prior to pyrolysis at a fixed mass ratio of waste:additive = 1:1 (w/w). After pyrolysis, the carbonized solids were dispersed in ultrapure water and sonicated for 30 min. Large, undissolved particles were removed by filtration through a 0.22 µm membrane filter. The resulting CNDs-containing solution was further purified using HPLC-SEC-FD to isolate the nanoparticle fraction. To obtain solid CNDs, the purified fractions were freeze-dried (lyophilized), yielding dry CND powders for storage and further characterization.

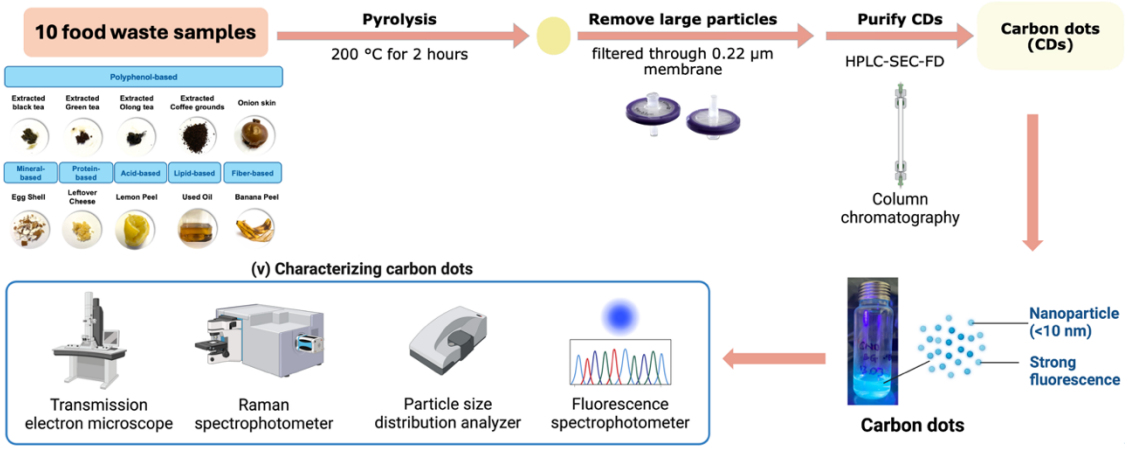


Figure 14. Workflow for synthesizing carbon nanodots (CNDs) from food waste via pyrolysis and subsequent purification and characterization steps.

3.4.2.2. Valorization of food wastes to produce CNDs: CCD and ML approach

3.4.2.2.1. Material

Fresh banana peels were collected from Dr. Aliment Company (Debrecen, Hungary), thoroughly washed with distilled water, freeze-dried, and ground into a fine powder for use as the carbon source.

3.4.2.2.2. Method

The experimental workflow for producing banana-peel-derived carbon nanodots (BP-CNDs) is summarized in **Figure 15** and consisted of three sequential stages.

Stage 1: Precursor screening (**Figure 15(1)**).

Lyophilized banana peel (BP) powder was mixed with four different precursors—urea, citric acid, glycine, and sugars—at predefined mass ratios (w/w). Each mixture was subjected to thermal treatment to induce carbonization and CNDs formation. After pyrolysis, the resulting carbonized solids were dispersed in ultrapure water, filtered to remove large insoluble residues, and the fluorescence intensity of the resulting CNDs suspensions was measured. The precursor yielding the highest fluorescence intensity of BP-CNDs was selected for further optimization studies.

Stage 2: Optimization using central composite design (CCD) (**Figure 15(2)**).

Based on the precursor screening results, urea was selected as the optimal additive for BP-CNDs synthesis. A central composite design (CCD) was then constructed to optimize the synthesis conditions. Three independent variables were investigated: (A) mass ratio between banana peel and urea (w/w), (B) pyrolysis time (h), and (C) pyrolysis temperature (°C). Each factor was evaluated at three coded levels (−1, 0, +1), as shown in **Table 3**.

Table 3. Independent variables and their coded levels used in CCD for optimizing BP-CNDs synthesis.

	Factor	-1	0	+1
A	Mass ratio between BP and Precursor (w/w)	4:1	4:2	4:3
B	Pyrolysis time (h)	1	2	3
C	Pyrolysis temperature (°C)	160	180	200

The CCD matrix consisted of factorial, axial, and center points, allowing the estimation of both linear and quadratic effects, as well as interaction terms. This design enabled an

efficient exploration of the synthesis space using a minimal number of experimental runs. The full experimental matrix with coded and actual levels for each condition is presented in **Table 4.**

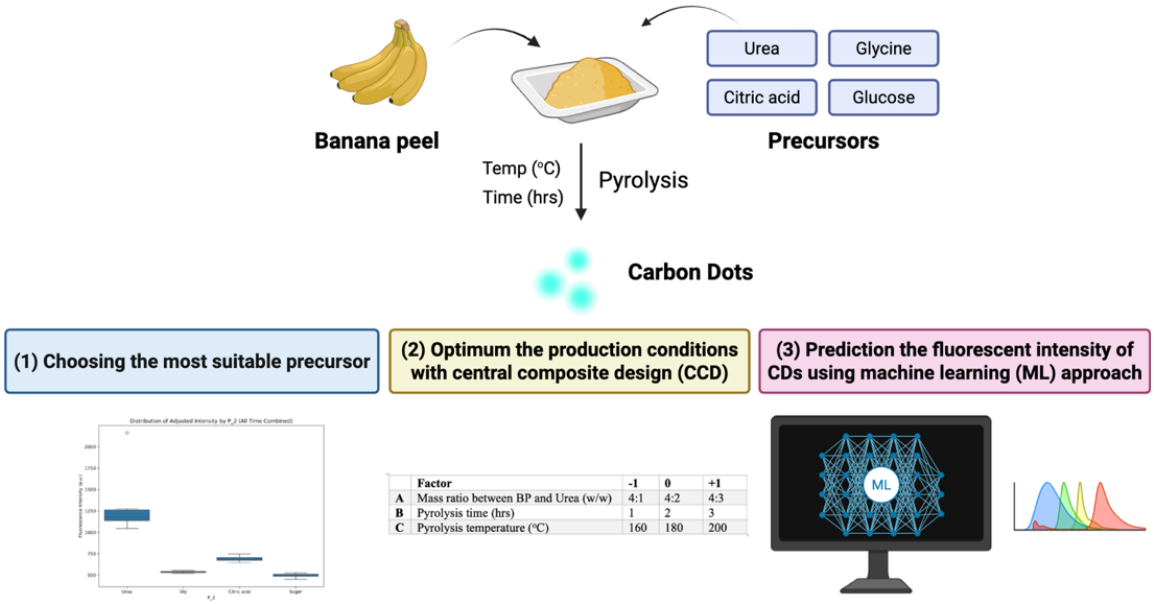
Table 4. Experimental CCD matrix for optimization of BP-CNDs synthesis.

Run	A_coded	B_coded	C_coded	Ratio (A)	Time (B)	Temp (C)
1	−1	−1	−1	4:1	1	160
2	−1	−1	0	4:1	1	180
3	−1	−1	+1	4:1	1	200
4	−1	0	−1	4:1	2	160
5	−1	0	0	4:1	2	180
6	−1	0	+1	4:1	2	200
7	−1	+1	−1	4:1	3	160
8	−1	+1	0	4:1	3	180
9	−1	+1	+1	4:1	3	200
10	0	−1	−1	4:2	1	160
11	0	−1	0	4:2	1	180
12	0	−1	+1	4:2	1	200
13	0	0	−1	4:2	2	160
14	0	0	0	4:2	2	180
15	0	0	+1	4:2	2	200
16	0	+1	−1	4:2	3	160
17	0	+1	0	4:2	3	180
18	0	+1	+1	4:2	3	200
19	+1	−1	−1	4:3	1	160
20	+1	−1	0	4:3	1	180
21	+1	−1	+1	4:3	1	200
22	+1	0	−1	4:3	2	160
23	+1	0	0	4:3	2	180
24	+1	0	+1	4:3	2	200
25	+1	+1	−1	4:3	3	160
26	+1	+1	0	4:3	3	180
27	+1	+1	+1	4:3	3	200

For each CCD run, BP–urea mixtures were pyrolyzed under the specified conditions. After cooling, the carbonized products were dispersed in ultrapure water, filtered to remove undissolved particles, and the fluorescence intensity of the obtained BP-CND solutions was recorded.

Stage 3: Machine learning (ML) modeling (Figure 15(3)).

All experimental data obtained from the CCD experiments were used to develop predictive machine-learning models for BP-CND fluorescence intensity. The dataset was split into training and testing sets using an 80:20 ratio. Seven ML algorithms—Random Forest, Support Vector Regression, Artificial Neural Networks (ANN), Gradient Boosting, Decision Tree, Linear Regression, and K-Nearest Neighbors Regression—were evaluated. Model performance was assessed using the coefficient of determination (R^2) and root mean square error (RMSE). The best-performing model was subsequently used to predict fluorescence intensity based on synthesis parameters, enabling data-driven optimization of BP-CND production.



	Factor	-1	0	+1
A	Mass ratio between BP and Urea (w/w)	4:1	4:2	4:3
B	Pyrolysis time (hrs)	1	2	3
C	Pyrolysis temperature (°C)	160	180	200

Figure 15. Schematic diagram of a 3-stage experimental design to optimize the production conditions of carbon nanodots from banana peel (BP-CNDs) using central composite design (CCD) and machine learning (ML) approach.

3.5. Analytical methods to study the properties of CNDs in foods.

3.5.1. Fluorescence Spectroscopy

The fluorescence properties of CNDs were evaluated using a FP-8500 fluorescence spectrophotometer (Jasco Co., Oklahoma, USA) in three replicates (D. Nguyen, Muthu, El-Ramady, Daróczi, et al., 2024). Excitation-emission matrices were recorded with excitation wavelengths ranging from 300 to 700 nm, and emission spectra were scanned between 300 and 700 nm. Fluorescence intensity values were compared across samples to assess quantum yield and determine optimal synthesis conditions. All spectra were corrected against the blank and normalized for inter-sample comparison.

3.5.2. UV-Visible Spectroscopy

UV-Vis absorption spectra were measured using a Lambda 35 spectrophotometer (PerkinElmer, Norwalk, USA). CNDs samples were diluted in ultrapure water and scanned over a wavelength range of 200 to 800 nm (Mintz et al., 2021). Absorbance peaks around 280–360 nm were recorded to indicate π–π* transitions of C=C bonds and n–π* transitions of C=O groups, which are typical of graphitic carbon structures. Measurements were performed in triplicate and spectra were baseline-corrected.

3.5.3. Transmission Electron Microscopy (TEM)

The morphology and particle size distribution of synthesized CNDs were examined using a transmission electron microscope (JEM-2000FXII model, JEOL Ltd., Tokyo, Japan) (Mintz et al., 2021). A drop of the CNDs solution was deposited onto a carbon-coated copper grid and dried under vacuum before imaging. TEM micrographs were taken at an accelerating voltage of 200 kV, and particle sizes were manually measured using ImageJ software from at least 100 individual particles per sample.

3.5.4. X-ray Diffraction (XRD)

The crystallographic structure of lyophilized CNDs powders was analyzed by X-ray diffraction (XRD) (Mintz et al., 2021). Diffractograms were obtained using a standard Cu-Kα radiation source (λ = 1.5406 Å), scanned from 5° to 80° (2θ) at a step size of 0.02°. The broad diffraction peak around 20–30° was used to confirm the amorphous or semi-crystalline nature of CNDs. Data interpretation focused on identifying structural disorder or graphitic domains.

3.5.5. Raman Spectroscopy

Raman spectra were recorded to evaluate the graphitic quality and defect density of the CNDs (Mintz et al., 2021). Measurements were carried out using a Raman spectrometer with a 532 nm excitation laser. The D-band (~1350 cm^{-1}) and G-band (~1580 cm^{-1}) were quantified, and the intensity ratio (I_D/I_G) was calculated to assess the degree of structural defects or disorder within the CNDs. Spectra were averaged from three replicates per sample.

3.5.6. Fourier-Transform Infrared Spectroscopy (FTIR)

Surface functional groups were analyzed using an Agilent 4300 Handheld FTIR with the diamond ATR module (Mintz et al., 2021). Lyophilized CNDs were gently pressed onto the ATR crystal (no further preparation). Spectra were collected from 4000–650 cm^{-1} at 4 cm^{-1} resolution with 32 co-added scans per sample, using an air background and automatic baseline correction.

3.5.7. Elemental (C/N) analysis and carbon quantification.

Bulk composition was determined on lyophilized CNDs using a elemental analyzer Primacs SNC 100. Samples (2–5 mg) were dried at 60 °C overnight, weighed into tin capsules, combusted in oxygen (≈1050–1100 °C), and the resulting gases were quantified against acetanilide standards; results are reported as %C and %N (mean ± SD, n = 3). For aqueous stock solutions used as fluorescence standards, total carbon was measured on the same instrument by drying known aliquots onto pre-weighed quartz boats (or by TOC when applicable), enabling calculation of CND concentration (mg dm^{-3}) for calibration and recovery studies.

3.5.8. High-Performance Liquid Chromatography with Fluorescence Detection (HPLC-SEC-FD)

HPLC-SEC-FD was employed to separate and quantify CNDs in complex food matrices. The system consisted of a size exclusion chromatography column coupled with a fluorescence detector (excitation: 380 nm; emission: 460 nm). Samples were filtered (0.22 μm) and injected in triplicate. Retention times and peak areas were used to confirm the presence and concentration of fluorescent CNDs. Calibration curves were constructed using standard solutions of known CND concentrations.

3.5.9. High-Performance Liquid Chromatography for the determination of caffeine

Using ISO 20481:2008 as the reference HPLC procedure (ISO 20481:2008, 2017), caffeine was quantified on an ECS05 gradient system with an ECDA2800 UV–Vis PDA

detector (ECOM, Praha). The analytical column was Nucleosil C18, 100 Å, 5 µm, 150 × 4.6 mm (Phenomenex, California). Conditions: 25 ± 2 °C; mobile phase = 0.01 M phosphate buffer (pH 6.4)/acetonitrile 90:10 (v/v); flow 2.0 mL min^{-1}; 8 min runtime; caffeine RT 5.3–5.6 min. A Sigma-Aldrich caffeine standard was used for calibration.

3.5.10. Quantum yield determination

The photoluminescence quantum yield (QY) of the carbon nanodots was obtained by the comparative method using quinine sulfate as the reference (Φr = 0.54 in 0.1 M H_2SO_4). Sample and reference solutions were prepared to give absorbance < 0.1 at the excitation wavelength (typically 360 nm) to minimize inner-filter effects. Emission spectra were collected on a fluorescence spectrophotometer under identical settings.

The QY of the sample (Φs) was calculated as:

$$\Phi_s = \Phi_r \left(\frac{I_s}{I_r}\right) \left(\frac{A_r}{A_s}\right) \left(\frac{n_s^2}{n_r^2}\right)$$

where I is the integrated emission intensity, A is the absorbance at the excitation wavelength, and n is the refractive index of the solvent (subscripts s and r denote sample and reference, respectively). All measurements were conducted at room temperature, with each experiment repeated in triplicate to ensure reproducibility.

3.5.11. Other methods

pH was measured using an FE30 pH meter (Mettler-Toledo, Schwerzenbach, Switzerland). Browning color development was assessed at 420 nm on a Lambda 35 UV–Vis spectrophotometer (Norwalk, USA) after 10-fold dilution with distilled water, following (Meydav et al., 1977). All measurements were performed in triplicate.

3.6. Statistical analysis

Statistical analyses were performed in IBM SPSS Statistics 25. TEM micrographs and particle-size distributions were processed in ImageJ 1.54d. Data handling and modeling combined Python 3.9 (NumPy, pandas, matplotlib, seaborn, scikit-learn), Microsoft Excel (Microsoft 365), and GraphPad Prism 9. Prism was used for hypothesis testing (e.g., ANOVA) and contour plotting, while Excel supported initial cleaning, matrix construction, and response-surface setup. Visualizations-including emission spectra, correlation heatmaps, model-fit curves, and feature-importance plots-were produced across Python and Prism to ensure a consistent style. Statistical significance was defined as $p < 0.05$.

4. RESULTS AND DISCUSSION

4.1. Results related to Objective 1: Synthesis and characterization of carbon nanodots (CNDs) using Maillard reaction model (addessing RQ1 – RQ3)

4.1.1. Synthesis of green carbon nanodots (CNDs) using the Maillard reaction model

4.1.1.1. The effect of different amino acids on the formation of CNDs.

The Maillard reaction is a well-known non-enzymatic reaction between amino acids and reducing sugars that leads to the formation of diverse compounds contributing to color, flavor, and aroma in thermally processed foods (Saltmarch & Labuza, 1982). Recently, carbon nanodots (CNDs) have been identified as one of the novel products of this reaction (Matiacevich & Pilarbuera, 2006). Aiming to synthesize green CNDs from safe and food-compatible sources, the Maillard reaction was selected as a model system using sucrose and various amino acids. Six amino acids (tyrosine, proline, glycine, arginine, glutamine, and phenylalanine) were used in this experiment. As shown in **Figure 16A**, each amino acid–sucrose combination produced CNDs with distinct fluorescence emission spectra, with excitation wavelengths set at 340 nm for tyrosine, 360 nm for proline and glycine, and 380 nm for the remaining amino acids.

Among the tested precursors, glycine-based CNDs (Gly-CNDs) yielded the highest fluorescence intensity, followed by phenylalanine and proline. This is likely due to glycine's small, non-aromatic structure and high reactivity in forming Schiff bases-key intermediates in the Maillard pathway that subsequently contribute to fluorescent melanoidins and carbon core structures (D. Li, Xie, et al., 2019).

The variation in fluorescence output can be attributed to the molecular structure of the amino acids. Aromatic amino acids like tyrosine and phenylalanine are inherently fluorescent (Alexander Ross et al., 2002), whereas non-aromatic amino acids such as glycine and arginine rely more on Maillard-driven transformations. Despite phenylalanine exhibiting higher native fluorescence (724.0 ± 4.0 a.u.), the synthesized Gly-CNDs surpassed Phe- CNDs in final intensity (2024.0 ± 3.7 a.u. vs. 1900.0 ± 9.1 a.u.), as shown in **Figure 16B**. These results suggest that glycine, due to its simple structure and strong reactivity, is an optimal precursor for producing high-fluorescence CNDs.

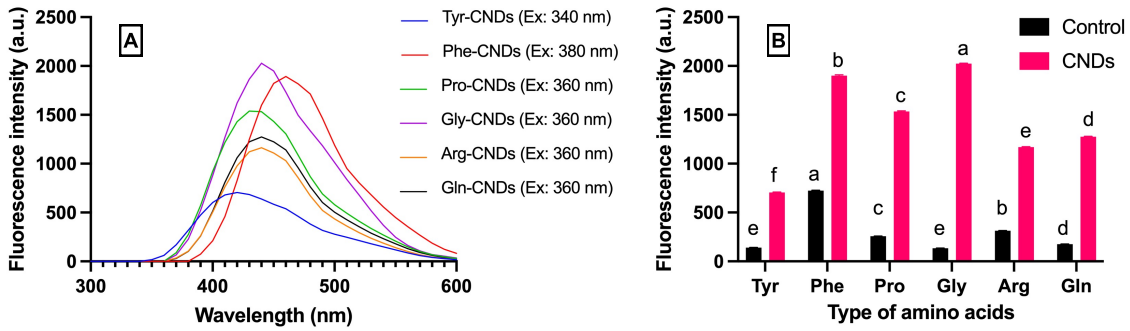


Figure 16. **A**. Fluorescence emission spectra of CNDs synthesized from sucrose and various amino acids: tyrosine (Tyr), proline (Pro), glycine (Gly), arginine (Arg), glutamine (Gln), and phenylalanine (Phe). Excitation wavelengths were adjusted per amino acid: 340 nm for Tyr, 360 nm for Pro and Gly, and 380 nm for Arg, Gln, and Phe. **B**. Fluorescence intensity of amino acid-based CNDs compared with native amino acids. Error bars represent standard deviation (n = 3); different letters indicate significant differences at $p < 0.05$ (Duncan's test) (D. Nguyen, Muthu, El-Ramady, Daróczi, et al., 2024).

4.1.1.2. Effect of the ratio between glycine and sugars (mmol/ mmol) on the formation of CNDs.

Following the identification of glycine as the optimal amino acid precursor, the excitation wavelength of 360 nm was employed to further study CNDs synthesis. Fluorescence emission spectra revealed that increasing the glycine-to-sucrose molar ratio led to enhanced CND fluorescence, with the highest intensity observed at a 1:1 (mmol:mmol) ratio (**Figure 17A**). This enhancement is likely linked to the efficient formation of Schiff base intermediates, which play a critical role in CNDs development. However, surpassing this ratio with excess glycine resulted in a notable decline in fluorescence. The reduced intensity at higher glycine levels suggests that surplus amino acid may disrupt Schiff base formation, thereby inhibiting effective carbonization. These results highlight the importance of precursor balance in optimizing fluorescence output and suggest that modulating precursor ratios may serve as a useful strategy to tailor CND properties for specific applications.

4.1.1.3. Effect of extraction solvents on the formation of CNDs

Extraction solvent type and pH were also found to significantly affect the yield and fluorescence intensity of CNDs (**Figure 17B**). Among aqueous solvents, deionized water adjusted to pH 9.0 produced the most intense fluorescence, while acidic conditions (pH

2.0) markedly suppressed CNDs formation. These findings are consistent with reports indicating that solvent pH can alter the surface charge and stability of carbon nanodots, thus influencing their optical behavior (Bai et al., 2019).

Moreover, ethanol was evaluated at varying concentrations. The highest fluorescence was observed with 40% ethanol, whereas further increases to 60%, 80%, and absolute ethanol resulted in reduced fluorescence intensity. Shen and Wu (2004) previously reported that ethanol facilitates Maillard reaction rates, which aligns with our findings at moderate concentrations (Shen & Wu, 2004). However, excessive ethanol may hinder Schiff base development, thereby compromising the carbonization process.

Together, these results demonstrate that CNDs synthesis via the Maillard reaction is highly sensitive to the extraction medium. Alkaline conditions and moderate ethanol concentrations promote Schiff base stability and enhance fluorescence output, providing a tunable approach to engineer CNDs with desirable optical properties for applications in sensing, imaging, and food analysis.

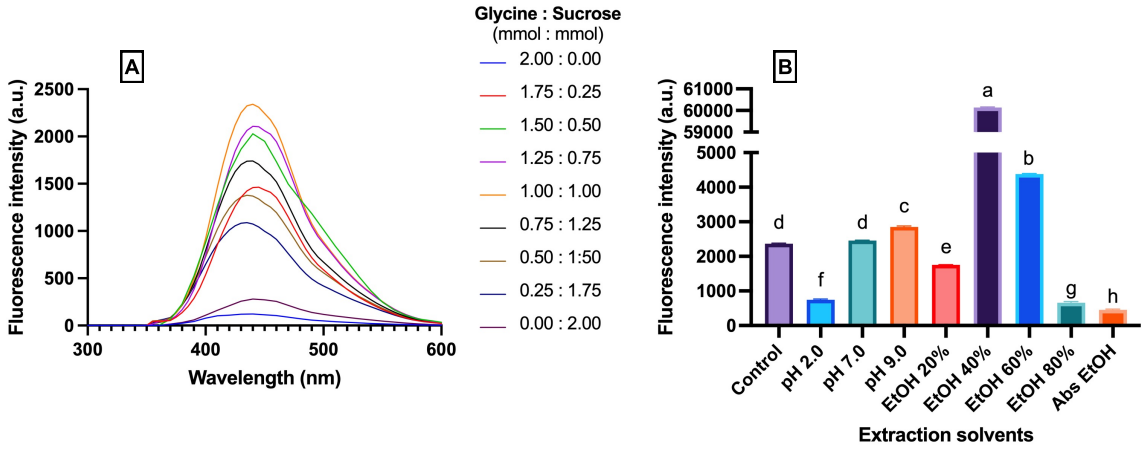


Figure 17. A. Fluorescence emission spectra of CNDs synthesized using different glycine-to-sucrose ratios (mmol/mmol), all measured at 360 nm excitation. The ratios tested included: 2:0, 1.75:0.25, 1.5:0.5, 1.25:0.75, 1:1, 0.75:1.25, 0.5:1.5, 0.25:1.75, and 0:2. **B**. Fluorescence intensity of CNDs extracted using solvents with varying pH (2.0, 7.0, 9.0) and ethanol concentrations (20% to 100%). The control was DI water at pH 6.0. Data represent mean ± SD (n = 3). Duncan letters indicate significant differences at $p < 0.05$ (D. Nguyen, Muthu, El-Ramady, Daróczi, et al., 2024).

4.1.2. Characterization of synthesized Carbon nanodots derived from glycine and sucrose (Gly-S-CNDs)

The structural and optical characteristics of Gly-S-CNDs were systematically analyzed and are presented in **Figure 18**. Transmission electron microscopy (TEM) confirmed successful synthesis, revealing predominantly spherical particles with uniform dispersion (**Figure 18A**). Size analysis indicated a narrow distribution centered at 4.2 ± 1.2 nm (**Figure 18B**), reflecting consistent nanoscale morphology.

Fluorescence spectra recorded across excitation wavelengths from 280 to 460 nm showed the strongest emission at 448 nm when excited at 360 nm (**Figure 18C**), consistent with earlier studies on CNDs from Maillard reactions (D. Li et al., 2018; D. Nguyen, Muthu, El-Ramady, Daróczi, et al., 2024). UV-Vis spectroscopy revealed a sharp absorption peak near 280 nm, attributed to π–π* transitions of aromatic sp^2 domains, along with a tail into the visible range, likely caused by surface defects and oxygen/nitrogen functionalities (D. Li et al., 2018; D. Nguyen, Muthu, El-Ramady, Daróczi, et al., 2024; H. Wang et al., 2020).

Raman analysis identified two characteristic peaks at ~1350 cm^{-1} (D-band) and ~1600 cm^{-1} (G-band), indicating a semi-graphitic structure typical of nitrogen-doped CNDs (W. Zhao et al., 2025). The relatively broad and weak bands suggest high surface functionalization, which may mask the graphitic core (**Figure 18D**).

X-ray diffraction (XRD) data (**Figure 18G**) showed a broad halo around 2θ = 25°, indicating an amorphous carbon structure with substantial disorder-typical of functionalized nanodots. Elemental composition analysis (**Figure 18E**) confirmed the presence of 33.1% carbon and 18.2% nitrogen, further supporting nitrogen incorporation into the CNDs structure.

Fourier-transform infrared spectroscopy (FTIR) was used to assess chemical transformation from glycine to CNDs (**Figure 18F**). Notable changes included enhanced peaks around 1600–1650 cm^{-1}, associated with aromatic C=C domains (X. Ma et al., 2025), and broader signals at 1500–1400 cm^{-1}, indicative of modified carboxyl groups (González-González et al., 2022). A strong peak at 1350 cm^{-1}, corresponding to CH/NH bending, likely reflects increased sp^2 carbon domains (Ferrari et al., 2003). Additional bands at 1100–1050 cm^{-1} and 900 cm^{-1} indicated C–N/C–O stretching and N–H/C–H wagging vibrations, respectively, confirming surface functionalization with nitrogen- or oxygen-containing groups (Groenewegen, 1972; Kolanowska et al., 2022; W. Zhao et al.,

2025). Minor shifts in the 700–800 cm^{-1} region suggest subtle structural rearrangements (W. Zhao et al., 2025).

High-performance liquid chromatography with size-exclusion and fluorescence detection (HPLC-SEC-FD) was used to validate the identity and purity of Gly-S-CNDs. The first fluorescence peak, corresponding to the nanodot fraction, was collected, lyophilized, and stored for subsequent use (Shafigulina et al., 2019) (**Figure 18H**).

4.1.3. Stability of synthesized Carbon nanodots derived from glycine and sucrose (Gly-S-CNDs)

The stability of Gly-S-CNDs was assessed under conditions relevant to food and biological applications. As shown in **Figure 19A**, Gly-S-CNDs maintained consistent fluorescence across a wide range of NaCl concentrations (0.1–1.0 M), indicating strong resistance to salt-induced aggregation-an essential feature for stability in physiological and food systems.

The fluorescence intensity of Gly-S-CNDs monitored in 60 minutes remains unchanged (**Figure 19B**), confirming good short-term stability. However, pH had a notable effect on fluorescence behavior (**Figure 19C–D**). Gly-S-CNDs showed the highest stability and fluorescence intensity at pH 4.0, while alkaline conditions led to a marked decline in emission, likely due to altered surface charge and disrupted functional groups. Despite this, the emission peak consistently remained around 440 nm across pH 4.0 to 11.0, suggesting structural resilience of the optical core.

Collectively, these results demonstrate that Gly-S-CNDs are stable under varying ionic strengths and timeframes, with optimal fluorescence preserved in mildly acidic environments. This makes them promising candidates for use in complex matrices such as food or biological fluids.

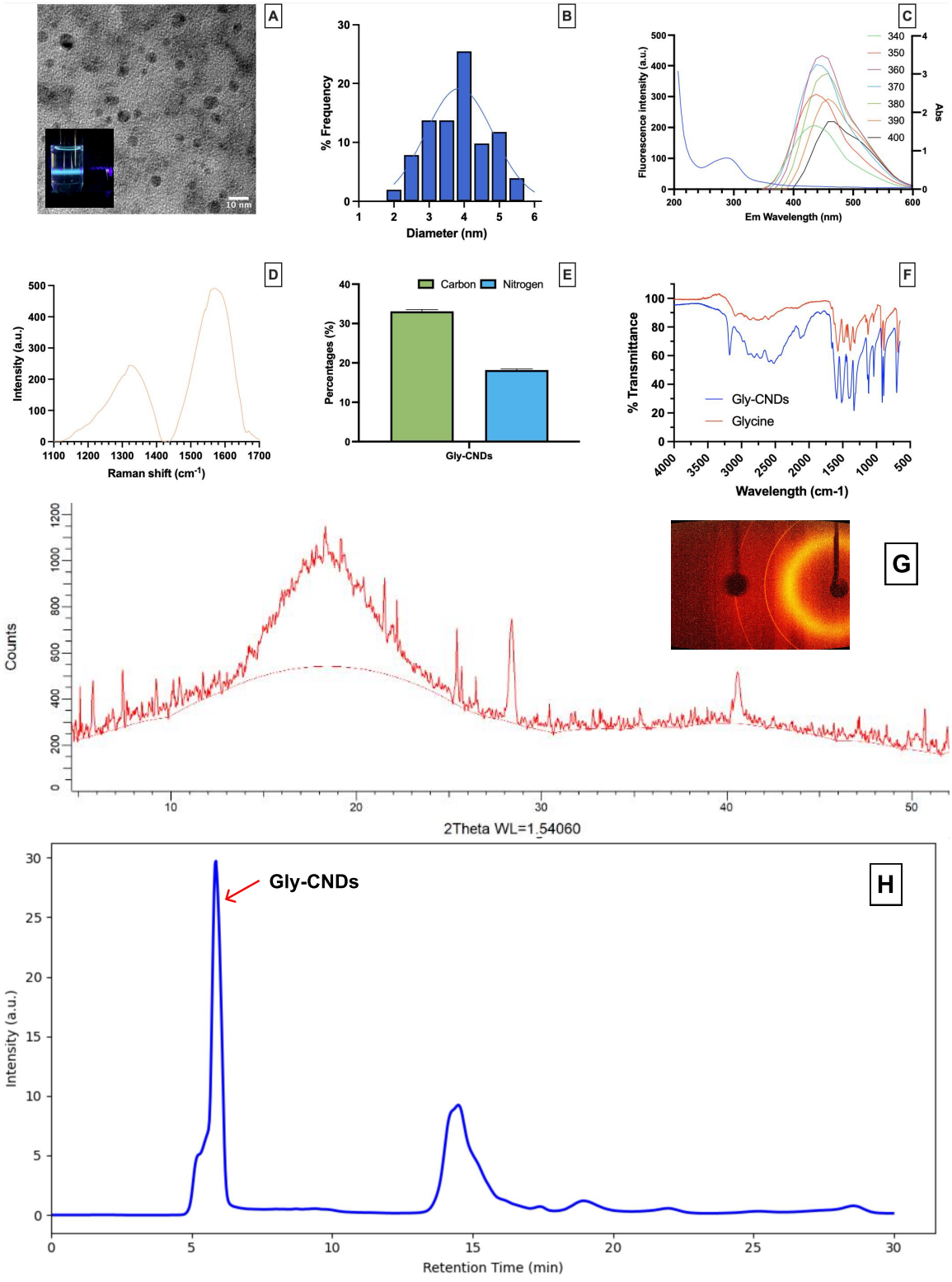


Figure 18. Characterization of carbon nanodots derived from glycine and sucrose (Gly-S-CNDs) including: **A**, TEM images with 10 nm scale. **B**, size distribution histogram with the average size at 4.2 ± 1.2 nm; **C**, the emission fluorescent spectra at different excitation wavelengths (right) and UV spectra with real sample under UV lamp (left). **D**, Raman

spectra. **E**, Carbon and nitrogen percentage. **F**, FTIR spectra of Gly-CNDs (blue line) and glycine (red line). **G**, X-ray diffraction (XRD) spectra. **H**, HPLC- SEC-FD chromatogram of isolated Gly-S-CNDs before the final purification (D. H. H. Nguyen, El-Ramady, & Prokisch, 2025).

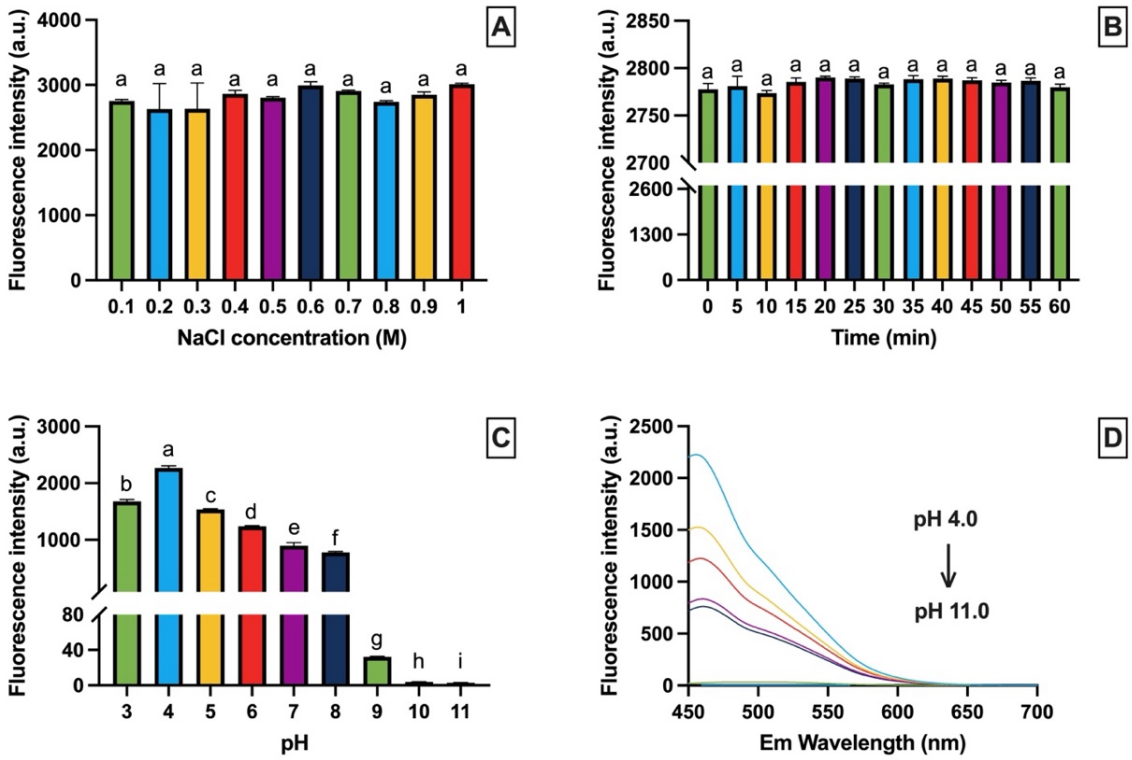


Figure 19. Stability of carbon nanodots derived from glycine and sucrose (Gly-S-CNDs) under different condition. **A**, Fluorescence intensity across varying NaCl concentrations (0.1–1.0 M). **B**, Temporal fluorescence stability over 60 minutes. **C**, Fluorescence behavior across a pH range of 4.0–11.0. **D**, Emission spectra of Gly-S-CNDs at 360 nm excitation under different pH conditions. Data represent means of triplicate measurements; different letters indicate statistically significant differences at $p < 0.05$. (D. H. H. Nguyen, El-Ramady, & Prokisch, 2025).

4.2. Results related to Objective 2: Development of methods to detect and quantify carbon nanodots (CNDs) in food matrices (addressing RQ3)

4.2.1. Quantitative measurement of CNDs using fluorescence spectroscopy

To establish a quantitative method for measuring carbon nanodots (CNDs) in food products, purified Gly-S-CNDs synthesized from the Maillard reaction were used as a standard, which synthesized from glycine and sugar in the ratio of 4:1 (w/w). The carbon content of the stock solution was determined using a Primacs SNC 100 elemental analyzer, resulting in a carbon concentration of 0.326%, equivalent to 3260 mg/kg. Calibration standards were freshly prepared and measured on the same day using a Jasco FP-8500 fluorescence spectrophotometer at an excitation wavelength of 360 nm. A five-point calibration curve was constructed in the range of 0 to 3200 mg/kg, demonstrating excellent linearity ($R^2 = 0.9995$) with the equation $y = 0.8441x + 6.61$ (**Figure 20**). The method showed high reproducibility (<0.1% RSD), with a detection limit (LOD) of 0.14 mg/kg and quantification limit (LOQ) of 0.47 mg/kg. After accounting for a 10-fold dilution in sample preparation, the effective LOD in solid food matrices was calculated as 1.4 mg/kg.

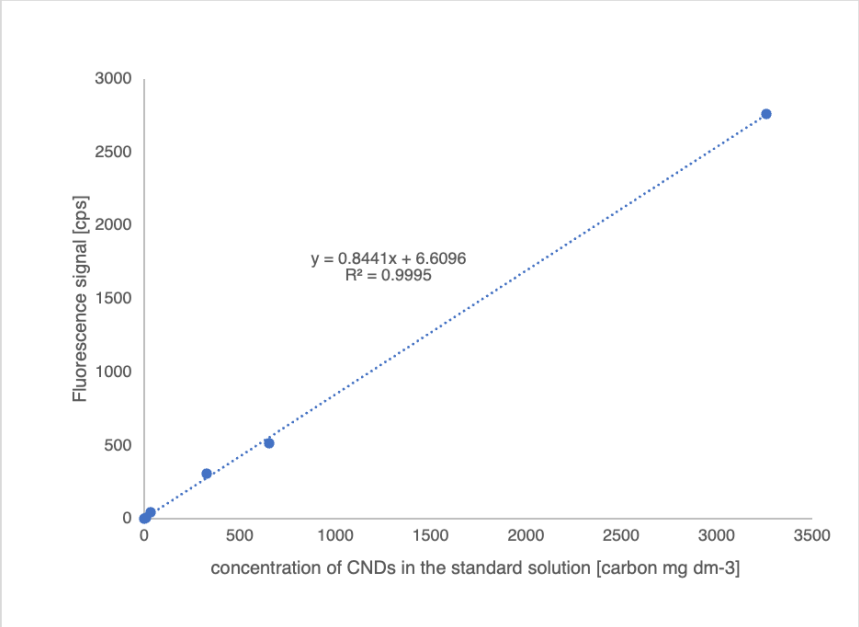


Figure 20. Calibration curve of carbon nanodots derived from glycine and sucrose (Gly-S-CNDs) standard solutions measured using the Jasco FP-8500 Spectrofluorometer in the range of 0 to 3200 mg dm^{-3}. Carbon content was determined using a certified elemental analyzer. Data represent mean values from triplicate measurements.

Method validation, including repeatability, inter-day precision, and accuracy, followed guidelines from AOAC International and the European Medicines Agency (AOAC International, 2016; ICH, 1995). Consistent results were also obtained using the standard addition approach, confirming the robustness of the method

Using this approach, CNDs concentrations in breadmaking samples were quantified (**Table 5**). After homogenization and sonication in distilled water, samples were treated with 40% ethanol (v/v), centrifuged, and filtered (0.22 µm) before fluorescence measurement. No CNDs were detected in dough, whereas significant amounts were found in baked components. The bread crust contained the highest concentration at 5120 ± 1 µg/kg DW, followed by the crumb at 3220 ± 4 µg/kg DW. These results support the hypothesis that thermal processing plays a critical role in CND formation, as previously reported (Sk et al., 2012b), with higher temperatures and direct heat exposure in the crust zone enhancing CND generation.

Table 5. Concentration of carbon nanodots (CNDs) in breadmaking samples measured by the fluorescent method.

Food Items	**CNDs concentration (µg/kg in DW)**
Dough	ND
Bread crumb	3220 ± 4^{a}
Bread crust	5120 ± 1^{b}

Values represent mean ± standard deviation. Different superscript letters indicate statistically significant differences ($p < 0.05$). ND: not detected

4.2.2. Quantitative Measurement of CNDs using high-performance liquid chromatography with size exclusion and fluorescence detection (HPLC-SEC-FD)

To quantify carbon nanodots (CNDs) in food matrices, a selective analytical method was developed using high-performance liquid chromatography with size exclusion and fluorescence detection (HPLC-SEC-FD).

Under identical conditions, four standards: Glycine-sucrose derived CNDs (Gly-S-CNDs), Glycine-citric acid derived CNDs (Gly-C-CNDs), Urea-citric acid derived CNDs (U-C-CNDs), Lysine-citric acid derived CNDs (Lys-C-CNDs) showed a dominant early peak at ~5–10 min in HPLC-SEC-FD chromatogram (**Figure 21**), consistent with nanoparticulate fractions. Based on the SEC column calibration, this elution window corresponds to an approximate molecular weight range of 200000 to 1000000 Da, which is consistent with the nanoscale size of CND aggregates or individual particles. Peak shape differed by precursor: Gly-S-CNDs gave a narrow, intense peak (tighter size distribution), whereas U-C-CNDs and Lys-C-CNDs were broader (greater polydispersity). Small late peaks likely reflect lower-molecular-weight fluorescent species.

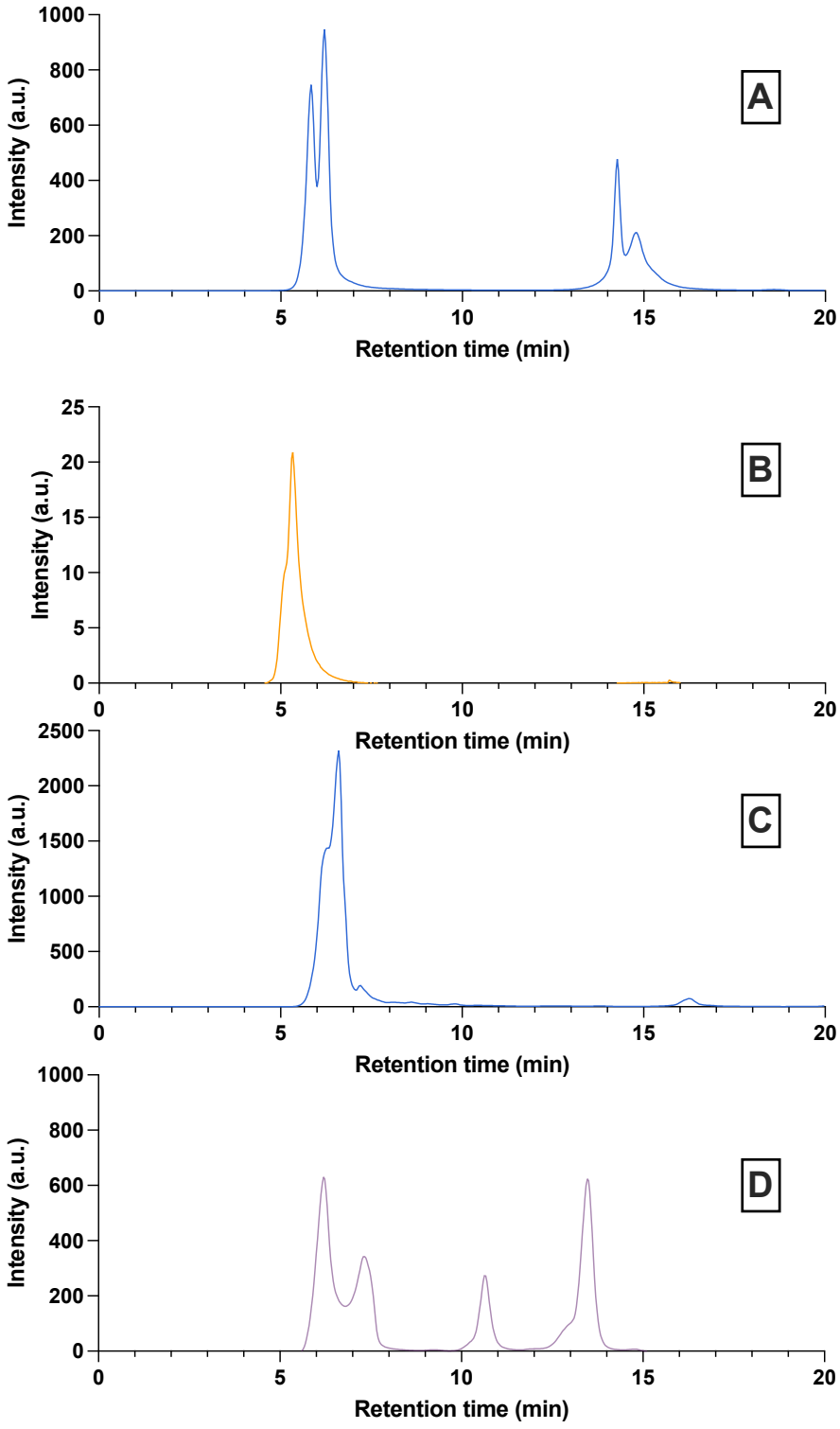


Figure 21. HPLC-SEC-FLD chromatograms of synthesized carbon nanodots (CNDs). Representative size exclusion chromatograms with fluorescence detection (Ex/Em: 380/460 nm) for: **(A)** glycine-sucrose derived CNDs (Gly-S-CNDs), **(B)** glycine-citric acid derived CNDs (Gly-C-CNDs), **(C)** urea-citric acid derived CNDs (U-C-CNDs), and **(D)** lysine-citric acid derived CNDs (Lys-C-CNDs).

4.2.2.1. Calibration curve and Method validation

For quantitative calibration, among the synthesized CNDs variants, glycine-sucrose carbon nanodots (Gly-S-CNDs) were chosen as the standard due to their stability, consistent size, and reliable fluorescence response. Gly-S-CNDs was synthesized from glycine and sucrose at the ratio of 4:1 (w/w). Fluorescence chromatograms of Gly-S-CNDs at concentrations ranging from 5 to 200 mg/L demonstrated consistent retention times and proportional increases in fluorescence intensity (**Figure 22A**). These results were used to construct a calibration curve, which showed excellent linearity across the tested range ($R^2 = 1$, **Figure 22B**). The method's sensitivity was evaluated using seven blank measurements. The limit of detection (LOD) was calculated as 0.068 mg/L, and the limit of quantification (LOQ) was 0.206 mg/L, indicating its capability for detecting low levels of CNDs in processed food samples.

Overall, this HPLC-SEC-FD approach offers a robust platform for precise CNDs quantification in food systems and holds potential for broader application in monitoring carbon-based nanomaterials.

The full HPLC-SEC-FLD workflow was reproduced at an external site (Lab B) using equivalent instrumentation. Overlaid chromatograms from both labs (**Figure 23**) showed closely matched elution profiles; small RT shifts were consistent with routine differences in system dead volume or column lot. For 6 and 12 mg/L standards, retention times and calculated concentrations (

Table 6) agreed well between laboratories, with RT variation < 0.5% and intra-lab %RSD < 4%. These outcomes demonstrate high precision, day-to-day stability, and straightforward portability for multi-center deployment, routine QC, and regulatory monitoring.

Table 6. Inter-laboratory Comparison of HPLC-SEC-FLD Method Performance

Gly-S-CNDs (mg/L)	Retention time, R_T (min)				CNDs (mg/L)			
	Lab A		Lab B		Lab A		Lab B	
	Mean	RSD (%)	Mean	RSD (%)	Mean	RSD (%)	Mean	RSD (%)
6	5.32 ± 0.02^{b}	0.36	6.81 ± 0.02^{a}	0.28	6.16 ± 0.24^{A}	3.9	6.4 ± 0.23^{A}	3.56
12	5.32 ± 0.02^{b}	0.36	6.8 ± 0.03^{a}	0.49	11.98 ± 0.23^{B}	1.91	12.21 ± 0.23^{B}	1.91

Values are expressed as mean ± standard deviation (n = 3). RSD: relative standard deviation. Superscript letters a, b within the same row denotes statistically significant differences in retention time between laboratories ($p < 0.001$). Superscript capital letters A, B indicate statistically significant differences in CND concentrations across spiking levels ($p < 0.001$, one-way ANOVA with Tukey's post hoc test). No significant differences were observed between laboratories for CND concentrations at the same spiking level ($p > 0.001$).

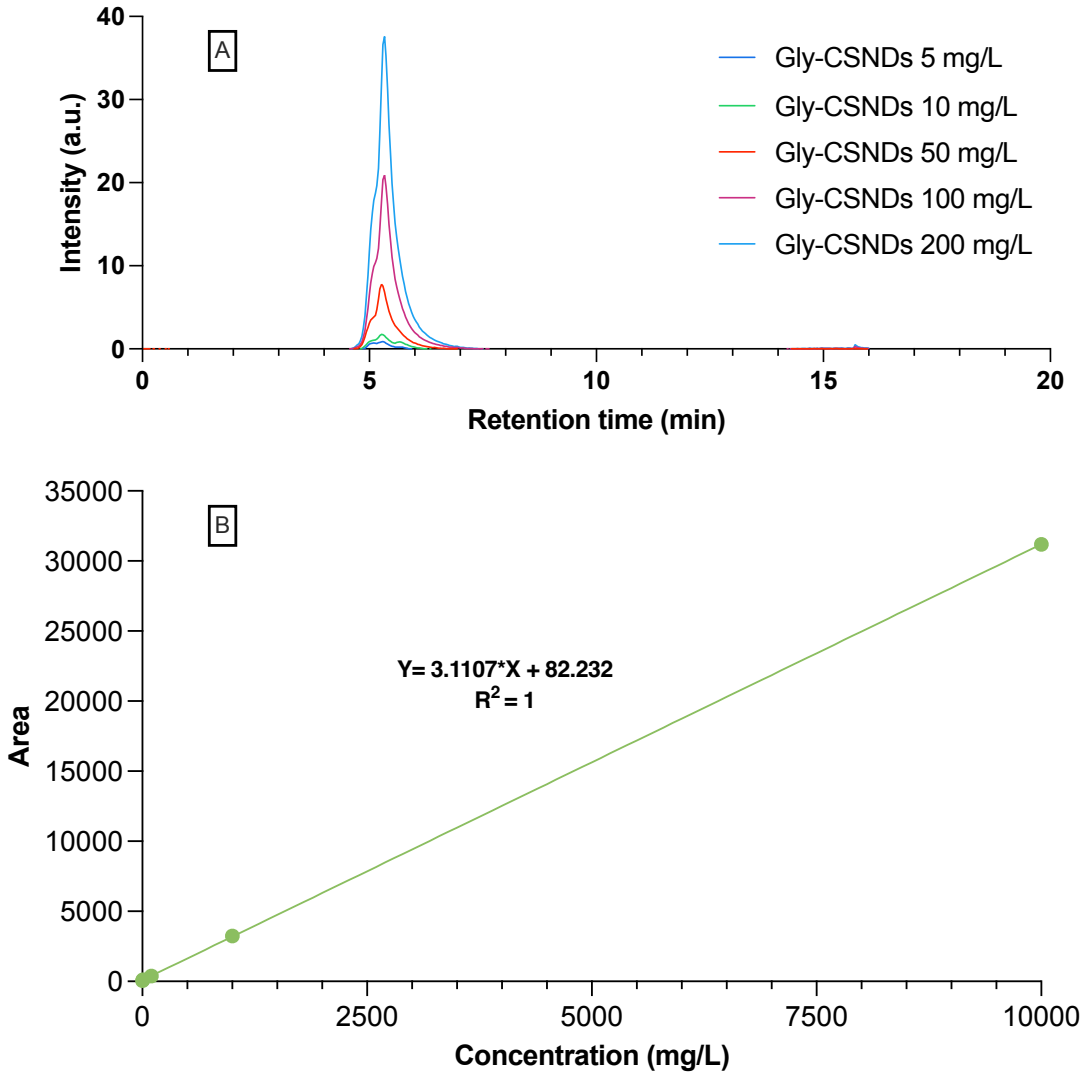


Figure 22. Calibration of HPLC-SEC-FD method using Gly-S-CNDs standards. **A**, Fluorescence chromatograms of Gly-S-CNDs at concentrations from 5 to 200 mg/L, showing consistent retention time and intensity. **B**, Calibration curve constructed from peak area versus concentration (0.1 – 10000 mmg/L), with high linearity ($R^2 = 1$), and method sensitivity defined by LOD = 0.068 mg/L and LOQ = 0.206 mg/L.

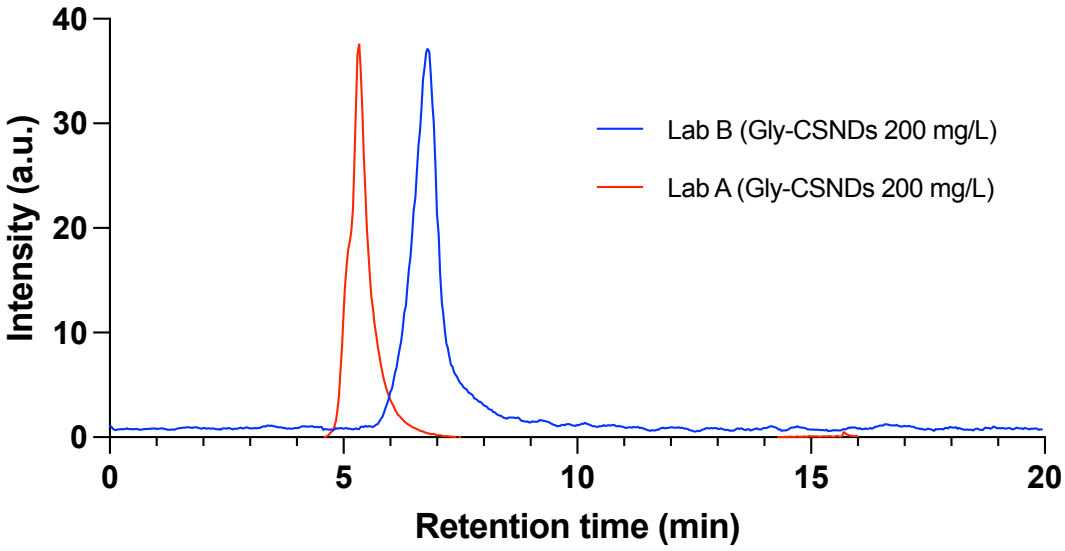


Figure 23. Inter-laboratory comparison of HPLC-SEC-FLD chromatograms for Gly-S-CNDs. Fluorescence chromatograms of Gly-S-CNDs recorded in two independent laboratories using different instruments and analysts. The red trace represents measurements conducted in Laboratory A, while the blue trace represents Laboratory B.

4.2.2.2. Accuracy and Recovery (Spiked samples).

Method accuracy and matrix effects were assessed via spike-recovery in a representative complex matrix (coffee extract). To assess method accuracy and matrix effects, coffee extracts were spiked with known concentrations of Gly-S-CNDs (5–200 mg/L) and analyzed in triplicate. As shown in

Table **7**, measured values closely tracked the fortification levels, giving recoveries of 98.51–101.20% with RSD < 2.2% across all points (n = 3). Consistent retention times and the absence of co-eluting signals further indicate minimal matrix interference. Collectively, these results support the HPLC-SEC-FLD method's accuracy, specificity, and suitability for quantifying CNDs in real food matrices such as coffee.

Table 7. Recovery of Gly-S-CNDs in coffee extract at varying spiking concentrations, demonstrating method accuracy and precision.

Added Gly-S-CNDs concentration (mg/L)	Measured Concentration (mg/L)	Recovery (%)	RSD (%)	n
0	93.19 ± 0.32	100	0.34	3

5	129.79 ± 0.15	100.66 ± 0.1	0.12	3
10	135.69 ± 2.87	101.2 ± 1.79	2.12	3
50	171.1 ± 2.13	98.67 ± 1.06	1.24	3
100	220.03 ± 2.12	98.51 ± 0.85	0.96	3
200	319.3 ± 2.01	98.73 ± 0.57	0.63	3

4.2.2.3. Validation of methods by measuring real samples

The validated HPLC-SEC-FLD method was applied to measure processed foods-coffee brew, black banana, black apple, and black-pearl. As illustrated in **Figure 24**, all measured sample detected a prominent fluorescent signal within the Gly-S-CNDs retention window (≈5.3–5.6 min), confirming CNDs presence. Peak height and bandwidth differed among products, consistent with variation in CND abundance and, potentially, hydrodynamic size or surface-state heterogeneity. The strongest responses were observed for black banana and black apple, which is plausible given extensive browning chemistry and sugar-rich Maillard pathways during over-ripening/darkening.

Concentrations derived from calibration (**Table 8**) mirrored these trends: black banana contained the highest CNDs level (977.75 ± 16.24 mg/L), followed by black apple (655.14 ± 8.13 mg/L) and coffee (384.97 ± 13.14 mg/L). The black-pearl showed the lowest amount (270.53 ± 11.70 mg/L), likely reflecting dilution and/or distinct formation routes. Collectively, the results indicate that both high-temperature processing (e.g., brewing/long time low temperature cooking) and oxidative–enzymatic browning in fruits can generate CNDs.

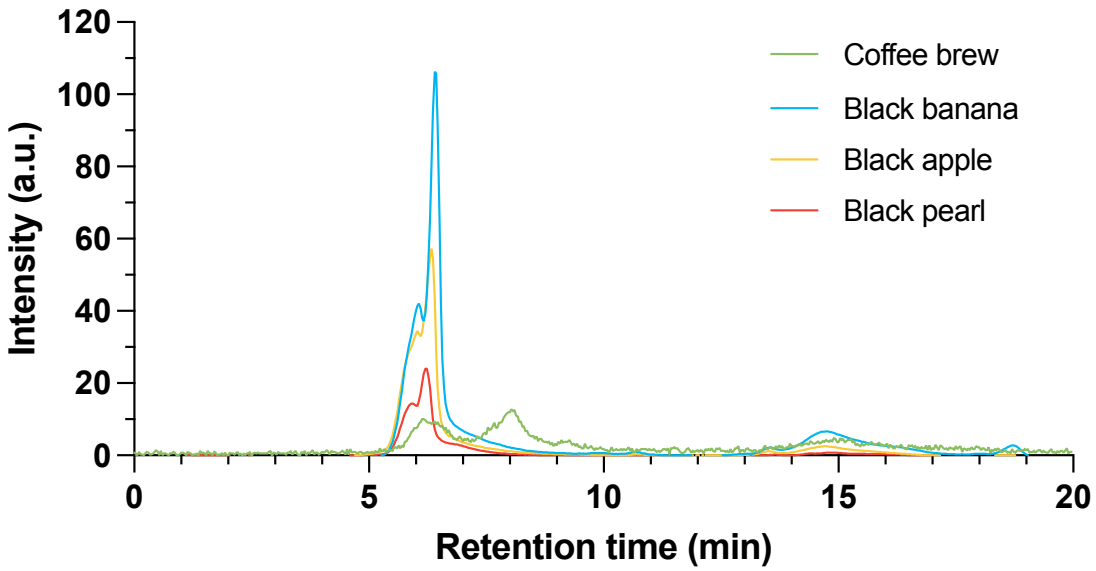


Figure 24. HPLC-SEC-FLD chromatograms of carbon nanodots (CNDs) detected in selected processed food samples.

Table 8. Concentration of CNDs in different food samples expressed in Gly-S-CNDs equivalent

Samples	**CNDs content (mg/L Gly-S-CNDs equivalent)**
Coffee brew	384.97 ± 13.14^{c}
Black banana	977.75 ± 16.24^{a}
Black apple	655.14 ± 8.13^{b}
Black pearl	270.53 ± 11.7^{d}

Values are presented as mean ± standard deviation (n = 3). Different superscript letters (a–d) indicate statistically significant differences among samples ($p < 0.001$, one-way ANOVA followed by Tukey's post hoc test).

4.3. Results related to Objective 3: Detection of carbon nanodots (CNDs) and elucidation of their formation mechanisms in food products (addressing RQ4–RQ5)

4.3.1. Detection of CNDs in food products

A validated high-performance liquid chromatography method with size-exclusion and fluorescence detection (HPLC-SEC-FD) was applied to quantify carbon nanodots (CNDs) in processed food samples. The calibration curve was linear across the tested range ($y = 3.1107x + 82.232$, $R^2 = 1.000$). The limit of detection (LOD) and limit of quantification (LOQ) were 0.068 mg/kg and 0.206 mg/kg, respectively. The method demonstrated excellent precision, repeatability, and inter-day reproducibility, confirming its suitability for routine CND analysis in food systems.

Using this validated method, CNDs were quantified in a wide range of processed foods. As shown in **Figure 25**,, measurable levels of CNDs were detected across six major food categories, including bakery products, chocolates, beverages, black foods, spices, cereals, and other processed goods. CNDs concentrations varied substantially among samples, reflecting differences in processing intensity, ingredient composition, and thermal exposure.

Overall, samples subjected to stronger thermal treatment (e.g., roasting, baking, or intensive processing) tended to show higher CNDs concentrations. Among all tested foods, coffee exhibited the highest CNDs concentration (3,860 mg/kg), followed by pretzel (3,480 mg/kg), roasted black beans (3,327 mg/kg), and roasted mung beans (2,700 mg/kg). Several roasted or extracted products also showed elevated levels, including roasted red chili (2,379 mg/kg), extracted black sesame (2,347 mg/kg), and extracted green tea leaves (1,985 mg/kg).

A clear heat-intensity gradient was observed in bakery products. Bread crust contained higher CNDs levels than breadcrumbs (1,829 vs. 501 mg/kg), whereas low CNDs were detected in dough (15 mg/kg). This bread crust > breadcrumbs > dough trend supports the role of thermal exposure in promoting CNDs formation, as the crust undergoes more direct and prolonged heating than the crumb, while dough is unbaked.

Spices such as turmeric (1,127 mg/kg), black pepper (1,382 mg/kg), and ginger (1,614 mg/kg) also exhibited appreciable CNDs concentrations, likely associated with drying or roasting during processing. In contrast, foods subjected to milder processing or lower thermal intensity generally showed lower CNDs levels (e.g., brewed green tea 560 mg/kg; brewed black tea 550 mg/kg; coke 31 mg/kg; black apple 43 mg/kg).

Overall, the distribution patterns shown in **Figure 25** are consistent with previous reports of CND formation in caramelized sugars and baked foods (Sk et al., 2012a), supporting the hypothesis that CNDs arise primarily through Maillard reactions and related thermal degradation pathways.

These findings demonstrate the widespread occurrence of CNDs in thermally processed foods and highlight the importance of processing conditions in governing their formation, with implications for food safety evaluation. The quantified CNDs here represent food-intrinsic nanoparticles generated during processing; therefore, their concentration reflects processing history rather than intentional formulation. This differs from added CNDs, where identity, surface functionalization, and exposure dose are defined by the manufacturer and should be evaluated separately for safety and compliance.

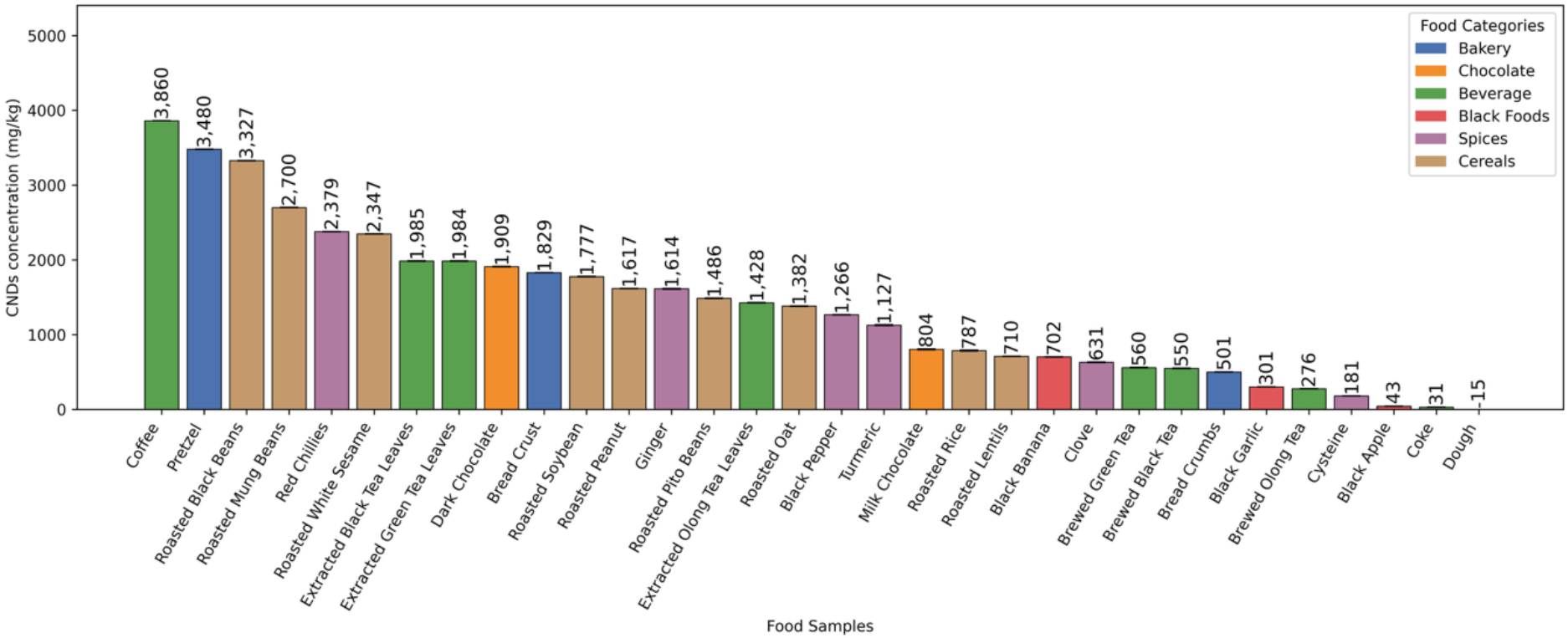


Figure 25. Concentration of carbon nanodots (CNDs) in selected food products grouped by category. CNDs levels (mg/kg) were quantified using a validated fluorescence spectroscopy method. Error bars represent standard deviation from triplicate measurements.

4.3.2. Characterization of food-derived carbon nanodots (F-CNDs)

4.3.2.1. Characterization of food-derived carbon nanodots (F-CNDs) in coffee brewing

To further understand the structure of food-derived carbon nanodots (F-CNDs), carbon nanodots naturally occurring in brewed coffee (C-CNDs) were extracted and subsequently characterized using transmission electron microscopy (TEM), fluorescence spectroscopy, and UV-visible spectrophotometry (**Figure 26)**. TEM analysis revealed spherical nanoparticles with uniform morphology and an average diameter of 3.2 ± 0.9 nm (**Figure 26A, C**). Fluorescence emission spectra collected across excitation wavelengths from 280 to 460 nm showed the strongest signal at 370 nm excitation and 438 nm emission (**Figure 26B, D**), consistent with previous findings from coffee grounds (Chu et al., 2023), though slightly blue-shifted compared to instant coffee CNDs (Ex: 390 nm, Em: 465 nm) reported by (Jiang et al., 2014). These spectral shifts may be attributed to differences in roasting duration, as previously discussed by (Chu et al., 2023). UV-Vis analysis (**Figure 26D**) revealed an absorbance peak near 300 nm, corresponding to π–π^* transitions in aromatic sp^2 domains, with a shoulder near 275 nm, further supporting the presence of graphitic structures (Chu et al., 2023; Ding et al., 2016).

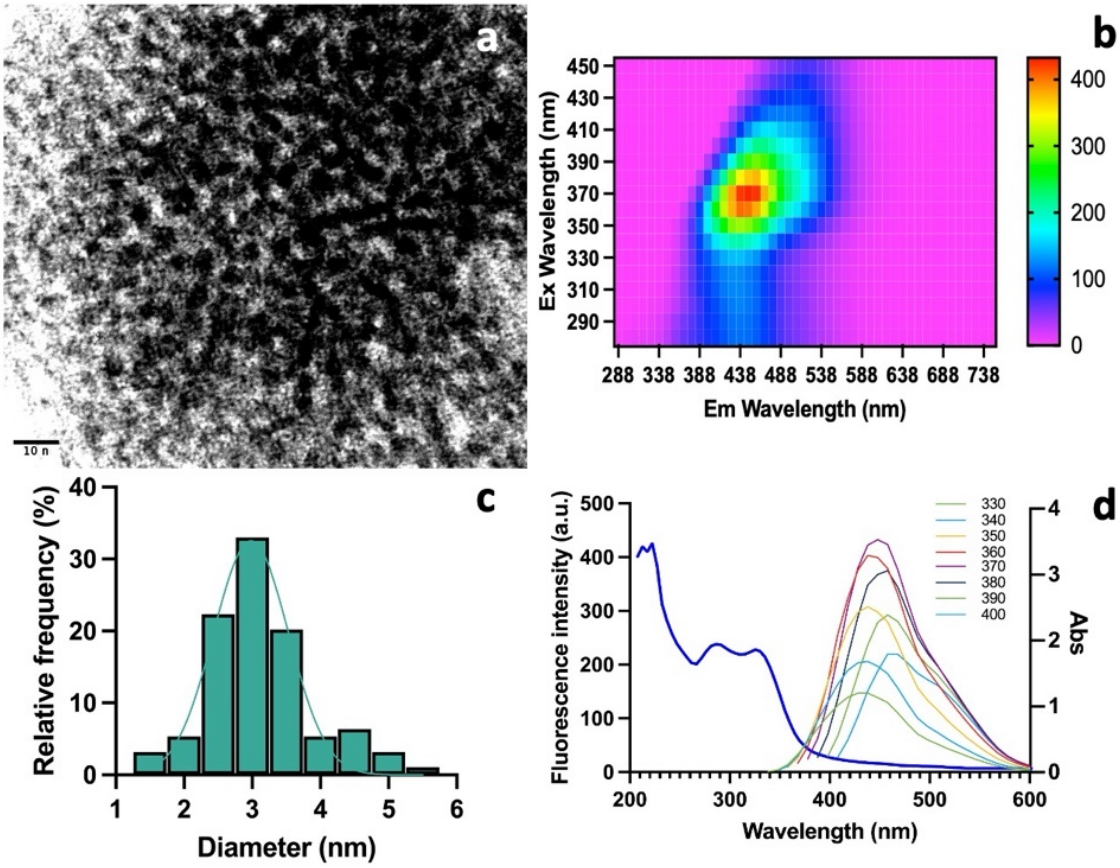


Figure 26. Optical Characterization of Carbon Nanodots Extracted from Brewed Coffee (C-CNDs). **A**, TEM image at 10 nm scale showing spherical morphology. **B**, 3D fluorescence excitation–emission spectra. **C**, Size distribution histogram (average diameter: 3.2 ± 0.9 nm). **D**, UV–Vis absorption spectrum (left) and 2D fluorescence emission spectra at varying excitation wavelengths (right).

4.3.2.2. Characterization of food-derived carbon nanodots (F-CNDs) in bakery products

CNDs were successfully extracted from pretzels using a previously established protocol (D. Nguyen, Muthu, El-Ramady, Daróczi, et al., 2024). The isolated nanodots were subsequently examined by transmission electron microscopy (TEM) and fluorescence spectroscopy (**Figure 27**). As shown in **Figure 27A–B**, the CNDs displayed strong photoluminescence, with a maximum excitation wavelength observed at 380 nm. This value was slightly higher than the typical 370 nm maximum reported for Maillard reaction-derived CNDs in model systems. TEM analysis at a 10 nm scale confirmed their predominantly spherical morphology (**Figure 27C**), while particle size distribution analysis revealed an average diameter of approximately 3.5 nm (**Figure 27D**).

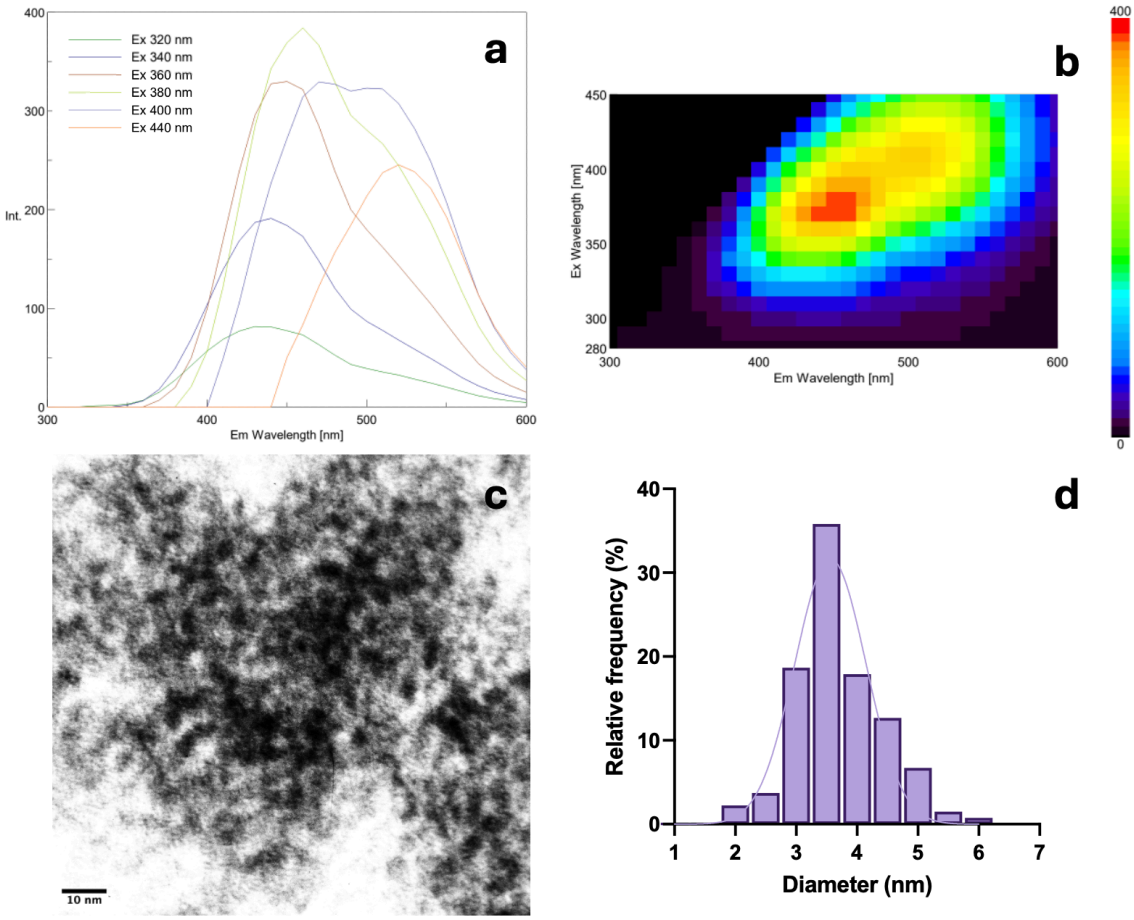


Figure 27. Characterization of carbon nanodots from bakery products (CNDs). **A**, The emission wavelength 300 – 600 nm of CNDs with different excitation wavelengths. **B**, 3D fluorescent spectra of CNDs. **C**, TEM images of CNDs with 10 nm scale. **D**, size distribution histogram of CNDs with an average size of 3.5 nm (Semsey et al., 2024).

4.3.2.3. Characterization of carbon nanodots (CNDs) in the presence of citric acid

To explore the influence of citric acid on CNDs synthesis, four types of nanodots were produced by combining nitrogen-rich precursors with either citric acid or glucose: glycine–citric acid (Gly-C-CNDs), glycine–sucrose (Gly-S-CNDs), urea–citric acid (U-C-CNDs), and lysine–citric acid (Lys-C-CNDs). The lyophilized powders exhibited clear visual differences depending on precursor type (**Figure 28**). Gly-S-CNDs appeared brownish, whereas Gly-C-CNDs and U-C-CNDs were greenish-yellow and dark brown, respectively. Lys-C-CNDs, by contrast, presented as pale yellow, reflecting variations in surface functionalities and reaction intermediates generated during pyrolysis.

Optical characterization confirmed that all four CNDs displayed excitation-dependent fluorescence (**Figure 29**), consistent with earlier reports that attribute this to heterogeneous emissive centers. Gly-S-CNDs showed a broad emission band centered at

~460 nm with an excitation window between 360–400 nm, suggesting relatively homogeneous surface states. Gly-C-CNDs emitted more narrowly at ~440 nm, while U-C-CNDs exhibited dual fluorescence with a broader tail extending toward 500 nm. Lys-C-CNDs displayed weaker but distinct emission characteristics.

EEM analysis confirmed that Gly-S-CNDs and Gly-C-CNDs formed clear hotspots, whereas U-C-CNDs showed a diffuse pattern, suggesting a wider range of emissive trap states. These distinct optical behaviors highlight the role of precursor composition in modulating surface chemistry and quantum confinement. Such variations not only confirm the structural diversity of food-derived CNDs but also demonstrate their potential as probes or calibration standards depending on the analytical context.

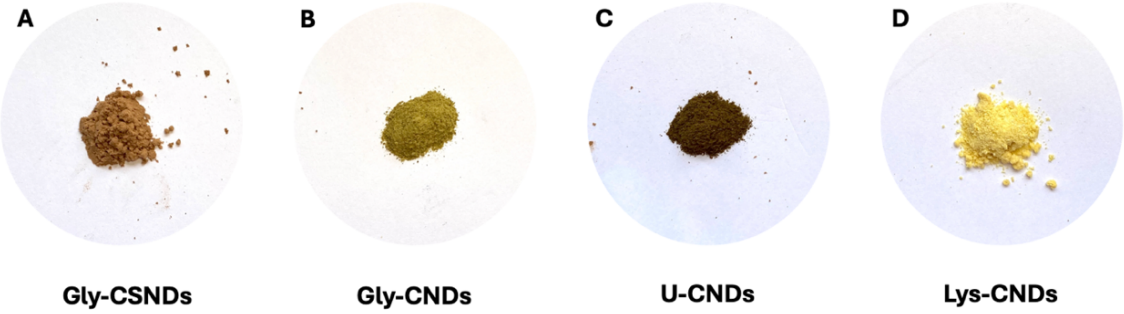


Figure 28. Visual comparison of lyophilized CNDs powders synthesized from different precursors: (A) glycine–sucrose (Gly-S-CNDs), (B) glycine–citric acid (Gly-C-CNDs), (C) urea–citric acid (U-C-CNDs), and (D) lysine-citric acid (Lys-C-CNDs).

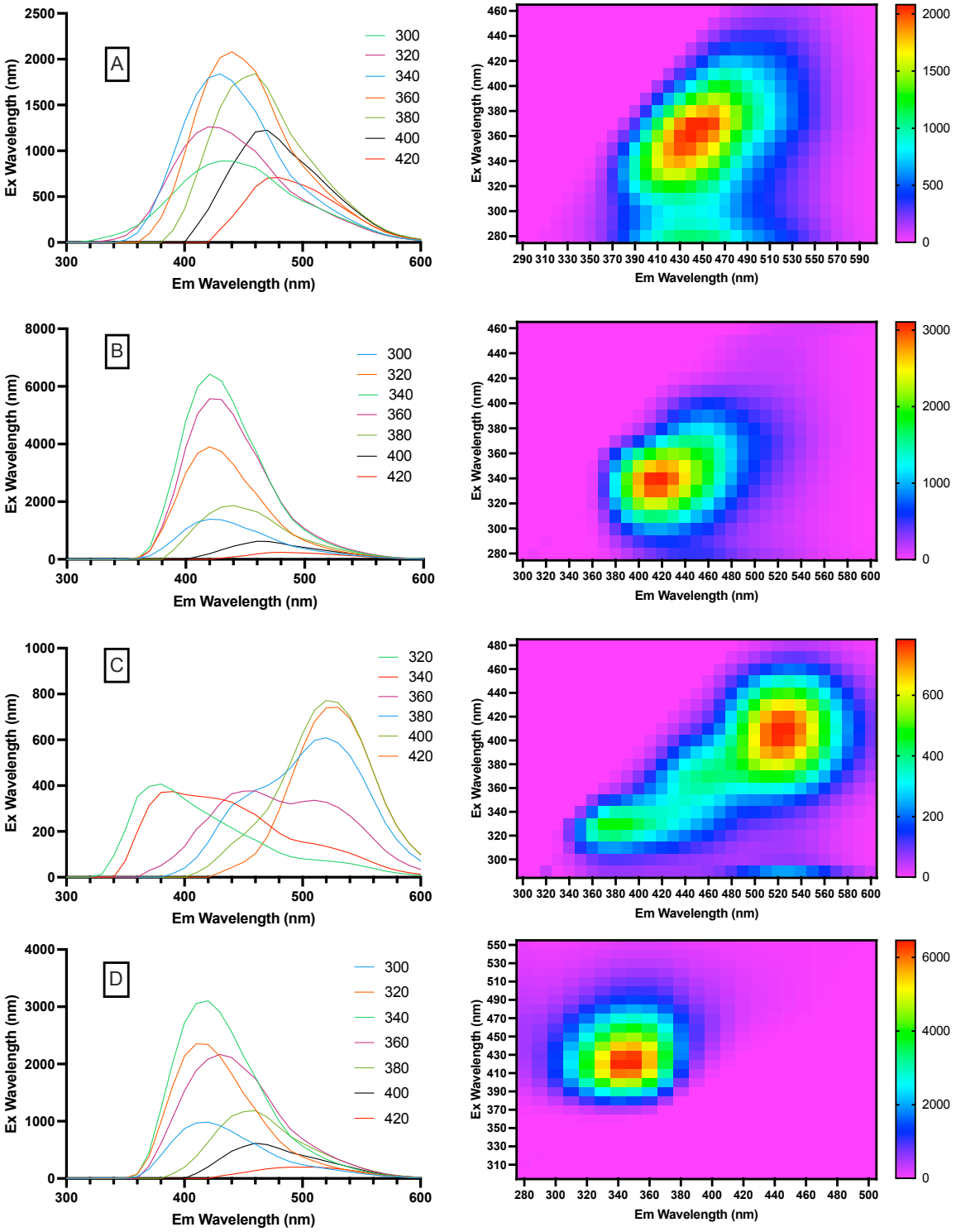


Figure 29. Optical characteristics of synthesized CNDs. **Left panels**: emission spectra recorded at multiple excitation wavelengths (300–480 nm). **Right panels**: excitation–emission matrices (EEMs) for (**A**) Gly-S-CNDs, (**B**) Gly-C-CNDs, (**C**) U-C-CNDs, and (D) Lys-C-CNDs illustrating differences in emission maxima and fluorescence distribution.

4.3.3. Understanding the formation mechanisms of carbon nanodots (CNDs) in food products

The widespread detection of CNDs across processed foods (**Section 4.3.1**) raises important questions about how these nanostructures originate during food preparation. Their consistent occurrence in baked, roasted, fried, and brewed products suggests that thermal processing is the key driver of their formation. To clarify these pathways, this section discusses a case study of coffee brewing and proposaed the formation mechanisms during processing.

4.3.3.1. A case study: Understanding the formation of food-derived carbon nanodots (F-CNDs) in coffee brewing

After confirming the occurrence of coffee-derived carbon nanodots (C-CNDs), we investigated how different brewing parameters influence their formation. Four experiments were designed to test the effects of bean type, grinding size, sample-to-water ratio, and brewing conditions (**Figure 30**).

4.3.3.2.1. Experiment 1: Effect of Coffee Bean Type

As shown in **Figure 30A**, bean type had a strong influence on C-CNDs yield. Arabica beans (*Coffea arabica* L.) generated fluorescence intensities of 5046 ± 15.3 a.u., over three times higher than Robusta beans (*Coffea canephora* L.) (1444.0 ± 28.4 a.u.). The 50:50 Arabica–Robusta blend produced an intermediate signal (≈2.3 × 10^3 a.u.), consistent with partial contribution from both bean types. These contrast can be attributed to compositional differences: Robusta beans typically contain less sucrose and more amino acids such as alanine and asparagine (Murkovic & Derler, 2006). During roasting, these compositional variations alter the rate and extent of Maillard reactions, affecting nanodot generation (D. Li et al., 2018; Z. Ma et al., 2020; D. Nguyen, Muthu, El-Ramady, Daróczi, et al., 2024). Previous work also showed that melanoidins produced during roasting diffuse into the brew and correlate with coffee's color and fluorescence (Bekedam et al. (2006)), suggesting a mechanistic link between melanoidins and CNDs (D. Li, Xie, et al., 2019).

4.3.3.2.2. Experiment 2: Effect of Grinding Size

Particle size of the grounds also influenced C-CND levels (**Figure 30B**). Coarse grinds (1.1 mm) yielded the highest fluorescence (6562.1 ± 32.7 a.u.), while fine grinds (0.3 mm) showed ~36% lower intensity (4183.4 ± 22.0 a.u.). Interestingly, this trend contrasted with caffeine extraction, which increases with finer grinds as reported by Bell

et al. (1996). The inverse pattern suggests caffeine may act as a quencher of CNDs fluorescence, consistent with known nanoparticle–molecule quenching mechanisms (Zu et al., 2017). Additionally, coarse grinds allow deeper water penetration and longer residence time, possibly enhancing nanodot formation within the matrix rather than at the particle surface.

4.3.3.2.3. Experiment 3: Effect of Coffee-to-Water Ratio

Figure 30C shows that a 1:15 coffee-to-water ratio produced the highest C-CNDs concentration. Ratios above this threshold led to reduced fluorescence, likely due to dilution of key precursors and limited interactions necessary for CNDs formation. Although increasing water improves extraction of soluble compounds, excessive dilution may hinder nanodot assembly from Maillard-derived intermediates (Barros et al., 2019; Nicoli et al., 1990).

4.3.3.2.4. Experiment 4: Effect of Brewing Temperature and Time

Temperature and brewing time exhibited a complex interaction (**Figure 30D**). At lower extraction temperatures (80–90°C), prolonged brewing enhanced C-CNDs formation, reaching a maximum of 5163.5 ± 25.8 a.u. at 80 °C for 300 seconds. In contrast, at 95 °C most nanodots were extracted within 150 seconds, after which prolonged heating decreased their fluorescence, possibly due to structural changes or degradation. These findings suggest that extended extraction at moderate temperatures is more favorable for nanodot stability compared to rapid, high-temperature conditions.

Overall, Arabica beans, medium grinding, and a 1:15 sample-to-water ratio under moderate extraction conditions produced the highest C-CNDs yields. These insights highlight the sensitivity of nanodot formation to brewing parameters and offer possible strategies for either enhancing or mitigating their occurrence. For example, pulsed electric field treatments have been reported to significantly reduce CND levels in coffee (Chu et al., 2023). Given their biocompatibility and fluorescence, C-CNDs could be considered “green” nanomaterials for applications in food and beverage systems.

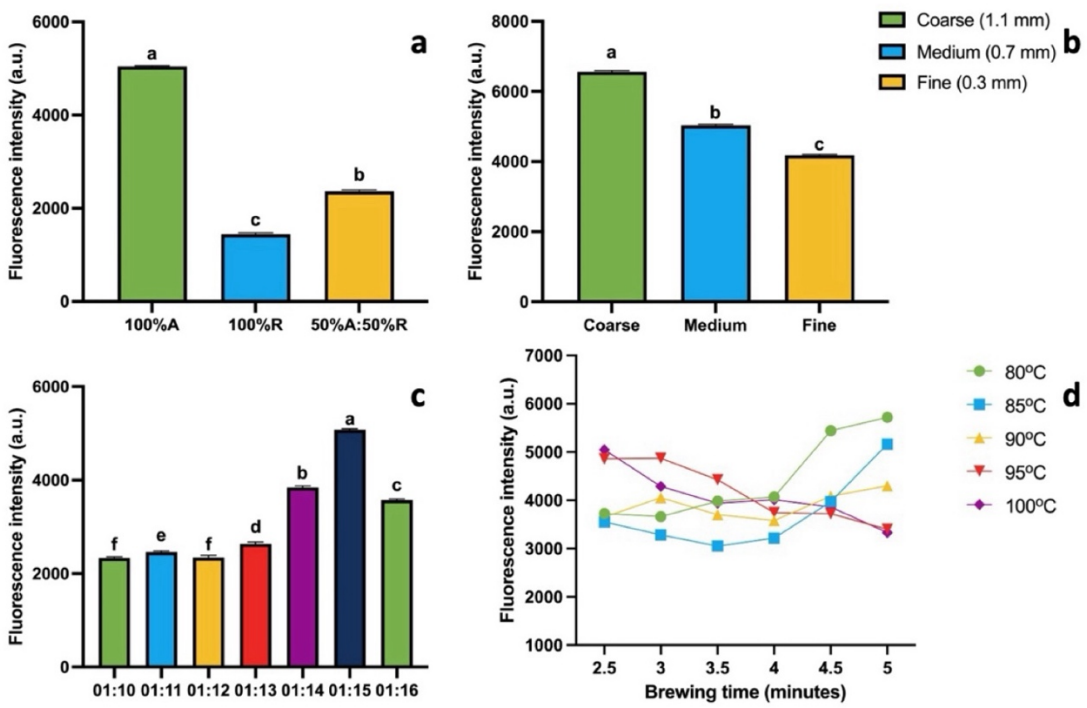


Figure 30. Fluorescence intensity of coffee-derived CNDs (C-CNDs) at excitation 370 nm under different brewing conditions: (A) bean type (100% Arabica, 100% Robusta, 50:50 blend); (B) grinding size (coarse, medium, fine); (C) coffee-to-water ratios (1:10 to 1:16 g/mL); (D) brewing time (150–300 s) at temperatures ranging 80–100 °C. Error bars show standard deviation (n=3); letters denote significant differences ($p < 0.05$).

4.3.3.2.5. Correlations Between C-CNDs and Coffee Components

To further explore interactions, correlation analysis was conducted between C-CNDs fluorescence and key brew parameters: caffeine, pH, total dissolved solids (TDS), and browning index. As shown in **Figure 31A**, C-CNDs levels were negatively correlated with all four factors, most strongly with caffeine ($r = –0.8$). This supports the hypothesis that caffeine directly suppresses CND fluorescence. Moderate correlations were observed with TDS (–0.48), pH (–0.33), and browning color (–0.62), reflecting the complex interplay of multiple extraction-driven processes.

Figure 31B further illustrates the strong negative correlation between caffeine and C-CNDs, reinforcing caffeine's potential role as a fluorescence quencher. This interaction aligns with quenching mechanisms previously described for CNDs with ions and organic molecules (J.-H. Hu et al., 2016; Laptinskiy et al., 2022; Xavier et al., 2018; Zu et al., 2017). While the exact mechanism requires clarification, possible pathways include

hydrogen bonding, π–π interactions, or electron transfer between caffeine and nanodot surfaces.

These results not only explain the observed variability in CNDs formation during brewing but also suggest a novel application: using CNDs as sensing platforms for caffeine quantification. Although electrochemical caffeine sensors based on carbon nanomaterials exist (Carolina Torres et al., 2014; Habibi et al., 2012), this study provides the first evidence linking CND fluorescence with caffeine concentration, opening a new direction for rapid beverage analysis.

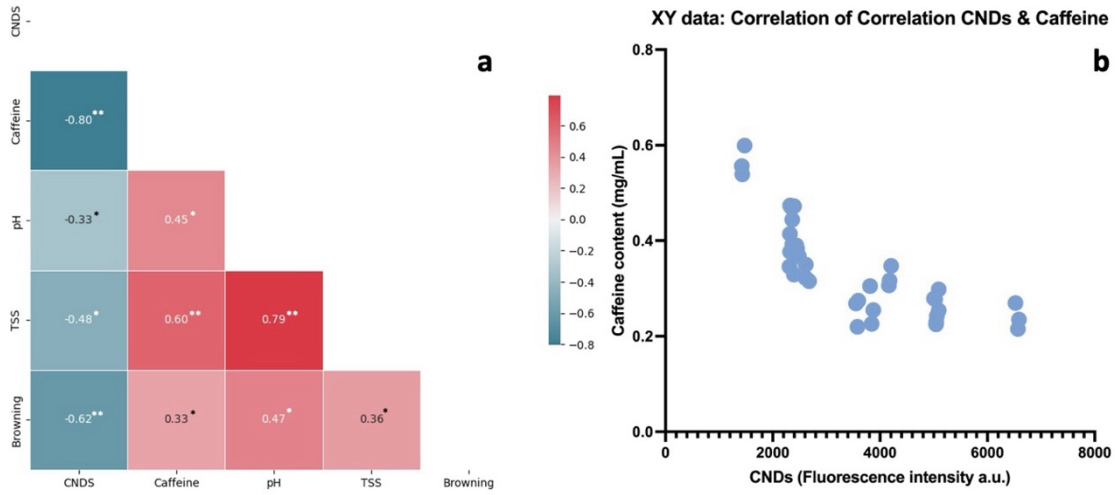


Figure 31. (a) Heatmap of Pearson correlations among C-CNDs (fluorescence intensity (a.u.), caffeine content (mg/mL), pH, total dissolved solids (TDS), and browning color (Abs at 420 nm) in coffee brews and **(b)** the correlation between C-CNDs and caffeine content in coffee brews. *Correlation coefficient at $p < 0.05$. **Correlation coefficient at $p < 0.001$.

4.3.3.2. Proposed Formation Mechanism during Food Processing

Quantitative analysis (**Section 4.3.1**, **Figure 25**) demonstrated that carbon nanodots (CNDs) are consistently present in a wide range of thermally processed foods. The measured concentrations spanned low tens of mg/kg (e.g., dough, ~15 mg/kg) to several thousand mg/kg (coffee, ~3,860 mg/kg), indicating a strong dependence on processing conditions and matrix composition rather than a single formation pathway.

Within bakery products, CNDs concentrations increased from raw dough to breadcrumbs and further to bread crust (~15 < 501 < 1,829 mg/kg, respectively). This gradient reflects

increasing thermal exposure during baking and supports the role of non-enzymatic browning reactions, particularly the Maillard reaction, in CNDs formation in protein–sugar rich systems. This interpretation is consistent with previous studies linking advanced Maillard reaction products and melanoidins to carbonaceous nanostructures (S. Li et al., 2018; Sk et al., 2012a).

Beverage samples exhibited marked differences. Coffee contained the highest CNDs concentration among all tested foods (~3,860 mg/kg), despite being processed under wet-heat conditions. This indicates that direct dry heating is not a prerequisite for CNDs formation; rather, the availability of reactive precursors (sugars, amino acids, polyphenols) and combined with prolonged extraction can promote nanoparticle formation in aqueous systems (D. Nguyen, El-Ramady, et al., 2024; Sk et al., 2012a; H. Wang et al., 2020). In contrast, brewed teas and unroasted cereal products showed substantially lower CNDs levels, highlighting the combined influence of thermal intensity and matrix composition on CNDs generation.

The coffee case study (**Section 4.3.3**) further demonstrated that CNDs formation and extraction are highly sensitive to brewing parameters. Bean type significantly influenced C-CNDs yield, with *Arabica* L. producing more than threefold higher fluorescence intensity than *Robusta* L., reflecting compositional differences in sugar and amino acid profiles that modulate Maillard reaction pathways during roasting. Grinding size also affected CNDs levels: coarse grinds yielded higher fluorescence than fine grinds, suggesting that matrix permeability and extraction kinetics influence nanodot release. Notably, fluorescence intensity was inversely correlated with caffeine content ($r = –0.8$), indicating caffeine-induced quenching and highlighting that apparent CND levels may reflect both formation and post-extraction molecular interactions. Brewing ratio and temperature–time combinations further modulated CND yield, with a 1:15 coffee-to-water ratio and moderate extraction conditions (e.g., 80 °C for 300 s) producing maximal fluorescence. These findings collectively demonstrate that CNDs occurrence in beverages depends not only on roasting chemistry but also on extraction dynamics, precursor availability, and nanoparticle–molecule interactions.

Moderate to elevated CNDs levels were also detected in spices and cereal-based samples. As these products were analyzed in their commercially available form, the detected CNDs are attributed to industrial drying and/or roasting steps commonly applied during processing, rather than to pyrolysis in the strict chemical sense. Similar associations between thermally treated plant matrices and carbonaceous nanostructures have been

reported in previous food and biomass studies (S. Li et al., 2018; Semsey et al., 2025; Sk et al., 2012a).

To contextualize these quantitative findings, **Figure 32** schematically illustrates the dominant thermal reaction pathways—Maillard reaction, caramelization, and high-temperature pyrolysis (>200 °C)—and their association with representative food categories analyzed in this study.

Overall, the concentration patterns observed across food categories indicate that CNDs formation is a general consequence of thermal food processing, governed by the interplay of temperature, exposure time, moisture content, and precursor availability. While multiple reaction pathways may contribute, the present results provide quantitative, processing-dependent evidence that complements the formation mechanisms discussed in **Section 2.2.2** and extends them through systematic measurement across diverse food matrices (S. Li et al., 2018; Sk et al., 2012a).

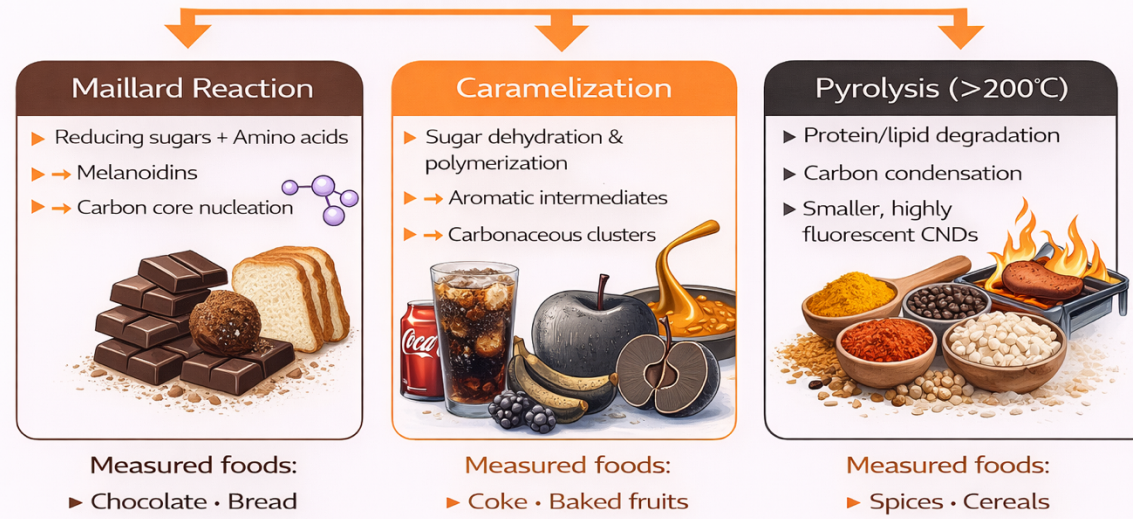


Figure 32. Schematic representation of major thermal reaction pathways (Maillard reaction, caramelization, and pyrolysis >200 °C) contributing to carbon nanodots (CNDs) formation in representative food categories.

4.4. Results related to Objective 4: Applications of carbon nanodots in the food and agricultural industry (addressing RQ7–RQ8)

4.4.1. Develop a Rapid Detection method to detect Caffeine in Beverages using glycine-sucrose derived carbon nanodots (Gly-S-CNDs)

4.4.1.1. Selectivity of this methods

Selectivity is a critical parameter for validating any sensing system. To test the specificity of glycine-sucrose derived carbon nanodots (Gly-S-CNDs), we evaluated their

fluorescence response in the presence of common beverage constituents and possible interferents, including sugars (glucose, fructose), additives (ascorbic acid, citric acid, benzoic acid, E210), inorganic ions (Na^+, K^+, Ca^{2+}, Mg^{2+}), and potentially hazardous compounds (acrylamide, 5-HMF). As shown in **Figure 33**, none of these substances significantly altered the fluorescence of Gly-S-CNDs at concentrations up to 500 µM. Even in the presence of high levels of interferents, Gly-S-CNDs maintained strong specificity toward caffeine, confirming their suitability for beverage analysis.

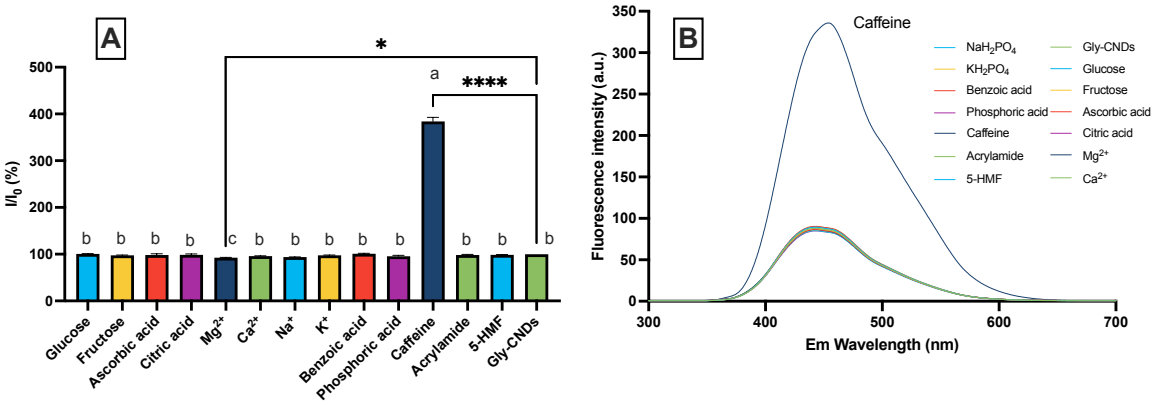


Figure 33. Selectivity of Gly-S-CNDs toward caffeine. (A) Relative fluorescence intensity (I/I_0) in the presence of common interferents (500 µM); bars sharing the same Duncan letter are not significantly different. (B) Representative emission spectra (λ_ex = 360 nm). Gly-CNDs (Gly-S-CNDs) served as the control sample. Data are mean ± SD (n = 3); significance vs control: * $p < 0.05$, **** $p < 0.001$.*

4.4.1.2. Fluorescence Assay for Caffeine Measurement

The fluorescence response of Gly-S-CNDs toward caffeine was evaluated under different conditions (**Figure 34**). Pure Gly-S-CNDs exhibited a strong emission peak (~2232.8 a.u.), while caffeine alone showed negligible fluorescence. Upon addition of 1717 µM caffeine to Gly-S-CNDs, the emission intensity increased by >50%, reaching ~3722.6 a.u. The enhancement clearly indicates direct interaction between caffeine and the nanodots. Notably, the signal from the Gly-S-CNDs + caffeine mixture was over 4000 times higher than that of caffeine alone, highlighting the probe's sensitivity.

Calibration was performed over a caffeine concentration range of 0–2060 nM. As shown in **Figure 35A**, the fluorescence enhancement factor (F/F_0) increased linearly with caffeine concentration, following the regression equation $y = 0.0008225x + 1.006$ ($R^2 = 0.9929$). The method achieved a detection limit (LOD) of 36.5 nM and a quantification limit (LOQ) of 122.1 nM. Emission spectra collected at increasing caffeine

concentrations (**Figure 35B, C**) confirmed a consistent emission wavelength, with intensity scaling proportionally to analyte levels. The fluorescence enhancement of Gly-S-CNDs in the presence of caffeine likely arises from specific surface interactions. TEM and FTIR confirmed abundant functional groups (–OH, –COOH, –NH_2) on Gly-CND surfaces, while Raman spectra indicated graphitic domains. Caffeine molecules are proposed to bind through hydrogen bonding and π–π stacking with aromatic graphitic regions, stabilizing surface states and suppressing non-radiative decay. Electrostatic interactions between nitrogen-containing groups and polar caffeine moieties may further contribute to passivation. This promotes radiative recombination, explaining the linear fluorescence enhancement observed in **Figure 35A–C**.

Table 9 compares CND-based caffeine sensors reported in the literature, including sulfur-doped CNDs (Nemati et al., 2018), Fe-doped red CNDs (Othman, 2024), and Gly-S-CNDs developed in this work. While sulfur-doped and Fe-doped CNDs show high sensitivity, the Gly-S-CNDs assay demonstrated the broadest linear range with a comparable LOD (0.043 µM). In addition, using glycine and sugars as precursors reduces potential toxicity, supporting suitability for food-related applications.

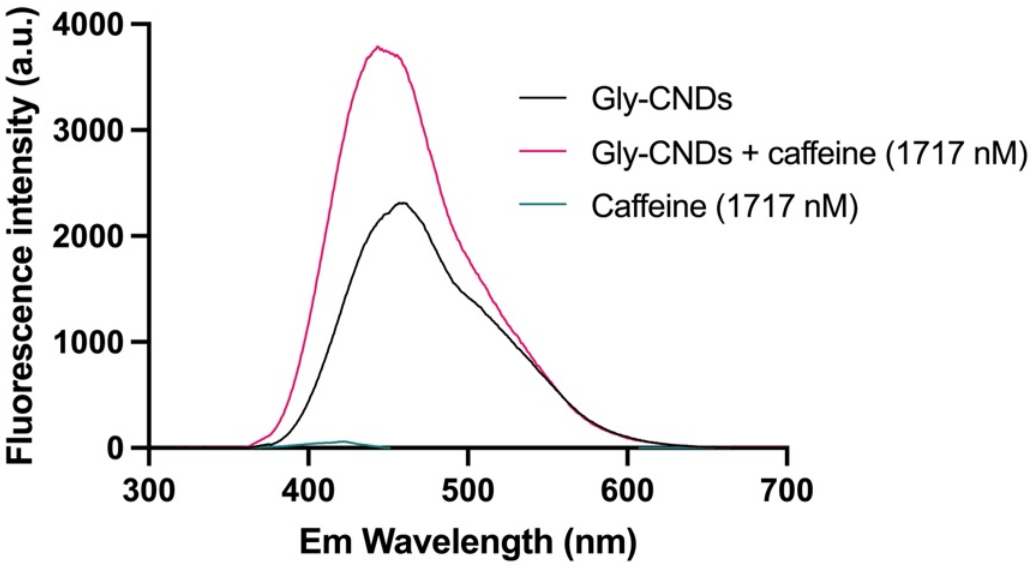


Figure 34. Fluorescence spectra of Gly-S-CNDs (black), Gly-S-CNDs + caffeine (red), and caffeine alone (green) at excitation 360 nm.

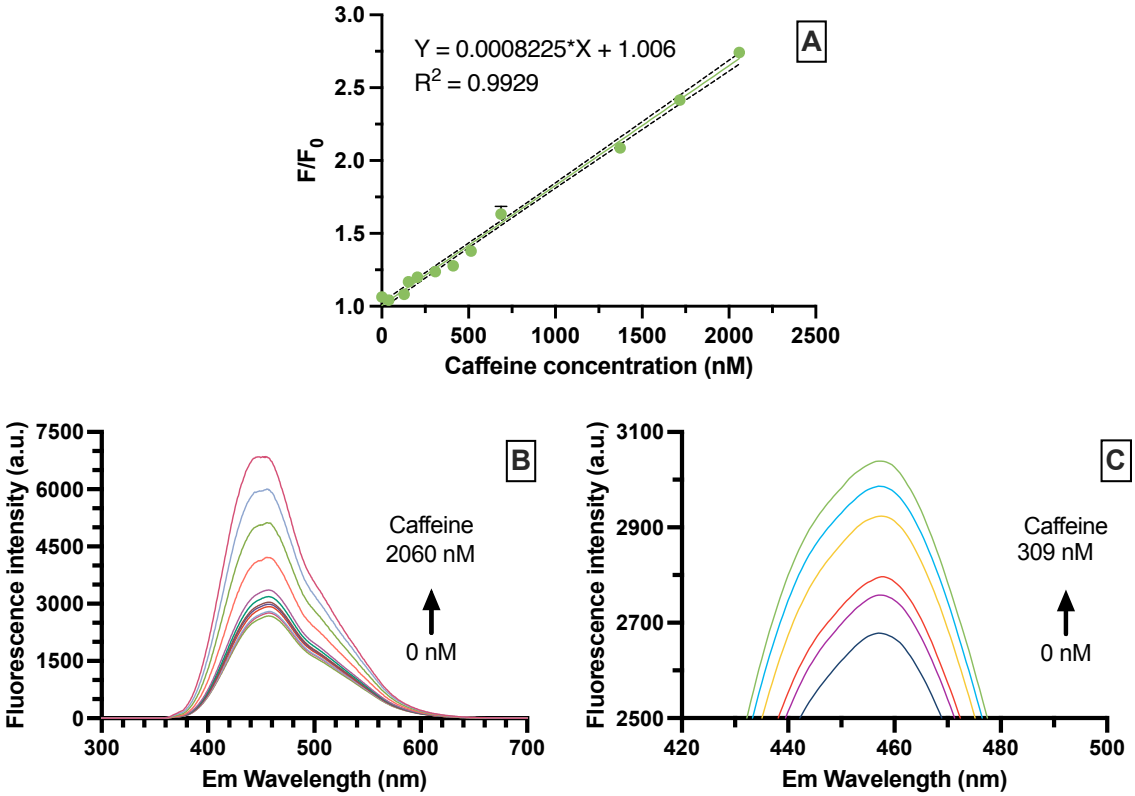


Figure 35. (**A**) Linear calibration curve of fluorescence enhancement (F/F_0) versus caffeine concentration (0–2060 nM). (**B, C**) Fluorescence spectra at increasing caffeine levels.

Table 9. Comparison of CNDs-based caffeine sensors.

Types of CNDs	Precursors	Linear ranges	LOD	References
Sulfur-doped CNDs	Citric acid, $Na_2S_2O_3$	0.2-70 µM	0.05 µM	(Nemati et al., 2018)
Fe-doped red CNDs	Neutral red, $FeCl_3$	1-40 µg/mL	0.024 µg/mL	(Othman, 2024)
Gly-S-CNDs	Glycine, sugars	50-2060 nM	0.0403 µM	**This work**

4.4.1.3. Optimization of Detection Conditions

The influence of pH, incubation time, and temperature was systematically studied to optimize sensing conditions (**Figure 36**). Fluorescence was stable between pH 3.0–5.0 but declined sharply above neutral pH, consistent with surface charge alterations (**Figure 36A–B**). Incubation studies indicated maximum intensity at 25 minutes, after which photobleaching effects became apparent (**Figure 36C**). Temperature dependence

revealed an optimum range of 40–50 °C, with higher values leading to thermal quenching (**Figure 36D**). Therefore, the recommended conditions for caffeine detection are pH 5.0, 25 min incubation, and 40 °C measurement.

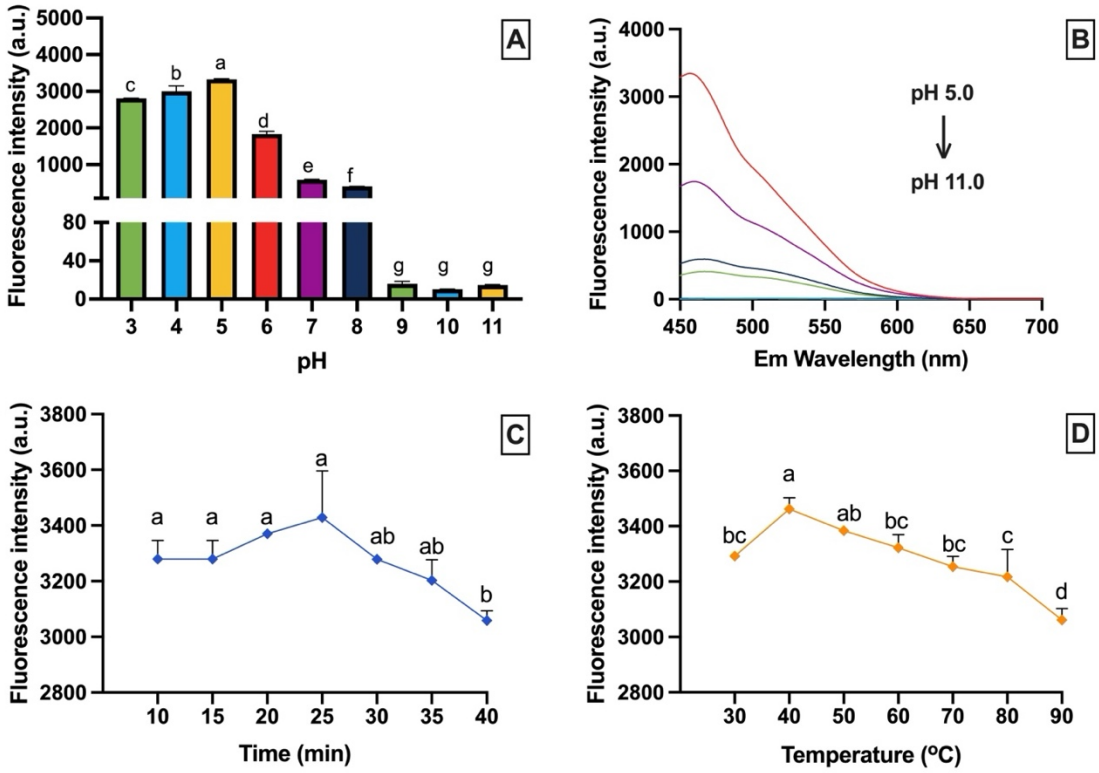


Figure 36. Optimization of Gly-S-CND fluorescence response to caffeine (1717 nM): (A) pH stability, (B) pH-dependent spectra, (C) incubation time, (D) incubation temperature.

4.4.1.4. Reference validation using HPLC

To demonstrate real-world applicability, caffeine levels were measured in six commercial beverages (three energy drinks, three teas) and one adulterated "fake coffee" sample. In energy drink spectra, the addition of Gly-S-CNDs caused an ~8-fold fluorescence enhancement compared to the sample alone (**Figure 37A**). Quantitative analysis (**Figure 37B**) showed excellent agreement between Gly-CNDs-based fluorescence detection and reference HPLC measurements ($p > 0.05$). Recovery experiments yielded 95.9–102.7% with RSD values <2%, confirming both accuracy and reproducibility (**Table 10**).

This study establishes glycine-derived CNDs as a green, food-grade nanomaterial for rapid caffeine sensing. The method provides broad linearity (50–2060 nM), low detection limits (36.5 nM), and strong selectivity, even in complex beverage matrices. Results in commercial samples were consistent with HPLC, validating its accuracy. To our

knowledge, this is the first demonstration of food-derived Gly-S-CNDs applied as fluorescent probes for caffeine, combining biocompatibility, sensitivity, and practicality for the food and beverage industry.

Table 10. Recovery validation of caffeine measurements using Gly-S-CNDs (n = 5).

Sample	**Added caffeine (mg)**	**Measured caffeine (mg)**	**Recovery (%)**	**RSD (%)***
Energy drink apple flavor (Hansen Natural Company, USA)	0	-	-	-
	0.020	0.020 ± 0.001	100.017 ± 6.048	1.968
	0.100	0.103 ± 0.002	102.703 ± 1.834	1.272
	0.200	0.192 ± 0.004	95.902 ± 2.173	1.863

*RSD (%) means relative standard deviation

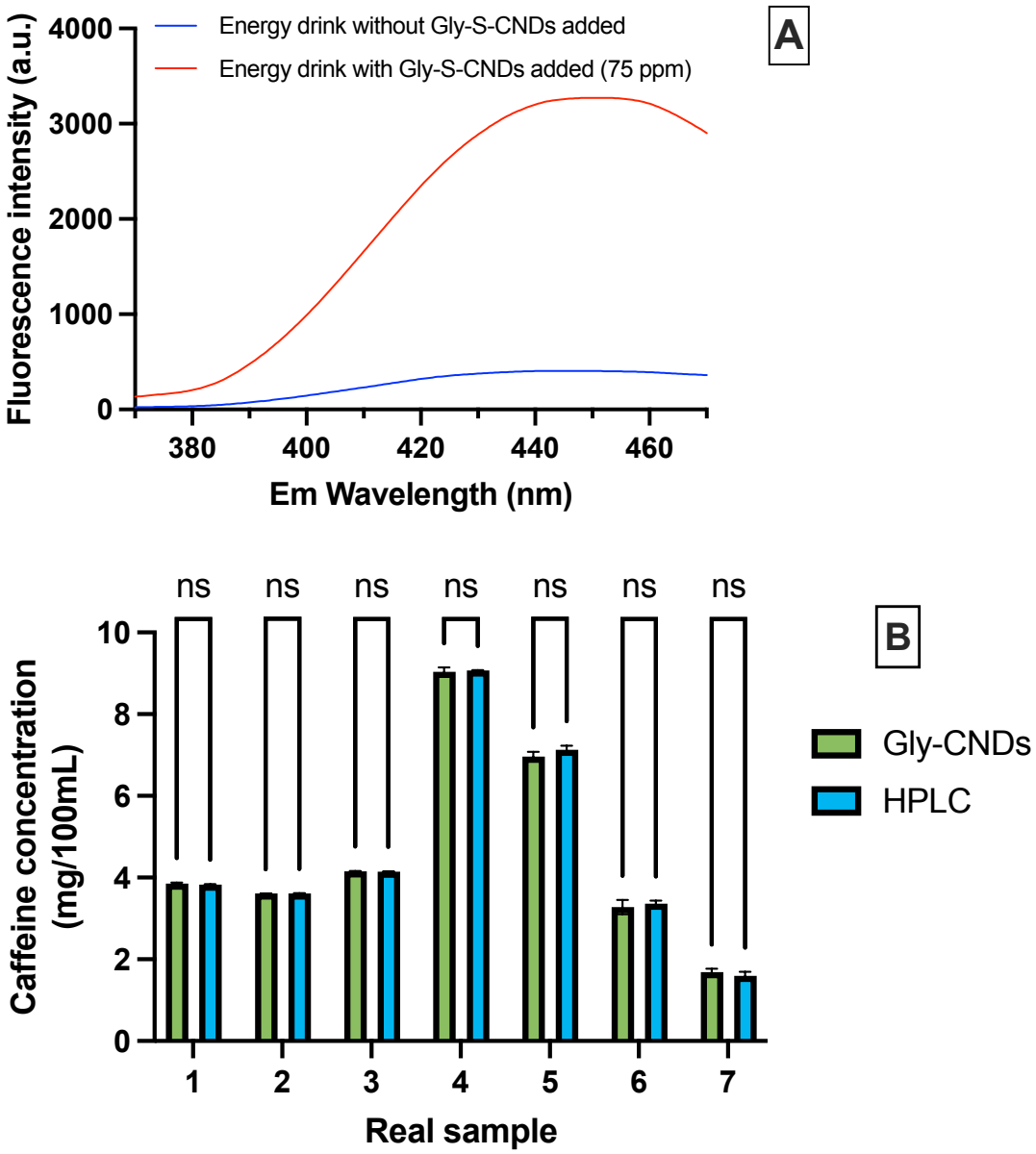


Figure 37. Application of Gly-S-CNDs for caffeine detection in commercial beverages. **(A)** Emission spectra of sample 1 (HELL Energy Drink, classic boxing kings edition, Hungary) with and without addition of Gly-S-CNDs at excitation 360 nm. **(B)** Comparison of caffeine concentrations in beverages measured by Gly-S-CNDs fluorescence assay and HPLC. Tested products included three energy drinks (sample 1: HELL, Hungary; sample 2: XIXO, Hungary; sample 3: Hansen Natural Co., USA), three teas (sample 4: green tea, Taiwan; sample 5: black tea, Taiwan; sample 6: oolong tea, Vietnam), and one adulterated sample (sample 7: fake coffee mixed with burnt corn, Vietnam). Data are shown as mean ± SD from triplicate analyses. Different letters (a–i) indicate significant differences ($p < 0.05$); ns = not significant.

4.4.2. Sustainable valorization of food waste into CNDs

4.4.2.1. Screening of Food Waste Precursors for Carbon Nanodot (CNDs) Production

To explore food waste as a renewable resource for producing carbon nanodots (CNDs), six representative categories-including polyphenol- rich wastes (exactred black tea leaves, exactred green tea leaves, exactred olong tea leaves, extracted coffee grounds, onion skin), mineral- rich wastes (egg shell), protein- rich wastes (leftover cheese), acid-rich wastes (lemon peel), lipid- rich wastes (used oil), and fiber-rich wastes (banana peel)-were selected and subjected to pyrolysis-based synthesis. Representative excitation–emission fluorescence maps of food-waste-derived CNDs are shown in **Figure 38**, confirming that all categories produced fluorescent nanoparticles, though emission intensities varied with precursor type. Notably, protein-based samples (e.g., cheese residues, eggshell) generated the strongest signals, while lipid-rich wastes (e.g., used oil) exhibited relatively weaker fluorescence. Comparative fluorescence intensities across waste categories (**Figure 39**) demonstrated that protein-based and polyphenol-rich wastes were the most efficient precursors, which similar with the collective liturature (D. H. H. Nguyen, El-Ramady, Törős, et al., 2025). Fiber-based and lipid-based samples produced CNDs with measurable but lower emission intensities, underscoring how precursor composition strongly influences synthesis efficiency.

To further enhance yields, precursor wastes were co-treated with citric acid or sucrose during pyrolysis. The statistical analysis in **Figure 40** revealed that citric acid markedly improved CNDs formation in nearly all categories, particularly for polyphenol, mineral, and fiber-based wastes. Schneider et al. (2017) revealed that nitrogen-doped carbon nanodots from citric acid contain fluorescent derivatives of citrazinic acid, which contribute to blue spectral emission In contrast, sucrose supplementation provided only modest improvement, and in protein-rich wastes reduced CNDs output in case of leftover chesse. These findings suggest that citric acid facilitates carbonization and surface passivation during nanodot synthesis, while sucrose may interfere with protein-based pathways.

Collectively, these results highlight that both waste type and additive treatment critically affect CNDs yield and properties. Protein- and polyphenol-rich wastes stand out as the most promising soucres, and citric acid is generally the most effective enhancer. This sustainable valorization strategy not only addresses food waste management but also enables scalable production of green, biocompatible CNDs for food and agricultural applications.

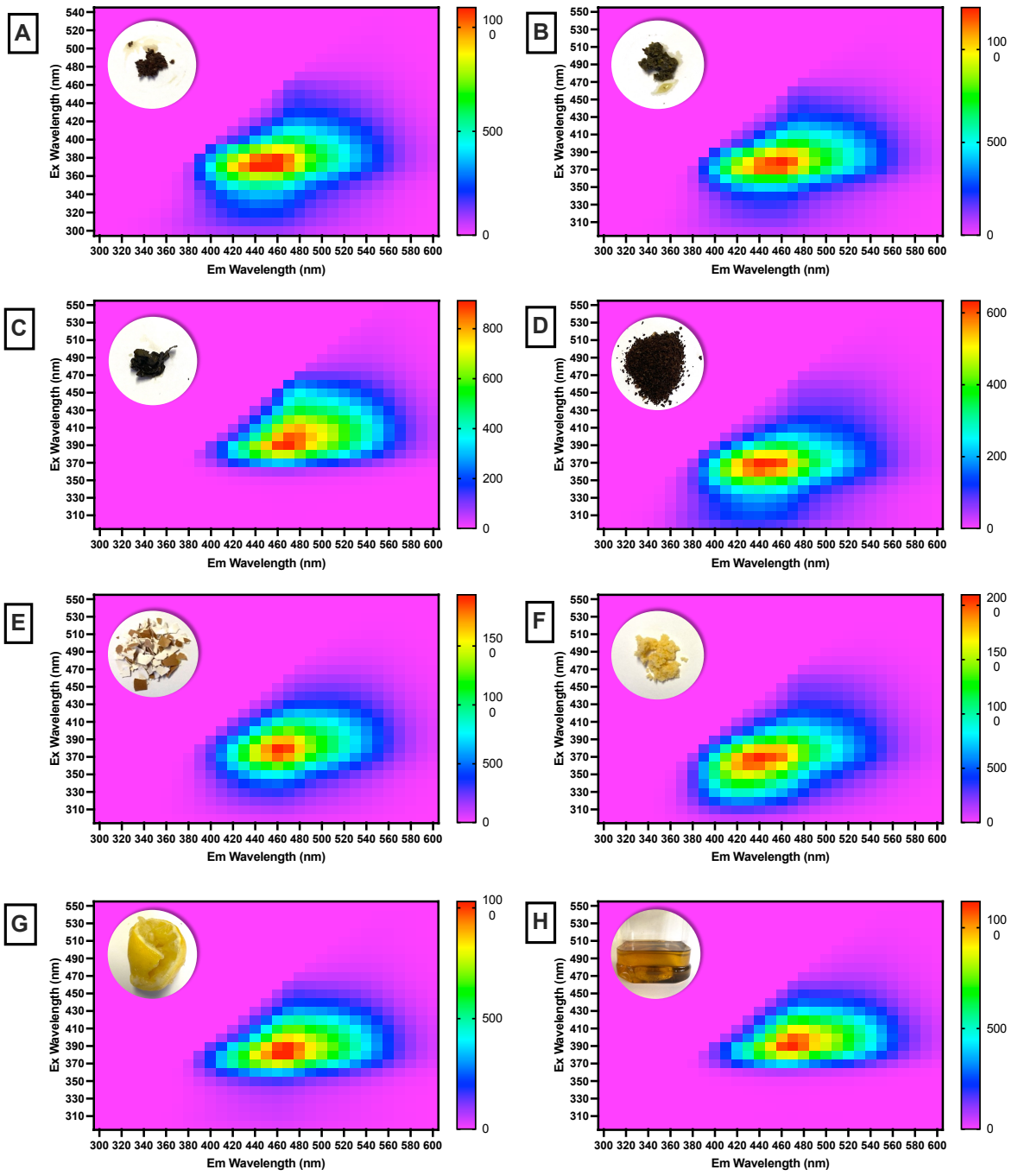


Figure 38. Representative excitation–emission fluorescence maps of CNDs derived from food-waste precursors, showing blue–green emission across diverse sources: (A) extracted black tea, (B) extracted green tea, (C) extracted oolong tea, (D) extracted ground coffee, (E) eggshell, (F) leftover cheese, (G) lemon peel, and (H) used cooking oil.

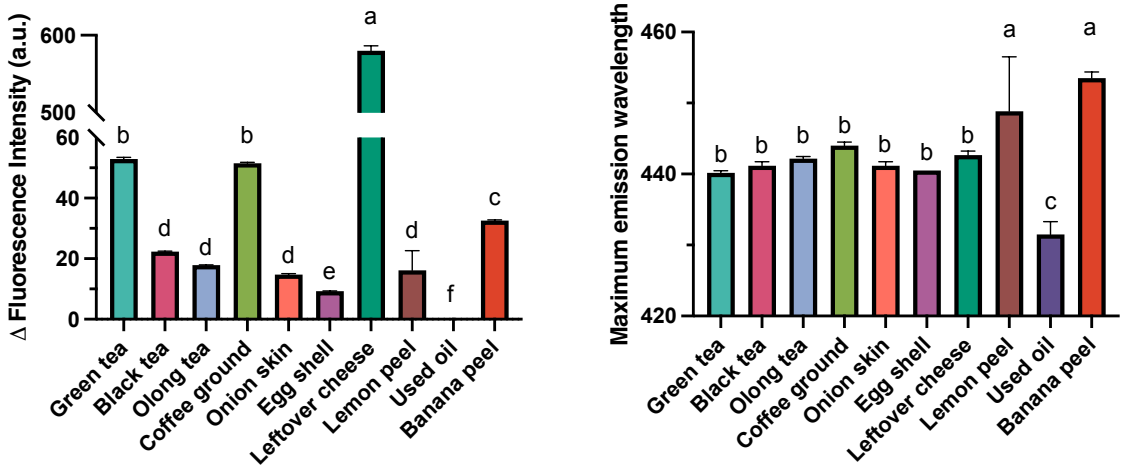


Figure 39. Comparative fluorescence intensities (right panel) and corresponding maximum emission wavelengths (left panel) of CNDs synthesized from ten different food waste categories under identical pyrolysis conditions.

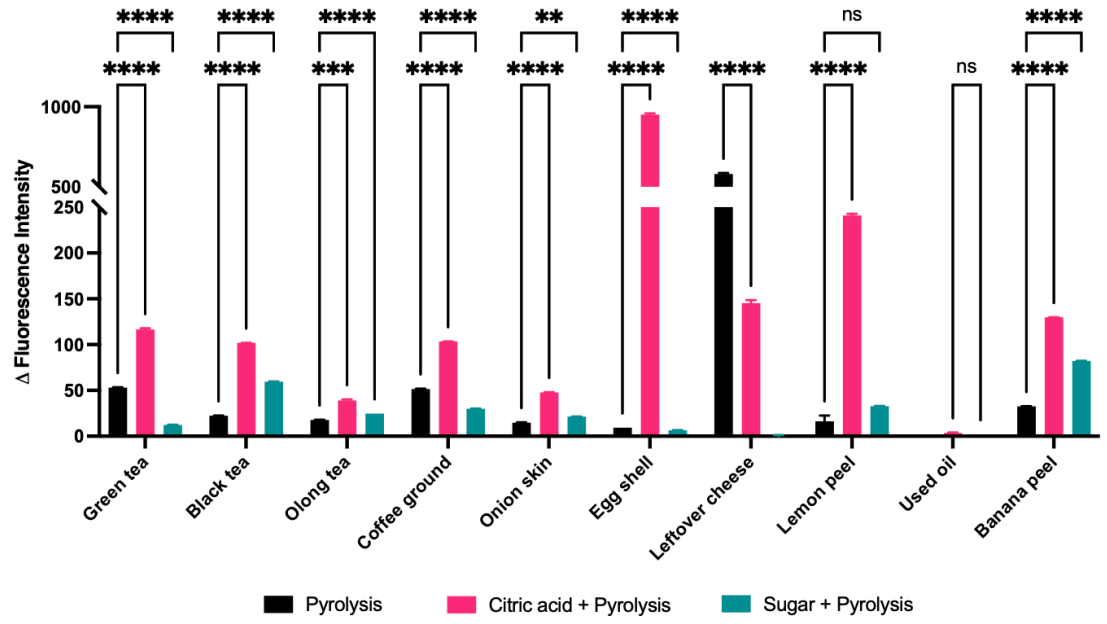


Figure 40. Statistical comparison of fluorescence enhancement (Δ intensity) of food-waste-derived CNDs under different synthesis conditions (pyrolysis alone, citric acid + pyrolysis, and sucrose + pyrolysis). Significance levels: ns = not significant; ** $p < 0.01$; *** $p < 0.001$; **** $p < 0.0001$.

4.4.2.2. A Case Study: Production of Carbon Nanodots from Banana Peel Using CCD and ML Approaches

Banana peel (BP), a common agricultural byproduct, was selected as a model substrate for producing carbon nanodots (CNDs) due to its abundance, rich organic content, and

potential for sustainable valorization. BP is produced in large volumes annually by food-processing industries, creating disposal challenges but offering valuable opportunities for biorefinery applications (Bishnoi et al., 2023). The chemical composition of BP includes cellulose, hemicelluloses, lignin, and simple sugars, making it an ideal substrate for nanomaterial synthesis (Jamal et al., 2011). Recent research demonstrates BP's successful conversion into CNDs through hydrothermal processes, producing fluorescent nanoparticles with 5 nm average size and 20% QY suitable (Atchudan et al., 2021). To enhance carbonization and fluorescence performance, BP was thermally treated with different nitrogen-containing precursors, including urea, glycine, citric acid, and sugar. The study followed a two-phase approach: (i) precursor screening to identify the most effective additive and (ii) statistical and machine learning-assisted optimization of synthesis parameters to maximize CND yield and performance.

4.4.2.2.1. Synthesis of Carbon nanodots from Banana Peel (BP-CNDs) via Pyrolysis

Banana peel was collected from the supplier, then freeze-dried for further use (**Figure 41D**). Banana peel powder was mixed with precursors at a specific mass ratio and subjected to pyrolysis in an oven at a temperature of 100 °C – 200 °C for 1- 4 hours. The obtained samples were mixed with ultrapure water in the ratio of 1:10 (w/w) and subjected to ultrasound for 30 min for extraction. The isolated CNDs solution was collected by filtering the sample with a 0.22 μm filter paper. BP-CNDs were obtained by collecting the first peak of the HPLC-SEC-FD chromatogram (high-performance liquid chromatography – size exclusion column – fluorescence detection). The synthesized CNDs were characterized by UV-Vis absorption spectroscopy, fluorescence spectroscopy, quantum yield measurements, and HPLC-SEC-FD characterized the synthesized CNDs.

To ensure the suitability of the banana peel (BP) biomass for CND synthesis, we first evaluated the fluorescence behavior and composition of the freeze-dried banana peel. As shown in **Figure 41**, emission spectra were recorded across a range of excitation wavelengths. The strongest fluorescence intensity was observed at an excitation wavelength of 360 nm, which was therefore selected for all subsequent fluorescence measurements. This choice is consistent with our previous findings on optimal excitation conditions for detecting CNDs in food matrices (D. Nguyen, Muthu, El-Ramady, Daróczi, et al., 2024). Elemental analysis confirmed adequate carbon and nitrogen content in the BP material, supporting its suitability for carbonization and in-situ nitrogen doping.

The physical appearance and integrity of the freeze-dried peels were also documented to ensure batch consistency prior to synthesis.

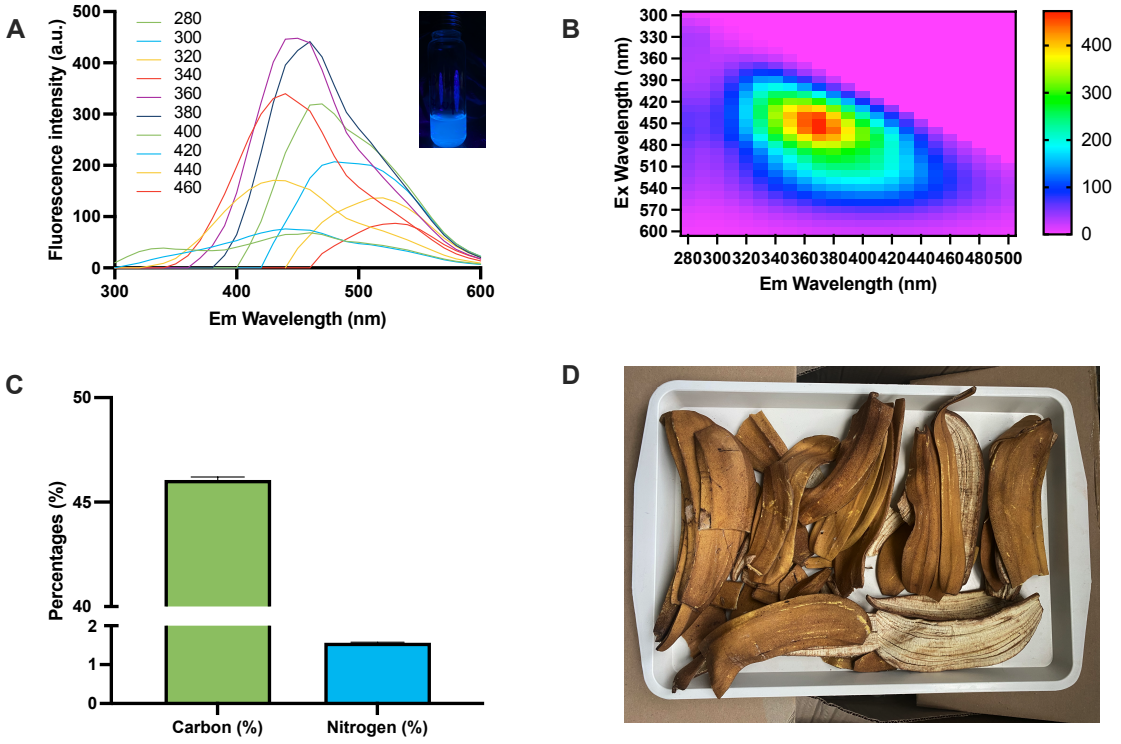


Figure 41. Evaluation of quality of freeze-dried banana peel (BP) for carbon nanodots (CNDs) synthesis. **A**, Fluorescence emission spectra of BP extract at different excitation wavelengths **(**color-coded by excitation wavelength (nm)) with the real image of BP extract under UV light. **B**, Excitation-emission matrix (EEM) plot of BP extract. **C**, Carbon and nitrogen content (%) of BP. **D**, Photographic image of BP samples collected from the supplier.

4.4.2.2.2. Screening of Nitrogen- and Carbon-Containing Precursors

Banana peel (BP) was selected as a sustainable carbon source for CND synthesis, and its performance was tested with four common additives: urea, glycine, citric acid, and sucrose. All mixtures were thermally treated at 180 °C for varying durations (1–4 h). The fluorescence profiles (**Figure 43A**) revealed clear differences in precursor performance: urea consistently generated the strongest emission, peaking after 3 h, whereas the other precursors showed relatively weak and time-independent signals. The distribution of intensities (**Figure 43B**) highlighted the broad response range of urea-BP CNDs, indicating both higher brightness and more structural diversity. Elemental composition further supported this result (**Figure 42**): nitrogen incorporation in the urea-treated

samples reached ~10.3%, while all others remained below 5.2%. This confirms urea's superior role as a nitrogen dopant during pyrolysis.

HPLC-SEC-FD chromatographic separation (**Figure 43C**) also emphasized the distinction: urea-derived BP-CNDs produced intense, broad peaks, particularly at ~6 min retention, suggestive of larger conjugated or nitrogen-enriched fluorescent structures. Other treatments yielded narrower, less intense peaks, consistent with more uniform but chemically simpler products. Optical evaluation affirmed urea as the optimal precursor, yielding a quantum efficiency near 40% (**Figure 43D**), far higher than BP-CNDs prepared with glycine, citric acid, or sucrose. UV–Vis spectra (**Figure 43E**) displayed broad UV absorption with clear π–π* and n–π* transitions, reflecting contributions from aromatic carbon domains and nitrogen-containing functional groups. Excitation–emission maps (**Figure 44**) also showed urea-BP-CNDs had broader, more intense fluorescence distributions than the others, particularly at 360 nm excitation, which was subsequently used for all fluorescence analyses. In conclusion, these findings establish that urea is the most effective additive for BP-CND synthesis, boosting nitrogen incorporation, surface defect states, and fluorescence efficiency.

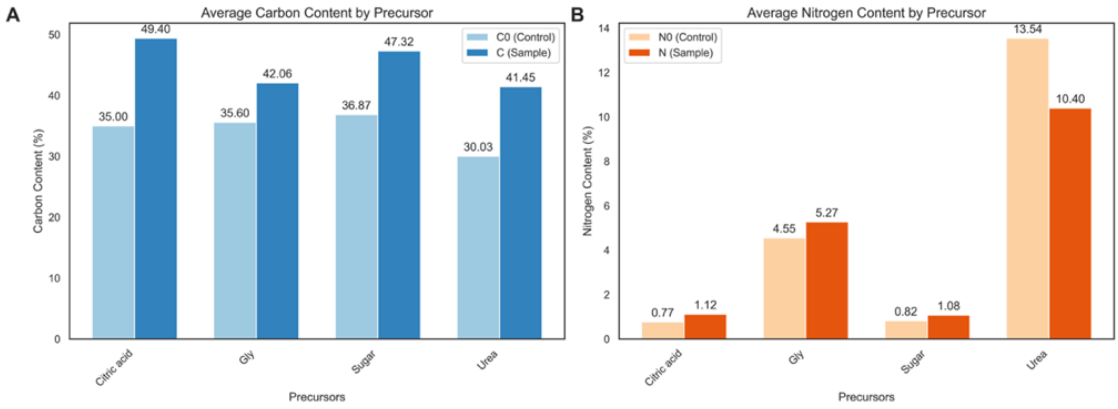


Figure 42. Carbon and nitrogen content (%) of BP-CNDs synthesized with different precursors (urea, citric acid, sugar, glycine), before and after heat treatment.

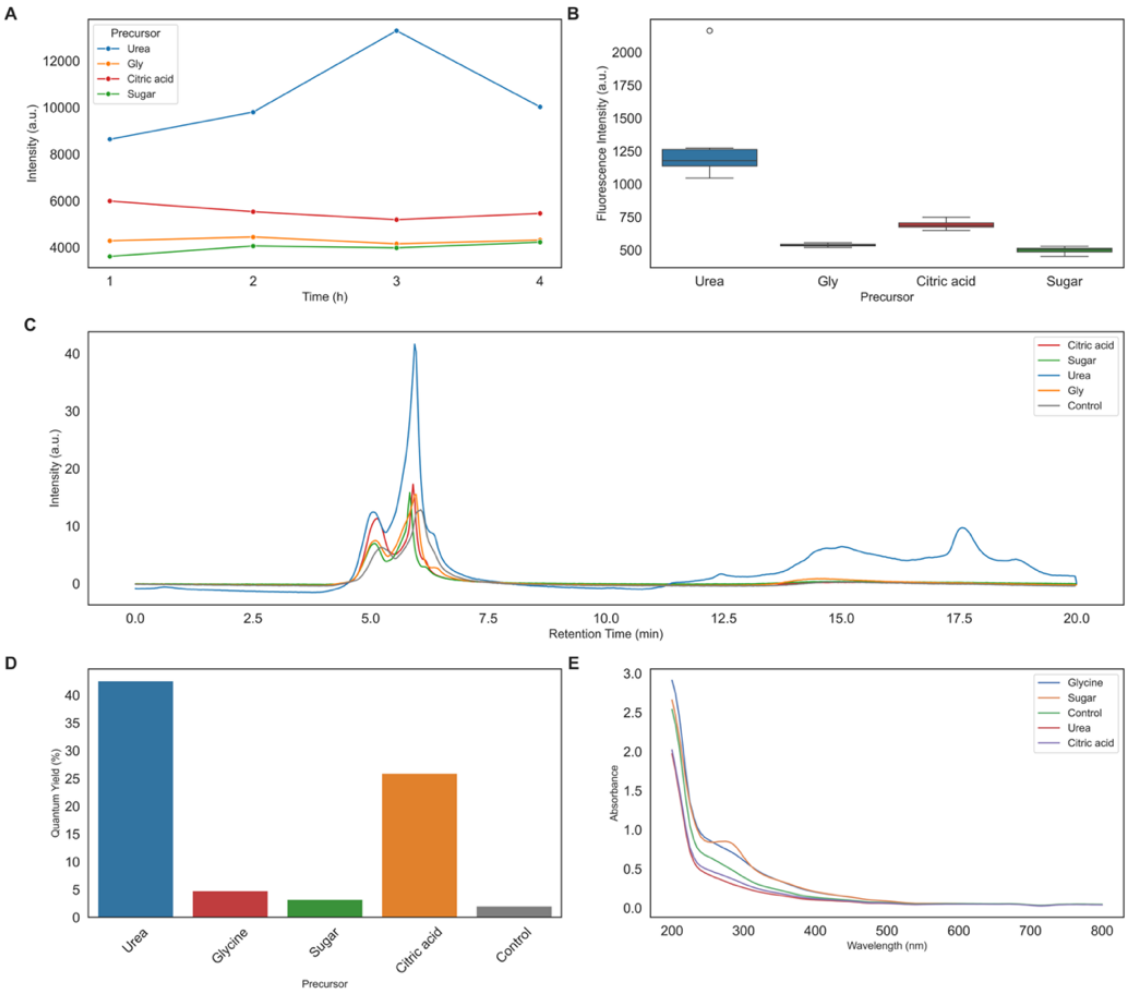


Figure 43. Effect of different precursors on banana peel-derived CNDs: (**A**) time-dependent fluorescence intensity (180 °C, 1–4 h); (**B**) box plot of fluorescence intensity grouped by precursor; (**C**) HPLC-SEC-FD chromatograms; (**D**) quantum yield (%) of CNDs from each precursor; (**E**) UV–Vis absorption spectra.

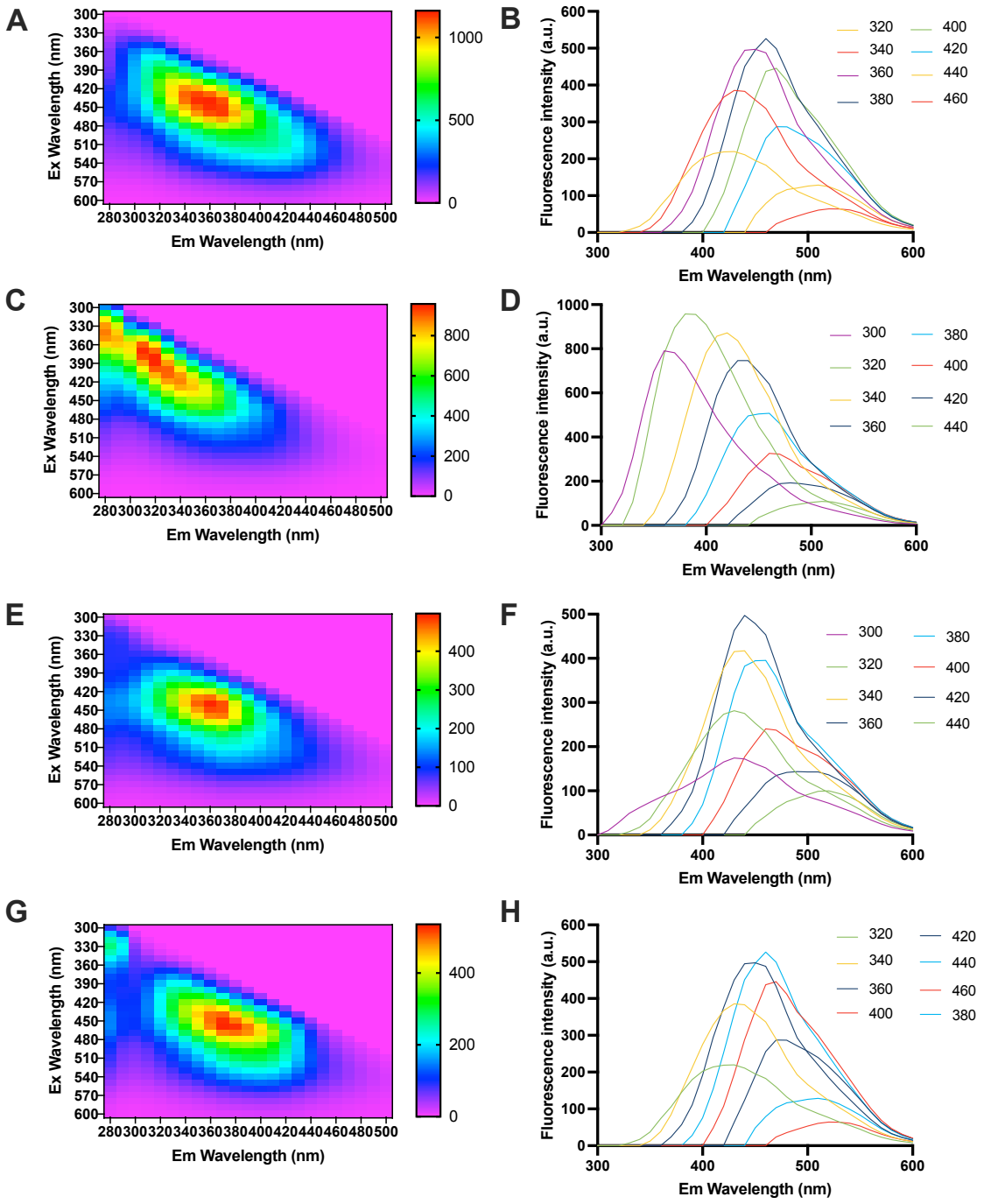


Figure 44. Excitation–emission matrix (EEM) maps and emission spectra of BP-CNDs prepared with different precursors: (A–B) urea, (C–D) citric acid, (E–F) sugar, and (G–H) glycine. In panels B, D, F, and H, each colored curve represents an emission spectrum recorded at a different excitation wavelength (nm).

4.4.2.2.3. Optimization with Central Composite Design (CCD)

After identifying urea as the preferred precursor, a Central Composite Design (CCD) was applied to optimize three synthesis parameters: mass ratio (urea:BP), pyrolysis

temperature, and reaction time. The quadratic regression model demonstrated strong predictive performance ($R^2 = 0.886$), with actual vs. predicted intensity values aligning closely (**Figure 45**). The fitted quadratic regression equation in coded form was:

$$Y = 9057.30 + 4147.28 \times A + 272.20 \times B + 1900.59 \times C + 592.56 \times A^2 + 143.28 \times AB + 1456.38 \times AC - 572.51 \times B^2 + 892.25 \times BC - 1193.28 \times C^2$$

where A, B, and C represent the coded values for mass ratio, reaction time, and temperature, respectively.

Analysis of variance (ANOVA, **Figure 46)** revealed that mass ratio and reaction temperature were statistically significant factors ($p < 0.001$ and $p = 0.002$, respectively), while reaction time showed limited impact. Importantly, the interaction between mass ratio and reaction temperature was also significant ($p = 0.023$), highlighting their synergistic role in enhancing fluorescence.

Response surface contour plots (**Figure 47**) confirmed that increasing both urea content and pyrolysis temperature synergistically boosted fluorescence intensity, whereas extending reaction time had little additional effect. The correlation matrix (**Figure 48**) further supported these results: mass ratio ($r = 0.80$) showed the strongest positive association with intensity, followed by temperature ($r = 0.31$), while reaction time ($r = 0.13$) was negligible.

The optimized synthesis conditions were identified as: BP:urea mass ratio of 4:2 (w/w), pyrolysis temperature of 200 °C, and reaction time of 3 h, yielding a predicted maximum fluorescence intensity of ~16,696 a.u. These results demonstrate that precursor composition and temperature are the dominant factors, consistent with previous reports emphasizing the role of nitrogen doping and thermal treatment in controlling CNDs emission properties (Y. Liu et al., 2022; Papaioannou et al., 2019; Ren et al., 2020).

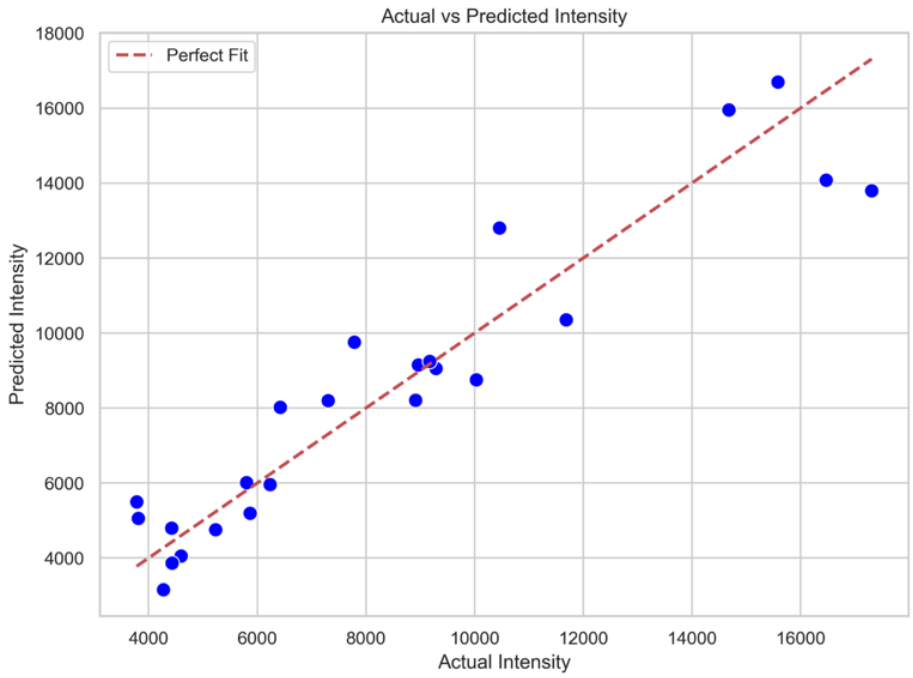


Figure 45. Predicted vs. observed fluorescence intensity for urea-BP-CNDs under varying mass ratio, time, and temperature conditions from CCD modeling.

OLS Regression Results

Dep. Variable:	actual_intensity	R-squared:	0.886
Model:	OLS	Adj. R-squared:	0.812
Method:	Least Squares	F-statistic:	12.05
Date:	Mon, 30 Jun 2025	Prob (F-statistic):	3.59e-05
Time:	20:46:45	Log-Likelihood:	-207.41
No. Observations:	24	AIC:	434.8
Df Residuals:	14	BIC:	446.6
Df Model:	9		
Covariance Type:	nonrobust		

	coef	std err	t	P>|t|	[0.025	0.975]
const	9057.3007	938.309	9.653	0.000	7044.828	1.11e+04
A_coded	4147.2813	470.081	8.822	0.000	3139.059	5155.504
B_coded	272.2049	502.039	0.542	0.596	-804.562	1348.972
C_coded	1900.5913	488.309	3.892	0.002	853.272	2947.910
A_coded^2	592.5591	781.412	0.758	0.461	-1083.402	2268.520
A_coded B_coded	143.2842	602.520	0.238	0.815	-1148.992	1435.560
A_coded C_coded	1456.3845	568.505	2.562	0.023	237.062	2675.707
B_coded^2	-572.5126	780.908	-0.733	0.476	-2247.395	1102.369
B_coded C_coded	892.2471	634.301	1.407	0.181	-468.193	2252.688
C_coded^2	-1193.2813	812.646	-1.468	0.164	-2936.234	549.672

Omnibus:	1.572	Durbin-Watson:	2.610
Prob(Omnibus):	0.456	Jarque-Bera (JB):	0.812
Skew:	0.448	Prob(JB):	0.666
Kurtosis:	3.095	Cond. No.	5.19

Figure 46. Full ANOVA table with F-values. Three variables include A: mass ratio, B: reaction time, and C: reaction temperature.

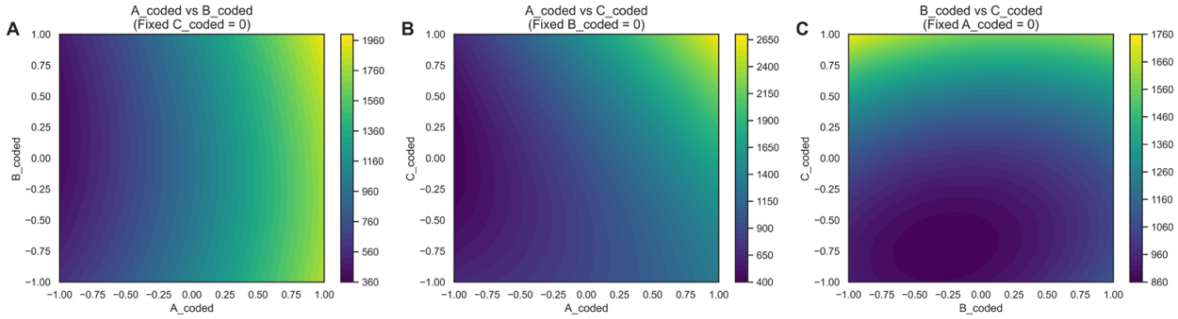


Figure 47. Response surface contour plots of predicted intensity for carbon nanodots produced from banana peel with urea added (U-BP-CNDs), illustrating interactions of coded mass ratios (A), reaction time (B), and temperatures (C) from Central Composite Design (CCD).

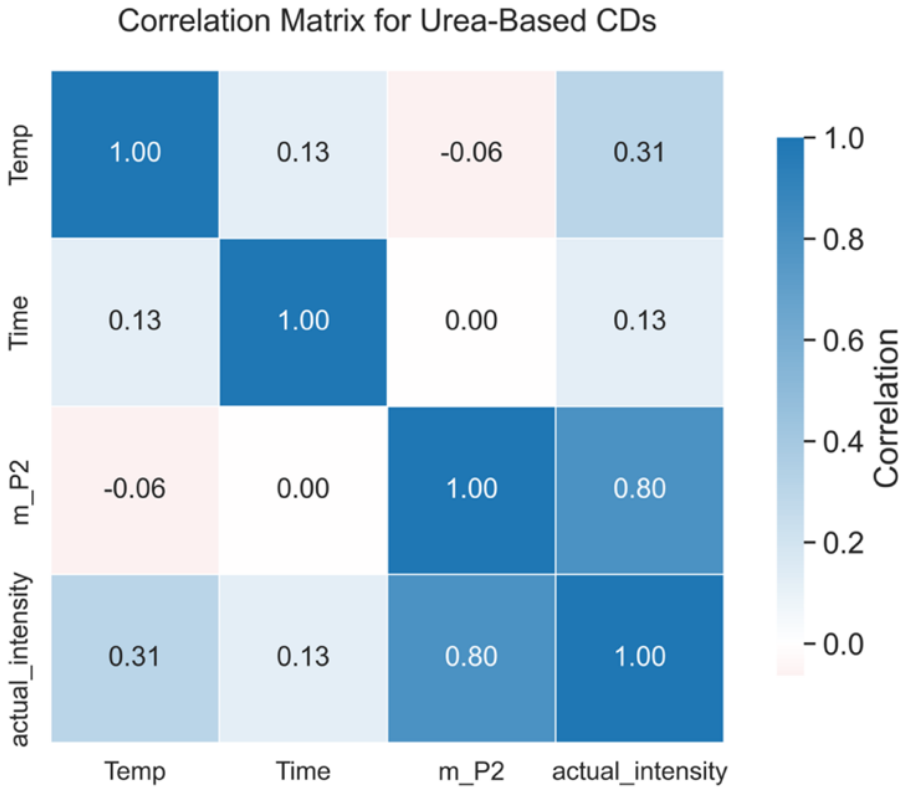


Figure 48. Correlation matrix of experimental factors (m_P2 = BP:urea mass ratio (w/w), reaction time, and temperature) and fluorescence intensity (predicted and measured) for banana-peel-derived carbon nanodots synthesized with urea in the central composite design (CCD) study.

4.4.2.2.4. Machine Learning Model Screening and Application

To further validate and extend CCD findings, seven machine learning (ML) models were trained on the CCD dataset: Linear Regression, K-Nearest Neighbors (KNN), Support Vector Regression (SVR), Decision Tree, Random Forest, Gradient Boosting, and Artificial Neural Network (ANN). Their predictive performance was evaluated using R^2 and RMSE values (**Table 11**). The Random Forest model achieved the best performance, with an R^2 of 0.843 and RMSE of 1209.37, outperforming all other approaches. Gradient Boosting also performed strongly (R^2 = 0.776), while simpler models such as Linear Regression and KNN offered only moderate accuracy. SVR and ANN models failed to capture the nonlinear patterns, yielding negative R^2 values.

Figure 49 illustrates the strong agreement between predicted and experimental values for the Random Forest model, with data points clustering along the identity line. Feature importance analysis (**Figure 50**) identified the urea:BP mass ratio as the most critical parameter, followed by temperature and reaction time, closely mirroring CCD statistical outcomes. This confirms the reliability of ensemble ML models for extracting key trends from complex experimental datasets.

Table 11. RMSE and R^2 for seven machine learning models predicting fluorescence intensity of BP-CNDs

Model	**RMSE**	**R^2**
Random Forest	1209.365831	0.843477
Gradient Boosting	1446.158552	0.776182
Decision Tree	1872.747239	0.624663
Linear Regression	1996.618776	0.573368
K-Neighbors Regression	2080.528265	0.536756
Support Vector Regression	3225.932897	-0.113714
ANN (MLPRegressor)	6257.512279	-3.190505

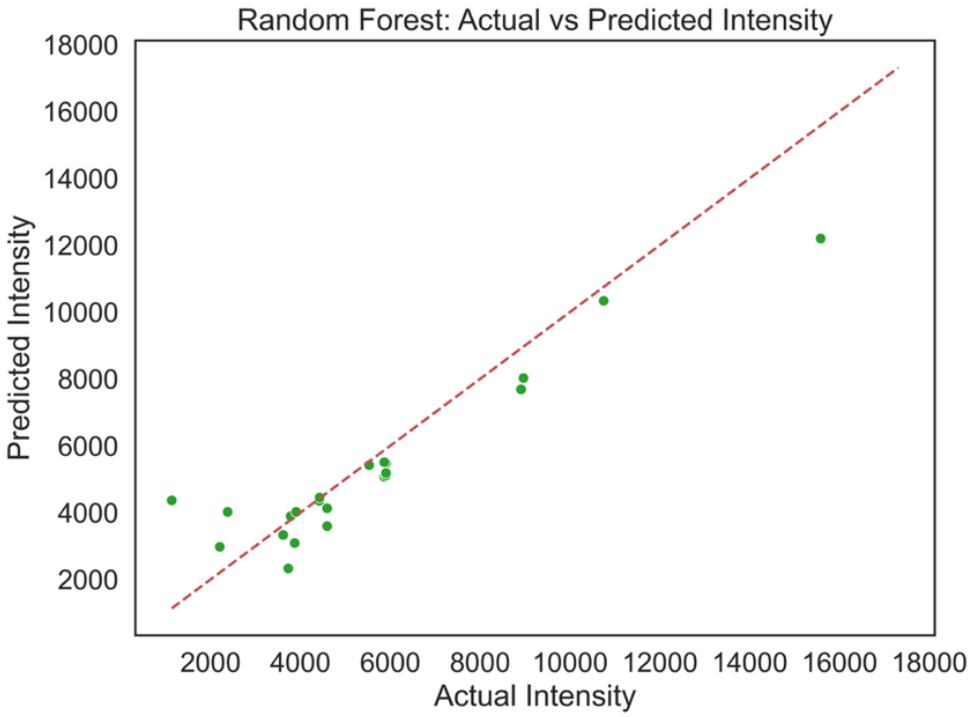


Figure 49. Random Forest regression model performance: predicted vs. experimental fluorescence intensities of BP-CNDs.

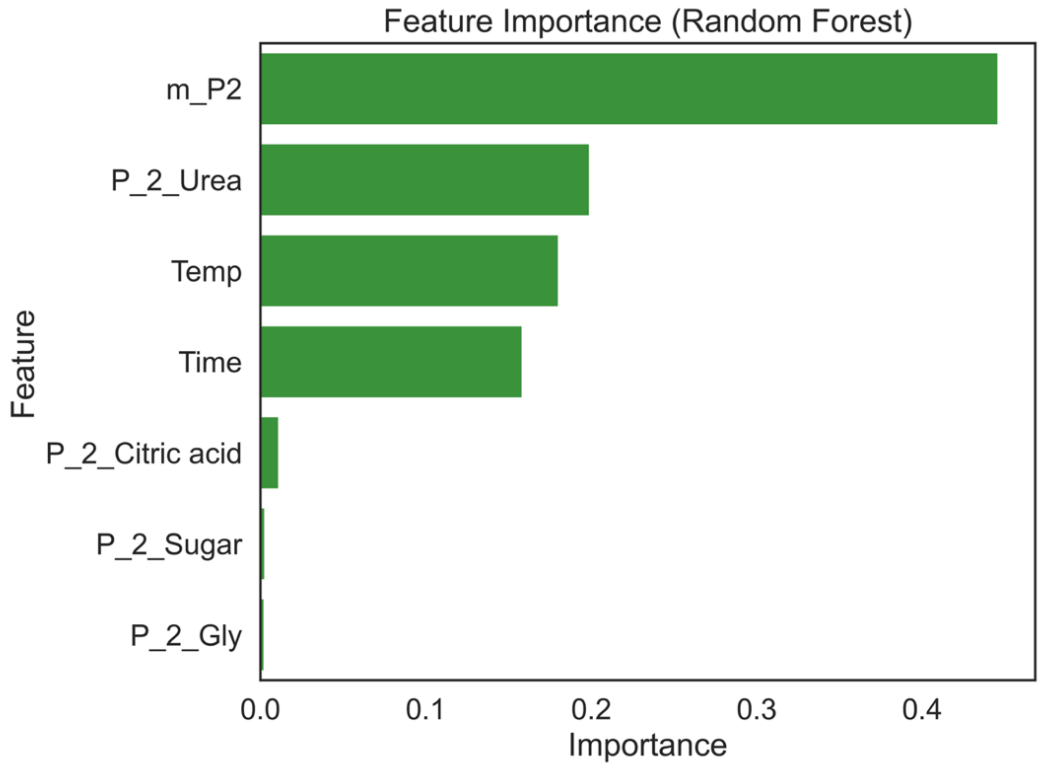


Figure 50. Feature Importance from Random Forest Model for Predicting Carbon Dot Intensity synthesis from Banana Peel and Urea

The combined use of Central Composite Design (CCD) and machine learning (ML) provides a robust framework for understanding and optimizing the synthesis of banana peel-derived carbon nanodots (BP-CNDs). Initial screening clearly established urea as the most effective precursor, producing significantly higher fluorescence compared to citric acid, glycine, and sugar. This superior performance can be explained by urea's dual role as a carbon and nitrogen source, which promotes nitrogen doping during pyrolysis and creates surface passivation states that enhance photoluminescence. Elemental analysis supported this conclusion, with urea-treated samples showing nitrogen contents exceeding 10%, far higher than the other treatments (<5%). Nitrogen incorporation into the CND lattice is widely recognized as a key driver of optical enhancement, consistent with reports where nitrogen-doped CNDs demonstrated increased quantum yields and altered emission spectra (Prado et al., 2023; Yorozuya et al., 2025). In this case study, the quantum yield of urea-assisted BP-CNDs approached 40%, a value notably higher than most biomass-derived CNDs such as lemon juice (14–25%) (Hoan et al., 2019), and even comparable to synthetic systems where external nitrogen doping raised yields from ~3% to >35% (Y. Liu et al., 2022).

Optimization with CCD provided a statistical understanding of process-variable effects. Both mass ratio and pyrolysis temperature emerged as critical factors, while reaction time contributed minimally beyond 3 hours, suggesting rapid saturation of the carbonization and doping process. This is in line with other experimental studies showing that precursor ratios and thermal intensity govern CNDs yield and emission behavior more strongly than reaction duration (Papaioannou et al., 2019; Ren et al., 2020).

The CCD-generated response surfaces and correlation analyses highlighted a synergistic effect between urea loading and temperature, with the optimal synthesis window at a 4:2 banana peel-to-urea ratio and 200 °C pyrolysis. This condition produced highly fluorescent CNDs without requiring excessive energy input, supporting the strategy's scalability and alignment with green chemistry principles.

Machine learning added predictive power and generalization to the CCD findings. Among the seven models tested, ensemble-based approaches-particularly Random Forest-showed the best performance ($R^2 = 0.843$, RMSE ≈ 1209), surpassing both linear regression and single-tree models. Feature importance analysis confirmed that mass ratio was the dominant predictor, followed by temperature and, to a lesser extent, reaction time, reinforcing the experimental and CCD results. Although Gradient Boosting also performed strongly, Random Forest offered a more balanced trade-off between accuracy

and interpretability. This performance is consistent with recent reports where tree-based ensemble methods have outperformed traditional regression in modeling fluorescence properties of CNDs (Chen et al., 2023; Hong et al., 2022; Senanayake et al., 2022). Unlike deep neural networks, which require large datasets and extensive tuning, Random Forest remains computationally efficient and interpretable, making it especially well-suited for experimental datasets with limited sample sizes.

This work shows that combining Central Composite Design with machine-learning delivers a powerful, low-waste pathway to engineer high-performance CNDs from food by-products. CCD quantified the effects of key synthesis variables, while ML provided accurate prediction and feature ranking-forming a feedback loop that cut trial-and-error and sharpened mechanistic insight. Using banana peel as a model feedstock, the optimized BP-CNDs achieved strong fluorescence, high quantum yield, and good photostability, matching or exceeding many conventionally synthesized dots. Beyond the technical gains, this approach advances circular economy goals by valorizing agricultural waste into low-cost, green nanomaterials suited for sensing, bioimaging, and smart packaging. In short, the integration of designed experiments and data-driven modeling offers a scalable blueprint for sustainable, application-ready nanotechnology.

5. CONCLUSION AND RECOMMENDATIONS

5.1. Research contribution

This dissertation contributes to the emerging field of food-derived nanomaterials by systematically exploring the formation, detection, and application of carbon nanodots (CNDs) within the food system. Three key areas of novelty are highlighted:

1. **Synthesis and Characterization of Green CNDs:** We demonstrated that CNDs can be effectively synthesized via Maillard reaction models and pyrolysis of food waste, with glycine identified as a superior nitrogen-rich precursor. Detailed characterization using TEM, FTIR, Raman, UV–Vis, XRD and fluorescence spectroscopy revealed nanoscale particles (3–5 nm) with strong blue-green emission and surface functional groups essential for solubility and stability.
2. **Analytical methods**: Developed and validated fluorescence spectroscopy and HPLC-SEC-FD protocols for sensitive and reliable quantification of CNDs in complex food matrices.
3. **Detection of Naturally Occurring CNDs in Foods:** For the first time, CND concentrations were systematically reported across seven food categories, with significant variation depending on food composition and processing intensity. This provides baseline data for assessing dietary exposure. Case studies on coffee brewing advanced mechanistic understanding of precursor, temperature, and processing effects.
4. **Applications in Food and Agriculture:** Glycine-derived CNDs were successfully applied as a rapid and selective sensor for caffeine, demonstrating a detection limit of 36.5 nM-superior to many previously reported carbon-based probes. Furthermore, banana peel was valorized as a sustainable feedstock for CNDs, with Central Composite Design (CCD) and machine learning approaches employed to optimize synthesis, reducing experimental burden while enhancing yield.

Together, these findings advance both the fundamental understanding of CND formation in foods and their potential use as functional nanomaterials in food safety, sensing, and valorization strategies.

5.2. Limitations and Future Research

While the study provides important insights, several limitations should be acknowledged:

- **Matrix complexity:** Detection of CNDs in food is complicated by coexisting fluorophores such as melanoidins, requiring further refinement of separation and purification methods.
- **Toxicological assessment:** Although food-derived CNDs are generally regarded as safe, systematic studies on cytotoxicity, genotoxicity, and bioavailability remain limited. Long-term safety evaluations are necessary before industrial applications.
- **Scalability:** Laboratory-scale pyrolysis and extraction methods may not directly translate to industrial-scale production. Energy efficiency, cost, and reproducibility need optimization.
- **Machine learning models:** Although Random Forest provided robust predictions, larger datasets and more advanced ML frameworks (e.g., deep learning, transfer learning) could further enhance predictive accuracy and generalization.

Future research directions include:

1. Development of standardized reference materials and certified methods for CND detection in food.
2. Expansion of toxicological and bioaccessibility studies across different food-derived CNDs.
3. Exploration of hybrid synthesis approaches combining food waste valorization with surface functionalization for targeted applications (e.g., pathogen detection, smart packaging).
4. Integration of advanced machine learning and artificial intelligence to accelerate optimization and predictive modeling of nanomaterial's properties.

5.3. Conclusion

5.3.1. Synthesis and Characterization of Green Carbon Nanodots (CNDs)

This dissertation demonstrated that carbon nanodots (CNDs) can be synthesized sustainably from safe food-grade precursors and agricultural residues. Glycine was identified as a particularly effective precursor, producing uniform, stable, and highly fluorescent nanodots. Valorization of banana peel further confirmed the feasibility of converting biowaste into functional nanomaterials, highlighting both low-cost production and alignment with green chemistry principles.

5.3.2. Development of Detection Methods for Carbon Nanodots (CNDs) in Foods

Two validated approaches - fluorescence spectroscopy and HPLC-SEC-FD - were successfully developed for quantitative detection of CNDs in food matrices. Both methods achieved high reproducibility and sensitivity, with HPLC-SEC-FD providing enhanced selectivity by separating nanoscale fractions from interfering compounds. In complex food matrices, the effective limits of detection are primarily constrained by matrix background signals and potential interferences; therefore, fluorescence spectroscopy is most suitable for simpler or pre-treated matrices, while HPLC-SEC-FLD offers more reliable low-level detection in complex samples through size-based separation. These protocols establish the first reliable analytical framework for monitoring CNDs in foods and enable systematic assessment of dietary exposure.

5.3.3. Detection and Formation Mechanisms of CNDs in Food Products

CNDs were detected across a broad range of food categories, with concentrations strongly influenced by processing methods and thermal conditions. Bread crust, biscuits, chocolate, cola, and black tea emerged as significant dietary sources, in some cases reaching tens of thousands of μg/kg. Experimental case studies on breadmaking and coffee brewing confirmed that Maillard chemistry, caramelization, and pyrolysis underpin CND formation, with precursor composition, temperature, and time shaping yield and optical properties. Correlation analyses revealed complex interactions with caffeine, pH, TDS, and browning index, advancing mechanistic understanding of how nanodots arise in real food systems.

5.3.4. Applications in Food and Agriculture

Applications developed in this work demonstrate the promise of food-derived CNDs as functional nanomaterials. A Gly-CND–based fluorescence assay enabled rapid, sensitive, and low-cost detection of caffeine in beverages, with performance comparable to HPLC.

Additionally, integration of Central Composite Design (CCD) and Machine Learning (ML) established an efficient framework for optimizing nanodot synthesis from banana peel, reducing experimental burden while maximizing yield and quantum efficiency. Collectively, these applications illustrate how food-derived CNDs can serve as safe, sustainable tools for biosensing, food quality monitoring, and circular bioeconomy-driven nanomaterial innovation.

6. NEW SCIENTIFIC RESULTS

1. I found that six amino acids - tyrosine, proline, glycine, arginine, glutamine, and phenylalanine - reacting with sucrose under Maillard-reaction conditions form fluorescent CNDs with distinct excitation-dependent emission spectra, using excitation wavelengths of 340 nm (Tyr), 360 nm (Pro, Gly), and 380 nm (Arg, Gln, Phe). Glycine–sucrose-derived CNDs (Gly-CNDs) showed the highest fluorescence intensity (2024.0 ± 3.7 a.u.), identifying glycine as the optimal amino acid precursor.
2. I synthesized and characterized Gly-S-CNDs from glycine and sucrose as ~ 4 nm spherical, nitrogen-doped nanodots with blue fluorescence ($\lambda_{em} \approx 448$ nm at 360 nm excitation) and a UV–Vis band near 280 nm extending into the visible region. Raman/XRD confirmed semi-graphitic, mainly amorphous carbon, while elemental/FTIR analyses showed nitrogen- and oxygen-containing surface groups; HPLC-SEC-FD isolated a single fluorescent fraction, confirming identity and purity. The nanodots retained fluorescence in 0.1–1.0 M NaCl and over time, with maximal intensity at pH 4 and a nearly constant emission maximum (~440 nm) from pH 4–11, indicating a stable emissive core with pH-sensitive surface states.
3. I developed and validated two complementary methods for quantifying CNDs in foods using purified Gly-S-CNDs as the calibration standard. A fluorescence spectroscopy method (λ_{ex} = 360 nm) enabled bulk CNDs quantification with excellent linearity (R^2 = 0.9995), low LOD/LOQ (down to ~0.14 mg/kg), and high precision (RSD < 0.1%), revealing that CNDs were absent in dough but formed during baking, reaching 501 mg/kg DW in breadcrumbs and 1,829 mg/kg DW in bread crust. In parallel, I established an HPLC-SEC-FD method that separates CNDs by size and quantifies them with very high sensitivity (R^2 = 1.000, LOD = 0.068 mg/kg), accuracy (coffee spike-recovery ~98 -101%), and robustness (low inter- and intra-laboratory variability), demonstrating a practically superior approach for selective CNDs monitoring in complex food matrices.
4. Using the validated HPLC-SEC-FD method, I showed that CNDs are widespread in thermally processed foods, with the highest levels in coffee (~3,860mg/kg), followed by extracted tea leaves, dark chocolate, and bread (501 mg/kg in breadcrumb, 1,829 mg/kg in bread crust), confirming the key role of heating. By synthesizing four model nanodots (Gly-S-CNDs, Gly-C-CNDs, U-C-CNDs, Lys-C-CNDs), I demonstrated that precursor composition and citric acid strongly modulate optical properties,

supporting distinct formation pathways. Integrating model and food data, I proposed a unified framework in which Maillard reactions, caramelization, pyrolysis, and wet-heat brewing (coffee, ≥ 90 °C, ~3.2 nm C-CNDs) all contribute to CNDs formation. I further showed that coffee brewing parameters markedly affect C-CNDs yield (higher for Arabica, coarse grinds, and a 1:15 ratio at 80 °C for 300 s) and that fluorescence is inversely correlated with caffeine (r = - 0.8), indicating caffeine-induced quenching and the potential of coffee-derived CNDs as caffeine sensors.

5. I developed a rapid, highly selective caffeine sensing system based on Gly-S-CNDs. The method showed a linear response from 50–2060 nM (R^2 = 0.9929) with LOD = 36.5 nM and LOQ = 122.1 nM, outperforming reported CND-based caffeine sensors. Optimized conditions (pH 5.0, 25 min incubation, 40 °C) enabled accurate caffeine quantification in commercial energy drinks, teas, and a "fake coffee" sample, with 8-fold fluorescence enhancement, good agreement with HPLC ($p > 0.05$), and recoveries of 95.9–102.7% (RSD < 2%, n = 5), confirming suitability for real-world applications.
6. I screened ten food-waste categories as precursors for CNDs via pyrolysis (200 °C, 2 h) and HPLC-SEC-FD and found that all produced CNDs, with protein- and polyphenol-rich wastes giving the highest fluorescence and lipid-rich the lowest. Citric acid co-treatment strongly enhanced yields, especially for polyphenol-, mineral-, and fiber-rich wastes, while sucrose had limited or negative effects. Thus, protein/polyphenol-rich wastes plus citric acid were identified as key levers for maximizing food-waste-derived CNDs production.
7. I upcycled banana peel into highly fluorescent CNDs by optimizing co-pyrolysis conditions with nitrogen/acid precursors using Central Composite Design and machine learning. Urea produced the brightest BP-CNDs, with a dominant SEC peak, elevated nitrogen (~10.3%), and a quantum yield of 40%, outperforming glycine, citric acid, and sucrose (<5.2% N). CCD identified an optimal urea:banana peel ratio of 4:2 (w/w), 200 °C, 3 h, yielding ~16,700 a.u. fluorescence, while Random Forest models (R^2 = 0.843) highlighted mass ratio and temperature as key predictors. This integrated strategy enables efficient, data-driven upcycling of banana peel into CNDs with reduced experimental workload.

7. PRACTICAL RESULTS

- I developed an environmentally friendly and cost-effective process to convert banana peel and other food waste into carbon nanodots (CNDs), using pyrolysis and food-grade precursors like urea and glycine. This sustainable approach not only addresses food waste disposal issues but also creates high-quality nanomaterials that can be used in various applications, ranging from food safety to biomedical fields.
- I quantified CND concentrations in various everyday foods such as bread crust, coffee, tea, and chocolate, providing critical baseline data for food safety assessments. This data can be leveraged by food scientists, nutritionists, and regulatory bodies to assess the potential dietary exposure to CNDs, enabling the development of standards and guidelines for safe consumption in food products.
- I validated a fast, cost-effective fluorescence-based assay using glycine-sucrose derived CNDs, which can be used as an alternative or complement to traditional HPLC methods in food quality control laboratories. This assay demonstrated high selectivity, sensitivity, and reproducibility for caffeine detection in various beverage matrices, making it a practical tool for routine monitoring of caffeine levels in commercial beverages such as energy drinks, teas, and coffee.
- I identified key parameters such as temperature, precursor composition, and water ratio that influence the formation of CNDs during food processing. This provides valuable insights into how food preparation techniques, such as baking or brewing, can be optimized to either enhance or mitigate CND formation. These findings offer practical strategies for food manufacturers to control the formation of nanomaterials in their products, with implications for both product safety and functionality.
- I applied a robust experimental design combined with machine learning models to optimize the synthesis of CNDs from food waste. This framework not only improved the efficiency of the process but also minimized experimental workload by reducing the need for extensive trial-and-error. This data-driven approach can be applied to the production of other nanomaterials, accelerating innovation in sustainable food nanotechnology and providing a scalable model for future applications in food and agriculture.

8. SUMMARY

This dissertation explores the emerging field of food-derived carbon nanodots (CNDs), focusing on their synthesis, detection, occurrence in foods, and applications within the food and agricultural sectors. CNDs are fluorescent nanomaterials generated during thermal processing, yet their pathways of formation, dietary prevalence, and analytical detection have remained largely underexplored. By integrating model systems, real food matrices, advanced analytical tools, and sustainable valorization strategies, this work provides a comprehensive understanding of CNDs in the context of food science and nanotechnology.

The first part of the research addressed the sustainable synthesis and characterization of CNDs from food-grade precursors and food waste. Model Maillard systems demonstrated that glycine was the most effective amino acid for producing small, stable, and strongly fluorescent CNDs, highlighting the role of nitrogen doping in enhancing optical properties. Banana peel was further valorized as a low-cost feedstock, confirming the feasibility of converting agricultural waste into nanomaterials. Advanced characterization using transmission electron microscopy, UV–Vis spectroscopy, Raman spectroscopy, FTIR, and fluorescence techniques revealed nanosized particles (3–5 nm) with strong blue-green emission and abundant surface functionalities that contribute to solubility and stability.

A second focus was the development of robust detection methods for quantifying CNDs in complex food matrices. Fluorescence spectroscopy was validated according to international standards, offering high sensitivity with detection limits down to 0.14 mg/dm³ in solution and 1.4 mg/kg in solid foods. To further enhance selectivity, a high-performance liquid chromatography platform coupled with size-exclusion separation and fluorescence detection (HPLC-SEC-FD) was established. This approach enabled reliable discrimination of CNDs from overlapping fluorescent compounds such as melanoidins, providing a reproducible and sensitive analytical framework for dietary exposure assessments.

The third part of the study investigated the occurrence and formation mechanisms of CNDs in real food systems. Using the validated methods, CNDs were detected in seven major food categories, including bakery products, beverages, chocolates, spices, cereals, and processed black foods. Concentrations varied widely, ranging from several tens of mg/kg to approximately 3,860 mg/kg, depending on food type and processing intensity. Controlled breadmaking experiments demonstrated that CNDs are absent in raw dough

but accumulate in crumb and crust, reflecting the influence of temperature and exposure time. A case study on coffee brewing further revealed that bean type, grind size, extraction ratio, and temperature significantly affect CND levels, supporting the role of Maillard and caramelization reactions as primary pathways for CND formation.

Finally, this work demonstrated practical applications of food-derived CNDs in the food and agricultural industry. Glycine-derived CNDs were employed as a fluorescent probe for rapid caffeine detection in beverages, achieving a detection limit of 36.5 nM, comparable to high-performance liquid chromatography but with lower cost and faster analysis. In parallel, the valorization of banana peel into CNDs was optimized using Central Composite Design (CCD) and machine learning approaches. These tools identified mass ratio and temperature as dominant factors influencing fluorescence yield, while predictive modeling reduced the need for exhaustive experimentation. The integration of experimental design with data-driven modeling offers a scalable and efficient route for sustainable nanomaterial production from agricultural waste.

In conclusion, this dissertation advances the fundamental understanding of food-derived CNDs, establishes reliable detection methods, and demonstrates their practical applications in sensing and waste valorization. It provides the first systematic quantification of CNDs across diverse food categories, confirms their formation through thermal processing pathways, and highlights their potential as safe, functional nanomaterials. The findings contribute to both food safety research and green nanotechnology, aligning with principles of sustainable development and the circular bioeconomy.

REFERENCES

1. Abinaya, S., Baby, A., Gurunathan, K., Sreeja, P. B., & Jose, S. P. (2022). Structural and morphological characterization of hydrothermally synthesized N-Carbon Dot @ Fe3O4 composites for heavy metal ion detection. *Materials Today: Proceedings*, *64*, 1854–1858. https://doi.org/10.1016/j.matpr.2022.06.321
2. Ahn, J., Song, Y., Kwon, J. E., Woo, J., & Kim, H. (2019). Characterization of food waste-driven carbon dot focusing on chemical structural, electron relaxation behavior and Fe3+ selective sensing. *Data in Brief*, *25*, 104038. https://doi.org/10.1016/j.dib.2019.104038
3. Alexander Ross, J. B., Laws, W. R., Rousslang, K. W., & Wyssbrod, H. R. (2002). Tyrosine Fluorescence and Phosphorescence from Proteins and Polypeptides. In J. R. Lakowicz (Ed.), *Topics in Fluorescence Spectroscopy* (Vol. 3, pp. 1–64). Kluwer Academic Publishers. https://doi.org/10.1007/0-306-47059-4_1
4. AOAC International. (2016). *Guidelines for Standard Method Performance Requirements. AOAC Official Methods of Analysis Appendix F, 1-18.* https://www.aoac.org/wp-content/uploads/2019/08/app_f.pdf
5. Astefanei, A., Núñez, O., & Galceran, M. T. (2015). Characterisation and determination of fullerenes: A critical review. *Analytica Chimica Acta*, *882*, 1–21. https://doi.org/10.1016/j.aca.2015.03.025
6. Atchudan, R., Jebakumar Immanuel Edison, T. N., Shanmugam, M., Perumal, S., Somanathan, T., & Lee, Y. R. (2021). Sustainable synthesis of carbon quantum dots from banana peel waste using hydrothermal process for in vivo bioimaging. *Physica E: Low-Dimensional Systems and Nanostructures*, *126*, 114417. https://doi.org/10.1016/j.physe.2020.114417
7. Bai, J., Ma, Y., Yuan, G., Chen, X., Mei, J., Zhang, L., & Ren, L. (2019). Solvent-controlled and solvent-dependent strategies for the synthesis of multicolor carbon dots for pH sensing and cell imaging. *Journal of Materials Chemistry C*, *7*(31), 9709–9718. https://doi.org/10.1039/C9TC02422K
8. Bao, L., Liu, C., Zhang, Z., & Pang, D. (2015). Photoluminescence-Tunable Carbon Nanodots: Surface-State Energy-Gap Tuning. *Advanced Materials*, *27*(10), 1663–1667. https://doi.org/10.1002/adma.201405070
9. Barros, K. M. A., Ribeiro Paulino, M., Batista, M. I. H. D. M., Gueiros, L. A. M., Souza, P. R. E. D., Leão, J. C., & De Albuquerque Tavares Carvalho, A. (2019). Absence of influence of polymorphisms of the MBL2 gene in oral infections by HSV-1 in individuals with HIV. *Brazilian Journal of Microbiology*, *50*(3), 663–668. https://doi.org/10.1007/s42770-019-00074-6
10. Bekedam, E. K., Schols, H. A., Van Boekel, M. A. J. S., & Smit, G. (2006). High Molecular Weight Melanoidins from Coffee Brew. *Journal of Agricultural and Food Chemistry*, *54*(20), 7658–7666. https://doi.org/10.1021/jf0615449
11. Bell, L. N., Wetzel, C. R., & Grand, A. N. (1996). Caffeine content in coffee as influenced by grinding and brewing techniques. *Food Research International*, *29*(8), 785–789. https://doi.org/10.1016/S0963-9969(97)00002-1

12. Bhatlawande, A. R., Ghatge, P. U., Shinde, G. U., Anushree, R. K., & Patil, S. D. (2024). Unlocking the future of smart food packaging: Biosensors, IoT, and nano materials. *Food Science and Biotechnology*, *33*(5), 1075–1091. https://doi.org/10.1007/s10068-023-01486-9
13. Bi, J., Li, Y., Wang, H., Song, Y., Cong, S., Yu, C., Zhu, B.-W., & Tan, M. (2018). Presence and Formation Mechanism of Foodborne Carbonaceous Nanostructures from Roasted Pike Eel (*Muraenesox cinereus*). *Journal of Agricultural and Food Chemistry*, *66*(11), 2862–2869. https://doi.org/10.1021/acs.jafc.7b02303
14. Bishnoi, S., Sharma, S., & Agrawal, H. (2023). Exploration of the Potential Application of Banana Peel for Its Effective Valorization: A Review. *Indian Journal of Microbiology*, *63*(4), 398–409. https://doi.org/10.1007/s12088-023-01100-w
15. Bosu, S., Rajamohan, N., Sagadevan, S., & Raut, N. (2023). Biomass derived green carbon dots for sensing applications of effective detection of metallic contaminants in the environment. *Chemosphere*, *345*, 140471. https://doi.org/10.1016/j.chemosphere.2023.140471
16. Buiculescu, R., Stefanakis, D., Androulidaki, M., Ghanotakis, D., & Chaniotakis, N. A. (2016). Controlling carbon nanodot fluorescence for optical biosensing. *The Analyst*, *141*(13), 4170–4180. https://doi.org/10.1039/C6AN00783J
17. Cao, L., Meziani, M. J., Sahu, S., & Sun, Y.-P. (2013). Photoluminescence Properties of Graphene versus Other Carbon Nanomaterials. *Accounts of Chemical Research*, *46*(1), 171–180. https://doi.org/10.1021/ar300128j
18. Cao, L., Song, X., Song, Y., Bi, J., Cong, S., Yu, C., & Tan, M. (2017). Fluorescent nanoparticles from mature vinegar: Their properties and interaction with dopamine. *Food & Function*, *8*(12), 4744–4751. https://doi.org/10.1039/C7FO01475A
19. Carolina Torres, A., Barsan, M. M., & Brett, C. M. A. (2014). Simple electrochemical sensor for caffeine based on carbon and Nafion-modified carbon electrodes. *Food Chemistry*, *149*, 215–220. https://doi.org/10.1016/j.foodchem.2013.10.114
20. Carvalho, P. M., Felício, M. R., Santos, N. C., Gonçalves, S., & Domingues, M. M. (2018). Application of Light Scattering Techniques to Nanoparticle Characterization and Development. *Frontiers in Chemistry*, *6*, 237. https://doi.org/10.3389/fchem.2018.00237
21. Cayuela, A., Soriano, M. L., Carrillo-Carrión, C., & Valcárcel, M. (2016). Semiconductor and carbon-based fluorescent nanodots: The need for consistency. *Chemical Communications*, *52*(7), 1311–1326. https://doi.org/10.1039/C5CC07754K
22. Chahal, S., Macairan, J.-R., Bui, H.-N. N., Smith, A., Larsson, H. C. E., Naccache, R., & Tufenkji, N. (2024). A comparison of carbon dot and CdTe quantum dot toxicity in *Drosophila melanogaster*. *Environmental Science: Advances*, *3*(6), 912–924. https://doi.org/10.1039/D4VA00017J
23. Chen, J., Zhang, M., Xu, Z., Ma, R., & Shi, Q. (2023). Machine-learning analysis to predict the fluorescence quantum yield of carbon quantum dots in biochar. *Science of The Total Environment*, *896*, 165136. https://doi.org/10.1016/j.scitotenv.2023.165136

24. Chu, L., Zhang, Y., He, L., Shen, Q., Tan, M., & Wu, Y. (2023). Carbon Quantum Dots from Roasted Coffee Beans: Their Degree and Mechanism of Cytotoxicity and Their Rapid Removal Using a Pulsed Electric Field. *Foods*, *12*(12), 2353. https://doi.org/10.3390/foods12122353
25. Cong, S., Bi, J., Song, X., Yu, C., & Tan, M. (2018). Ultrasmall fluorescent nanoparticles derived from roast duck: Their physicochemical characteristics and interaction with human serum albumin. *Food & Function*, *9*(4), 2490–2495. https://doi.org/10.1039/C8FO00178B
26. Cong, S., Wang, N., Wang, K., Wu, Y., Li, D., Song, Y., Prakash, S., & Tan, M. (2019). Fluorescent nanoparticles in the popular pizza: Properties, biodistribution and cytotoxicity. *Food & Function*, *10*(5), 2408–2416. https://doi.org/10.1039/C8FO01944D
27. De, B., & Karak, N. (2013). A green and facile approach for the synthesis of water soluble fluorescent carbon dots from banana juice. *RSC Advances*, *3*(22), 8286. https://doi.org/10.1039/c3ra00088e
28. De Boëver, R., Town, J. R., Li, X., & Claverie, J. P. (2022). Carbon Dots for Carbon Dummies: The Quantum and The Molecular Questions Among Some Others. *Chemistry – A European Journal*, *28*(47), e202200748. https://doi.org/10.1002/chem.202200748
29. De Yro, P. A. N., Quaichon, G. M. O., Cruz, R. A. T., Emolaga, C. S., Que, M. C. O., Magdaluyo, E. R., & Basilia, B. A. (2019). *Hydrothermal synthesis of carbon quantum dots from biowaste for bio-imaging*. 020007. https://doi.org/10.1063/1.5094310
30. Ding, H., Yu, S.-B., Wei, J.-S., & Xiong, H.-M. (2016). Full-color light-emitting carbon dots with a surface-state-controlled luminescence mechanism. *ACS Nano*, *10*(1), 484–491.
31. Dwandaru, W. S. B., Fauzi, F., Sari, D. S., Sari, E. K., Santoso, I., & Suhendar, H. (2019). Optical Properties Comparison of Carbon Nanodots Synthesized from Kangkung (Ipomoea aquatica) with Deep Frying and Roasting Techniques. *Jurnal Penelitian Fisika Dan Aplikasinya (JPFA)*, *9*(2), 123–131. https://doi.org/10.26740/jpfa.v9n2.p123-131
32. Etefa, H. F., Tessema, A. A., & Dejene, F. B. (2024). Carbon Dots for Future Prospects: Synthesis, Characterizations and Recent Applications: A Review (2019–2023). *C*, *10*(3), 60. https://doi.org/10.3390/c10030060
33. Fawaz, W., Hasian, J., & Alghoraibi, I. (2023). Synthesis and physicochemical characterization of carbon quantum dots produced from folic acid. *Scientific Reports*, *13*(1), 18641. https://doi.org/10.1038/s41598-023-46084-1
34. Ferrari, A. C., Rodil, S. E., & Robertson, J. (2003). Interpretation of infrared and Raman spectra of amorphous carbon nitrides. *Physical Review B*, *67*(15), 155306. https://doi.org/10.1103/PhysRevB.67.155306
35. Fu, M., Ehrat, F., Wang, Y., Milowska, K. Z., Reckmeier, C., Rogach, A. L., Stolarczyk, J. K., Urban, A. S., & Feldmann, J. (2015). Carbon Dots: A Unique Fluorescent Cocktail of Polycyclic Aromatic Hydrocarbons. *Nano Letters*, *15*(9), 6030–6035. https://doi.org/10.1021/acs.nanolett.5b02215

36. Gao, X., Zhang, H., Liu, L., Jia, M., Li, X., & Li, J. (2024). Nano-biosensor based on manganese dioxide nanosheets and carbon dots for dual-mode determination of Staphylococcus aureus. *Food Chemistry*, *432*, 137144. https://doi.org/10.1016/j.foodchem.2023.137144
37. Geng, X., Congdon, T. R., Anees, P., Greschner, A. A., Vetrone, F., & Gauthier, M. A. (2020). Surface *vs.* core N/S/Se-heteroatom doping of carbon nanodots produces divergent yet consistent optical responses to reactive oxygen species. *Nanoscale Advances*, *2*(9), 4024–4033. https://doi.org/10.1039/D0NA00439A
38. Gong, X., Hu, Q., Chin Paau, M., Zhang, Y., Zhang, L., Shuang, S., Dong, C., & Choi, M. M. F. (2014). High-performance liquid chromatographic and mass spectrometric analysis of fluorescent carbon nanodots. *Talanta*, *129*, 529–538. https://doi.org/10.1016/j.talanta.2014.04.008
39. González-González, R. B., González, L. T., Madou, M., Leyva-Porras, C., Martinez-Chapa, S. O., & Mendoza, A. (2022). Synthesis, Purification, and Characterization of Carbon Dots from Non-Activated and Activated Pyrolytic Carbon Black. *Nanomaterials*, *12*(3), 298. https://doi.org/10.3390/nano12030298
40. Groenewegen, J. (1972). The infrared spectrum of glycine chemisorbed by supported nickel. *Journal of Catalysis*, *27*(3), 369–373. https://doi.org/10.1016/0021-9517(72)90172-8
41. Habibi, B., Abazari, M., & Pournaghi-Azar, M. H. (2012). A Carbon Nanotube Modified Electrode for Determination of Caffeine by Differential Pulse Voltammetry. *Chinese Journal of Catalysis*, *33*(11–12), 1783–1790. https://doi.org/10.1016/S1872-2067(11)60438-5
42. Haiyang, L., Guantong, L., Nan, Z., Zhanye, Y., Xinge, J., Bing, Z., & Tian, Y. (2024). Ag-carbon dots with peroxidase-like activity for colorimetric and SERS dual mode detection of glucose and glutathione. *Talanta*, *273*, 125898. https://doi.org/10.1016/j.talanta.2024.125898
43. Han, M., Wang, L., Li, S., Bai, L., Zhou, Y., Sun, Y., Huang, H., Li, H., Liu, Y., & Kang, Z. (2017). High-bright fluorescent carbon dot as versatile sensing platform. *Talanta*, *174*, 265–273. https://doi.org/10.1016/j.talanta.2017.05.067
44. Han, Y., Tang, B., Wang, L., Bao, H., Lu, Y., Guan, C., Zhang, L., Le, M., Liu, Z., & Wu, M. (2020). Machine-Learning-Driven Synthesis of Carbon Dots with Enhanced Quantum Yields. *ACS Nano*, *14*(11), 14761–14768. https://doi.org/10.1021/acsnano.0c01899
45. Havrdová, M., Urbančič, I., Tománková, K. B., Malina, L., Poláková, K., Štrancar, J., & Bourlinos, A. B. (2022). Intracellular Trafficking of Cationic Carbon Dots in Cancer Cell Lines MCF-7 and HeLa—Time Lapse Microscopy, Concentration-Dependent Uptake, Viability, DNA Damage, and Cell Cycle Profile. *International Journal of Molecular Sciences*, *23*(3), 1077. https://doi.org/10.3390/ijms23031077
46. Hoan, B. T., Tam, P. D., & Pham, V.-H. (2019). Green Synthesis of Highly Luminescent Carbon Quantum Dots from Lemon Juice. *Journal of Nanotechnology*, *2019*, 1–9. https://doi.org/10.1155/2019/2852816
47. Hoan, B. T., Van Huan, P., Van, H. N., Nguyen, D. H., Tam, P. D., Nguyen, K. T., & Pham, V. (2018). Luminescence of lemon-derived carbon quantum dot and its

potential application in luminescent probe for detection of Mo $^{6+}$ ions. *Luminescence*, *33*(3), 545–551. https://doi.org/10.1002/bio.3444

48. Hola, K., Zhang, Y., Wang, Y., Giannelis, E. P., Zboril, R., & Rogach, A. L. (2014). Carbon dots—Emerging light emitters for bioimaging, cancer therapy and optoelectronics. *Nano Today*, *9*(5), 590–603. https://doi.org/10.1016/j.nantod.2014.09.004
49. Hong, Q., Wang, X.-Y., Gao, Y.-T., Lv, J., Chen, B.-B., Li, D.-W., & Qian, R.-C. (2022). Customized Carbon Dots with Predictable Optical Properties Synthesized at Room Temperature Guided by Machine Learning. *Chemistry of Materials*, *34*(3), 998–1009. https://doi.org/10.1021/acs.chemmater.1c03220
50. Hu, J.-H., Sun, Y., Qi, J., Pei, P.-X., Lin, Q., & Zhang, Y.-M. (2016). A colorimetric and "turn-on" fluorimetric chemosensor for the selective detection of cyanide and its application in food samples. *RSC Advances*, *6*(102), 100401–100406. https://doi.org/10.1039/C6RA16378E
51. Hu, Q., Paau, M. C., Choi, M. M. F., Zhang, Y., Gong, X., Zhang, L., Liu, Y., & Yao, J. (2014). Better understanding of carbon nanoparticles via high-performance liquid chromatography-fluorescence detection and mass spectrometry. *ELECTROPHORESIS*, *35*(17), 2454–2462. https://doi.org/10.1002/elps.201400197
52. Huang, Z., & Ren, L. (2025). Large Scale Synthesis of Carbon Dots and Their Applications: A Review. *Molecules*, *30*(4), 774. https://doi.org/10.3390/molecules30040774
53. Hui, Y. Y., Chang, H., Dong, H., & Zhang, X. (Eds). (2019). *Carbon Nanomaterials for Bioimaging, Bioanalysis, and Therapy* (1st edn). Wiley. https://doi.org/10.1002/9781119373476
54. ICH, I. (1995). *Topic Q 2 (R1) Validation of Analytical Procedures: Text and Methodology. European Medicines Agency*. CPMP/ICH/381/95.
55. ISO 20481:2008. (2017). *Coffee and coffee products Determination of the caffeine content using high performance liquid chromatography (HPLC) Reference method*. https ://www.iso.org/home.html.
56. Jaleel, J. A., & Pramod, K. (2018). Artful and multifaceted applications of carbon dot in biomedicine. *Journal of Controlled Release*, *269*, 302–321. https://doi.org/10.1016/j.jconrel.2017.11.027
57. Jamal, P., K. Saheed, O., & Alam, Z. (2011). Bio-Valorization Potential of Banana Peels (Musa sapientum): An Overview. *Asian Journal of Biotechnology*, *4*(1), 1–14. https://doi.org/10.3923/ajbkr.2012.1.14
58. Jiang, C., Wu, H., Song, X., Ma, X., Wang, J., & Tan, M. (2014). Presence of photoluminescent carbon dots in Nescafe® original instant coffee: Applications to bioimaging. *Talanta*, *127*, 68–74. https://doi.org/10.1016/j.talanta.2014.01.046
59. John, B. K., Abraham, T., & Mathew, B. (2022). A Review on Characterization Techniques for Carbon Quantum Dots and Their Applications in Agrochemical Residue Detection. *Journal of Fluorescence*, *32*(2), 449–471. https://doi.org/10.1007/s10895-021-02852-8

60. Jurkiewicz, K., Pawlyta, M., & Burian, A. (2018). Structure of Carbon Materials Explored by Local Transmission Electron Microscopy and Global Powder Diffraction Probes. *C*, *4*(4), 68. https://doi.org/10.3390/c4040068
61. Kalytchuk, S., Wang, Y., Poláková, K., & Zbořil, R. (2018). Carbon Dot Fluorescence-Lifetime-Encoded Anti-Counterfeiting. *ACS Applied Materials & Interfaces*, *10*(35), 29902–29908. https://doi.org/10.1021/acsami.8b11663
62. Kolanowska, A., Dzido, G., Krzywiecki, M., Tomczyk, M. M., Łukowiec, D., Ruczka, S., & Boncel, S. (2022). Carbon Quantum Dots from Amino Acids Revisited: Survey of Renewable Precursors toward High Quantum-Yield Blue and Green Fluorescence. *ACS Omega*, *7*(45), 41165–41176. https://doi.org/10.1021/acsomega.2c04751
63. Kumar, J. V., & Rhim, J.-W. (2024). Fluorescent carbon quantum dots for food contaminants detection applications. *Journal of Environmental Chemical Engineering*, *12*(2), 111999. https://doi.org/10.1016/j.jece.2024.111999
64. Laptinskiy, K. A., Burikov, S. A., Chugreeva, G. N., & Dolenko, T. A. (2022). The mechanisms of fluorescence quenching of carbon dots upon interaction with heavy metal cations. *Fullerenes, Nanotubes and Carbon Nanostructures*, *30*(1), 46–52. https://doi.org/10.1080/1536383X.2021.1995365
65. Li, D., Na, X., Wang, H., Xie, Y., Cong, S., Song, Y., Xu, X., Zhu, B.-W., & Tan, M. (2018). Fluorescent Carbon Dots Derived from Maillard Reaction Products: Their Properties, Biodistribution, Cytotoxicity, and Antioxidant Activity. *Journal of Agricultural and Food Chemistry*, *66*(6), 1569–1575. https://doi.org/10.1021/acs.jafc.7b05643
66. Li, D., Na, X., Zhou, W., Wang, C., Li, Y., Zhu, B.-W., & Tan, M. (2019). Adverse effects of fluorescent carbon dots from canned yellow croaker on cellular respiration and glycolysis. *Food & Function*, *10*(2), 1123–1131. https://doi.org/10.1039/C8FO02602E
67. Li, D., Xie, Y., Na, X., Li, Y., Dai, C., Li, Y., & Tan, M. (2019). Insights into melanoidin conversion into fluorescent nanoparticles in the Maillard reaction. *Food & Function*, *10*(7), 4414–4422. https://doi.org/10.1039/C9FO00383E
68. Li, S., Jiang, C., Wang, H., Cong, S., & Tan, M. (2018). Fluorescent nanoparticles present in Coca-Cola and Pepsi-Cola: Physiochemical properties, cytotoxicity, biodistribution and digestion studies. *Nanotoxicology*, *12*(1), 49–62. https://doi.org/10.1080/17435390.2017.1418443
69. Li, Y., Bi, J., Liu, S., Wang, H., Yu, C., Li, D., Zhu, B.-W., & Tan, M. (2017). Presence and formation of fluorescence carbon dots in a grilled hamburger. *Food & Function*, *8*(7), 2558–2565. https://doi.org/10.1039/C7FO00675F
70. Liao, H., Jiang, C., Liu, W., Vera, J. M., Seni, O. D., Demera, K., Yu, C., & Tan, M. (2015). Fluorescent Nanoparticles from Several Commercial Beverages: Their Properties and Potential Application for Bioimaging. *Journal of Agricultural and Food Chemistry*, *63*(38), 8527–8533. https://doi.org/10.1021/acs.jafc.5b04216
71. Liao, J., Yao, Y., Lee, C.-H., Wu, Y., & Li, P. (2021). In Vivo Biodistribution, Clearance, and Biocompatibility of Multiple Carbon Dots Containing Nanoparticles

for Biomedical Application. *Pharmaceutics*, *13*(11), 1872. https://doi.org/10.3390/pharmaceutics13111872

72. Lin, L., Wang, X.-X., Lin, S.-Q., Zhang, L.-H., Lin, C.-Q., Li, Z.-M., & Liu, J.-M. (2012). Research on the spectral properties of luminescent carbon dots. *Spectrochimica Acta Part A: Molecular and Biomolecular Spectroscopy*, *95*, 555–561. https://doi.org/10.1016/j.saa.2012.04.049
73. Liu, M. (2020). Optical Properties of Carbon Dots: A Review. *Nanoarchitectonics*, *1*(1), 1–12. https://doi.org/10.37256/nat.112020124.1-12
74. Liu, M. L., Yang, L., Li, R. S., Chen, B. B., Liu, H., & Huang, C. Z. (2017). Large-scale simultaneous synthesis of highly photoluminescent green amorphous carbon nanodots and yellow crystalline graphene quantum dots at room temperature. *Green Chemistry*, *19*(15), 3611–3617. https://doi.org/10.1039/C7GC01236E
75. Liu, Y., Yong, C., Tong, B., Li, Y., Wang, N., & Lei, Y. (2022). Modification of carbon dots derived from biomass by exogenous nitrogen doping: Action mechanism and difference analysis. *Optical Materials*, *134*, 113144. https://doi.org/10.1016/j.optmat.2022.113144
76. Liu, Y.-Y., Yu, N.-Y., Fang, W.-D., Tan, Q.-G., Ji, R., Yang, L.-Y., Wei, S., Zhang, X.-W., & Miao, A.-J. (2021). Photodegradation of carbon dots cause cytotoxicity. *Nature Communications*, *12*(1), 812. https://doi.org/10.1038/s41467-021-21080-z
77. Ma, X., Ma, Y., Dong, L., Chang, X., Yang, T., Cao, X., Feng, L., Hu, Z., & Hu, T. (2025). Novel hydroxyl and carboxyl group-enriched nitrogen-doped carbon dots N-CDs as highly efficient corrosion inhibitors for carbon steel Q235 in 1 M HCl. *Inorganic Chemistry Communications*, *175*, 114167. https://doi.org/10.1016/j.inoche.2025.114167
78. Ma, Z., Ma, Y., Gu, M., Huo, X., Ma, S., Lu, Y., Ning, Y., Zhang, X., Tian, B., & Feng, Z. (2020). Carbon Dots Derived from the Maillard Reaction for pH Sensors and Cr (VI) Detection. *Nanomaterials*, *10*(10), 1924. https://doi.org/10.3390/nano10101924
79. Margraf, J. T., Strauss, V., Guldi, D. M., & Clark, T. (2015). The Electronic Structure of Amorphous Carbon Nanodots. *The Journal of Physical Chemistry B*, *119*(24), 7258–7265. https://doi.org/10.1021/jp510620j
80. Mary Alex, A., Kiran, M. D., Hari, G., Krishnan, A., Jayan, J. S., & Saritha, A. (2020). Carbon dots: A green synthesis from Lawsonia inermis leaves. *Materials Today: Proceedings*, *26*, 716–719. https://doi.org/10.1016/j.matpr.2019.12.409
81. Matiacevich, S., & Pilarbuera, M. (2006). A critical evaluation of fluorescence as a potential marker for the Maillard reaction. *Food Chemistry*, *95*(3), 423–430. https://doi.org/10.1016/j.foodchem.2005.01.027
82. Meiling, T. T., Schürmann, R., Vogel, S., Ebel, K., Nicolas, C., Milosavljević, A. R., & Bald, I. (2018a). Photophysics and Chemistry of Nitrogen-Doped Carbon Nanodots with High Photoluminescence Quantum Yield. *The Journal of Physical Chemistry C*, *122*(18), 10217–10230. https://doi.org/10.1021/acs.jpcc.8b00748
83. Meiling, T. T., Schürmann, R., Vogel, S., Ebel, K., Nicolas, C., Milosavljević, A. R., & Bald, I. (2018b). Photophysics and Chemistry of Nitrogen-Doped Carbon

Nanodots with High Photoluminescence Quantum Yield. *The Journal of Physical Chemistry C*, *122*(18), 10217–10230. https://doi.org/10.1021/acs.jpcc.8b00748

84. Meng, L., & Wu, H. (2024). Preparation of carbon quantum dots and their application in the detection of vitamin B2. *RSC Advances*, *14*(22), 15499–15506. https://doi.org/10.1039/D4RA01388C
85. Mewada, A., Pandey, S., Shinde, S., Mishra, N., Oza, G., Thakur, M., Sharon, M., & Sharon, M. (2013). Green synthesis of biocompatible carbon dots using aqueous extract of Trapa bispinosa peel. *Materials Science and Engineering: C*, *33*(5), 2914–2917. https://doi.org/10.1016/j.msec.2013.03.018
86. Meydav, S., Saguy, I., & Kopelman, I. J. (1977). Browning determination in citrus products. *Journal of Agricultural and Food Chemistry*, *25*(3), 602–604. https://doi.org/10.1021/jf60211a030
87. Mintz, K. J., Bartoli, M., Rovere, M., Zhou, Y., Hettiarachchi, S. D., Paudyal, S., Chen, J., Domena, J. B., Liyanage, P. Y., Sampson, R., Khadka, D., Pandey, R. R., Huang, S., Chusuei, C. C., Tagliaferro, A., & Leblanc, R. M. (2021). A deep investigation into the structure of carbon dots. *Carbon*, *173*, 433–447. https://doi.org/10.1016/j.carbon.2020.11.017
88. Mondal, D., Datta, S., & Jana, D. (2025). Navigating the evolution of two-dimensional carbon nitride research: Integrating machine learning into conventional approaches. *Physical Chemistry Chemical Physics*, *27*(9), 4531–4566. https://doi.org/10.1039/D4CP04309J
89. Moradi, M., Molaei, R., Kousheh, S. A., T. Guimarães, J., & McClements, D. J. (2023). Carbon dots synthesized from microorganisms and food by-products: Active and smart food packaging applications. *Critical Reviews in Food Science and Nutrition*, *63*(14), 1943–1959. https://doi.org/10.1080/10408398.2021.2015283
90. MoziOğlu, E. (2022). Microwave-Based Synthesis of Carbon Dots From Lemon Juice For Biotechnological Applications. *Osmaniye Korkut Ata Üniversitesi Fen Bilimleri Enstitüsü Dergisi*, *5*(2), 600–611. https://doi.org/10.47495/okufbed.1024008
91. Mukherjee, P., Chakraborty, A., Chakraborty, M., & Mukhopadhyay, G. (2022). Carbon Dot—An Updated Review. *International Journal of Pharmaceutical Investigation*, *12*(2), 136–140. https://doi.org/10.5530/ijpi.2022.2.25
92. Murdock, R. C., Braydich-Stolle, L., Schrand, A. M., Schlager, J. J., & Hussain, S. M. (2008). Characterization of Nanomaterial Dispersion in Solution Prior to In Vitro Exposure Using Dynamic Light Scattering Technique. *Toxicological Sciences*, *101*(2), 239–253. https://doi.org/10.1093/toxsci/kfm240
93. Murkovic, M., & Derler, K. (2006). Analysis of amino acids and carbohydrates in green coffee. *Journal of Biochemical and Biophysical Methods*, *69*(1–2), 25–32. https://doi.org/10.1016/j.jbbm.2006.02.001
94. Nemati, F., Hosseini, M., Zare-Dorabei, R., Salehnia, F., & Ganjali, M. R. (2018). Fluorescent turn on sensing of Caffeine in food sample based on sulfur-doped carbon quantum dots and optimization of process parameters through response surface methodology. *Sensors and Actuators B: Chemical*, *273*, 25–34. https://doi.org/10.1016/j.snb.2018.05.163

95. Neumann, S., Menter, C., Mahmoud, A. S., Segets, D., & Rafaja, D. (2020). Microstructure characteristics of non-monodisperse quantum dots: On the potential of transmission electron microscopy combined with X-ray diffraction. *CrystEngComm*, *22*(21), 3644–3655. https://doi.org/10.1039/D0CE00312C
96. Nguyen, D., El-Ramady, H., & Prokisch, J. (2024). Food safety aspects of carbon dots: A review. *Environmental Chemistry Letters*. https://doi.org/10.1007/s10311-024-01779-3
97. Nguyen, D. H. H., El-Ramady, H., & Prokisch, J. (2025). Carbon nanodots derived from glycine for rapid detection of caffeine in beverages. *Journal of Food Composition and Analysis*, *145*, 107784. https://doi.org/10.1016/j.jfca.2025.107784
98. Nguyen, D. H. H., El-Ramady, H., Törős, G., Muthu, A., Elsakhawy, T., Abdalla, N., Alibrahem, W., Kharrat Helu, N., & Prokisch, J. (2025). Food-Derived Carbon Dots: Formation, Detection, and Impact on Gut Microbiota. *Foods*, *14*(17), 2980. https://doi.org/10.3390/foods14172980
99. Nguyen, D. H. H., Muthu, A., Elsakhawy, T., Sheta, M. H., Abdalla, N., El-Ramady, H., & Prokisch, J. (2025). Carbon Nanodots-Based Sensors: A Promising Tool for Detecting and Monitoring Toxic Compounds. *Nanomaterials*, *15*(10), 725. https://doi.org/10.3390/nano15100725
100. Nguyen, D., Muthu, A., El-Ramady, H., Béni, Á., & Prokisch, J. (2024). Detection and formation of fluorescent carbon nanodots in coffee brews and its relationship with other compositions. *Journal of Food Composition and Analysis*, *132*, 106347. https://doi.org/10.1016/j.jfca.2024.106347
101. Nguyen, D., Muthu, A., El-Ramady, H., Daróczi, L., Nagy, L., Kéki, S., Béni, Á., Csarnovics, I., & Prokisch, J. (2024). Optimization of extraction conditions to synthesize green carbon nanodots using the Maillard reaction. *Materials Advances*, 10.1039.D4MA00037D. https://doi.org/10.1039/D4MA00037D
102. Nicoli, M. C., Rosa, M. D., & Lerici, C. R. (1990). Influence of some processing conditions on solid-liquid extraction of coffee. *Lebensmittel-Wissenschaft+ Technologie= Food Science+ Technology*, *23*(5).
103. Othman, H. O. (2024). Fe-Doped Red Fluorescent Carbon Dots for Caffeine Analysis in Energy Drinks Using a Paper-Based Sensor. *Journal of Fluorescence*. https://doi.org/10.1007/s10895-024-04062-4
104. Pajewska-Szmyt, M., Buszewski, B., & Gadzała-Kopciuch, R. (2020). Carbon dots as rapid assays for detection of mercury(II) ions based on turn-off mode and breast milk. *Spectrochimica Acta Part A: Molecular and Biomolecular Spectroscopy*, *236*, 118320. https://doi.org/10.1016/j.saa.2020.118320
105. Papaioannou, N., Titirici, M.-M., & Sapelkin, A. (2019). Investigating the Effect of Reaction Time on Carbon Dot Formation, Structure, and Optical Properties. *ACS Omega*, *4*(26), 21658–21665. https://doi.org/10.1021/acsomega.9b01798
106. Park, S. Y., Lee, H. U., Park, E. S., Lee, S. C., Lee, J.-W., Jeong, S. W., Kim, C. H., Lee, Y.-C., Huh, Y. S., & Lee, J. (2014). Photoluminescent Green Carbon Nanodots from Food-Waste-Derived Sources: Large-Scale Synthesis, Properties, and Biomedical Applications. *ACS Applied Materials & Interfaces*, *6*(5), 3365–3370. https://doi.org/10.1021/am500159p

107. Park, Y., Yoo, J., Lim, B., Kwon, W., & Rhee, S.-W. (2016a). Improving the functionality of carbon nanodots: Doping and surface functionalization. *Journal of Materials Chemistry A*, *4*(30), 11582–11603. https://doi.org/10.1039/C6TA04813G
108. Park, Y., Yoo, J., Lim, B., Kwon, W., & Rhee, S.-W. (2016b). Improving the functionality of carbon nanodots: Doping and surface functionalization. *Journal of Materials Chemistry A*, *4*(30), 11582–11603. https://doi.org/10.1039/C6TA04813G
109. Prado, M. B., Truong, N. T., & Wanekaya, A. K. (2023). Improving the quantum yield of nitrogen-doped carbon dots by varying dopant ratios and pH. *Sensors and Actuators Reports*, *6*, 100165. https://doi.org/10.1016/j.snr.2023.100165
110. Qu, S., Wang, X., Lu, Q., Liu, X., & Wang, L. (2012). A Biocompatible Fluorescent Ink Based on Water-Soluble Luminescent Carbon Nanodots. *Angewandte Chemie International Edition*, *51*(49), 12215–12218. https://doi.org/10.1002/anie.201206791
111. Ramanarayanan, R., & Swaminathan, S. (2020). Synthesis and characterisation of green luminescent carbon dots from guava leaf extract. *Materials Today: Proceedings*, *33*, 2223–2227. https://doi.org/10.1016/j.matpr.2020.03.805
112. Ren, J., Malfatti, L., & Innocenzi, P. (2020). Citric Acid Derived Carbon Dots, the Challenge of Understanding the Synthesis-Structure Relationship. *C*, *7*(1), 2. https://doi.org/10.3390/c7010002
113. Ren, J., Opoku, H., Tang, S., Edman, L., & Wang, J. (2024). Carbon Dots: A Review with Focus on Sustainability. *Advanced Science*, *11*(35), 2405472. https://doi.org/10.1002/advs.202405472
114. Ren, J., Weber, F., Weigert, F., Wang, Y., Choudhury, S., Xiao, J., Lauermann, I., Resch-Genger, U., Bande, A., & Petit, T. (2019). Influence of surface chemistry on optical, chemical and electronic properties of blue luminescent carbon dots. *Nanoscale*, *11*(4), 2056–2064. https://doi.org/10.1039/C8NR08595A
115. Righetto, M., Privitera, A., Fortunati, I., Mosconi, D., Zerbetto, M., Curri, M. L., Corricelli, M., Moretto, A., Agnoli, S., Franco, L., Bozio, R., & Ferrante, C. (2017). Spectroscopic Insights into Carbon Dot Systems. *The Journal of Physical Chemistry Letters*, *8*(10), 2236–2242. https://doi.org/10.1021/acs.jpclett.7b00794
116. Rodríguez-Varillas, S., Fontanil, T., Obaya, Á. J., Fernández-González, A., Murru, C., & Badía-Laíño, R. (2022). Biocompatibility and Antioxidant Capabilities of Carbon Dots Obtained from Tomato (Solanum lycopersicum). *Applied Sciences*, *12*(2), 773. https://doi.org/10.3390/app12020773
117. Rossini, E. L., Milani, M. I., & Pezza, H. R. (2019). Green synthesis of fluorescent carbon dots for determination of glucose in biofluids using a paper platform. *Talanta*, *201*, 503–510. https://doi.org/10.1016/j.talanta.2019.04.045
118. Sa, S., Mn, E., Ae, T., & An, K. (2017). Synthesis of Carbon Dots with Tunable Luminescence. *Journal of Material Science & Engineering*, *06*(05). https://doi.org/10.4172/2169-0022.1000376
119. Sahu, S., Behera, B., Maiti, T. K., & Mohapatra, S. (2012). Simple one-step synthesis of highly luminescent carbon dots from orange juice: Application as excellent bio-imaging agents. *Chemical Communications*, *48*(70), 8835. https://doi.org/10.1039/c2cc33796g

120. Saltmarch, M., & Labuza, T. P. (1982). Nonenzymatic Browning via the Maillard Reaction in Foods. *Diabetes*, *31*(Supplement_3), 29–36. https://doi.org/10.2337/diab.31.3.S29
121. Santos, N., Santana, P. A., Osorio-Roman, I., Jara-Gutiérrez, C., Villena, J., & Ahumada, M. (2025). Effect of temperature on the carbonization process of cationic carbon dots: A physicochemical and *in vitro* study. *RSC Advances*, *15*(16), 12814–12824. https://doi.org/10.1039/D5RA00062A
122. Schneider, J., Reckmeier, C. J., Xiong, Y., Von Seckendorff, M., Susha, A. S., Kasák, P., & Rogach, A. L. (2017). Molecular Fluorescence in Citric Acid-Based Carbon Dots. *The Journal of Physical Chemistry C*, *121*(3), 2014–2022. https://doi.org/10.1021/acs.jpcc.6b12519
123. Sciortino, A., Cayuela, A., Soriano, M. L., Gelardi, F. M., Cannas, M., Valcárcel, M., & Messina, F. (2017). Different natures of surface electronic transitions of carbon nanoparticles. *Physical Chemistry Chemical Physics*, *19*(34), 22670–22677. https://doi.org/10.1039/C7CP04548D
124. Semsey, D., Nguyen, D. H. H., Törős, G., Papp, V., Pénzes, J., Vida, T., Béni, Á., Rai, M., & Prokisch, J. (2025). Analysis of Fluorescent Carbon Nanodots Synthesized from Spices Through Thermal Processes Treatment. *Nanomaterials*, *15*(8), 625. https://doi.org/10.3390/nano15080625
125. Semsey, D., Nguyen, D., Törős, G., Muthu, A., Labidi, S., El-Ramady, H., Béni, Á., Rai, M., & József, P. (2024). Analysis of Fluorescent Carbon Nanodot Formation during Pretzel Production. *Nanomaterials*, *14*(13), 1142. https://doi.org/10.3390/nano14131142
126. Senanayake, R. D., Yao, X., Froehlich, C. E., Cahill, M. S., Sheldon, T. R., McIntire, M., Haynes, C. L., & Hernandez, R. (2022). Machine Learning-Assisted Carbon Dot Synthesis: Prediction of Emission Color and Wavelength. *Journal of Chemical Information and Modeling*, *62*(23), 5918–5928. https://doi.org/10.1021/acs.jcim.2c01007
127. Shafigulina, A. D., Revina, A. A., Platonova, N. P., Borovikova, S. A., & Buryak, A. K. (2019). The Use of Size-Exclusion Chromatography for Determining the Sizes of Metal Nanoparticles Synthesized in Reverse Micelles. *Colloid Journal*, *81*(3), 292–297. https://doi.org/10.1134/S1061933X19030128
128. Shen, S. C., & Wu, J. S. B. (2004). Maillard Browning in Ethanolic Solution. *Journal of Food Science*, *69*(4), FCT273–FCT279. https://doi.org/10.1111/j.1365-2621.2004.tb06328.x
129. Shi, Q.-Q., Li, Y.-H., Xu, Y., Wang, Y., Yin, X.-B., He, X.-W., & Zhang, Y.-K. (2014). High-yield and high-solubility nitrogen-doped carbon dots: Formation, fluorescence mechanism and imaging application. *RSC Adv.*, *4*(4), 1563–1566. https://doi.org/10.1039/C3RA45762A
130. Shi, X., Wei, W., Fu, Z., Gao, W., Zhang, C., Zhao, Q., Deng, F., & Lu, X. (2019). Review on carbon dots in food safety applications. *Talanta*, *194*, 809–821. https://doi.org/10.1016/j.talanta.2018.11.005
131. Shi, Y., Su, W., Yuan, F., Yuan, T., Song, X., Han, Y., Wei, S., Zhang, Y., Li, Y., Li, X., & Fan, L. (2023). Carbon Dots for Electroluminescent Light-Emitting

Diodes: Recent Progress and Future Prospects. *Advanced Materials*, *35*(44), 2210699. https://doi.org/10.1002/adma.202210699

132. Sk, M. P., Jaiswal, A., Paul, A., Ghosh, S. S., & Chattopadhyay, A. (2012a). Presence of Amorphous Carbon Nanoparticles in Food Caramels. *Scientific Reports*, *2*(1), 383. https://doi.org/10.1038/srep00383
133. Sk, M. P., Jaiswal, A., Paul, A., Ghosh, S. S., & Chattopadhyay, A. (2012b). Presence of amorphous carbon nanoparticles in food caramels. *Scientific Reports*, *2*(1), 383.
134. Song, X., Cao, L., Cong, S., Song, Y., & Tan, M. (2018). Characterization of Endogenous Nanoparticles from Roasted Chicken Breasts. *Journal of Agricultural and Food Chemistry*, *66*(28), 7522–7530. https://doi.org/10.1021/acs.jafc.8b01988
135. Song, X., Wang, H., Zhang, R., Yu, C., & Tan, M. (2018). Bio-distribution and interaction with dopamine of fluorescent nanodots from roasted chicken. *Food & Function*, *9*(12), 6227–6235. https://doi.org/10.1039/C8FO01159A
136. Song, Y., Cao, L., Li, J., Cong, S., Li, D., Bao, Z., & Tan, M. (2019). Interactions of carbon quantum dots from roasted fish with digestive protease and dopamine. *Food & Function*, *10*(6), 3706–3716. https://doi.org/10.1039/C9FO00655A
137. Soni, N., Singh, S., Sharma, S., Batra, G., Kaushik, K., Rao, C., Verma, N. C., Mondal, B., Yadav, A., & Nandi, C. K. (2021). Absorption and emission of light in red emissive carbon nanodots. *Chemical Science*, *12*(10), 3615–3626. https://doi.org/10.1039/D0SC05879C
138. Su, K., Xiang, G., Jin, X., Wang, X., Jiang, X., He, L., Zhao, W., Sun, Y., & Cui, C. (2022). Gram-scale synthesis of nitrogen-doped carbon dots from locusts for selective determination of sunset yellow in food samples. *Luminescence*, *37*(1), 118–126. https://doi.org/10.1002/bio.4152
139. Tan, M., Zhang, L., Tang, R., Song, X., Li, Y., Wu, H., Wang, Y., Lv, G., Liu, W., & Ma, X. (2013). Enhanced photoluminescence and characterization of multicolor carbon dots using plant soot as a carbon source. *Talanta*, *115*, 950–956. https://doi.org/10.1016/j.talanta.2013.06.061
140. Tepliakov, N. V., Kundelev, E. V., Khavlyuk, P. D., Xiong, Y., Leonov, M. Yu., Zhu, W., Baranov, A. V., Fedorov, A. V., Rogach, A. L., & Rukhlenko, I. D. (2019). Sp^2 –sp^3 -Hybridized Atomic Domains Determine Optical Features of Carbon Dots. *ACS Nano*, *13*(9), 10737–10744. https://doi.org/10.1021/acsnano.9b05444
141. Tian, X., & Yin, X. (2019). Carbon Dots, Unconventional Preparation Strategies, and Applications Beyond Photoluminescence. *Small*, *15*(48), 1901803. https://doi.org/10.1002/smll.201901803
142. Tomskaya, A. E., Egorova, M. N., Kapitonov, A. N., Nikolaev, D. V., Popov, V. I., Fedorov, A. L., & Smagulova, S. A. (2018). Synthesis of Luminescent N-Doped Carbon Dots by Hydrothermal Treatment. *Physica Status Solidi (b)*, *255*(1), 1700222. https://doi.org/10.1002/pssb.201700222
143. Törős, G., Béni, Á., Balláné, A. K., Semsey, D., Ferroudj, A., & Prokisch, J. (2025). Production of Myco-Nanomaterial Products from Pleurotus ostreatus (Agaricomycetes) Mushroom via Pyrolysis. *Pharmaceutics*, *17*(5), 591. https://doi.org/10.3390/pharmaceutics17050591

144. Trubetskaya, O. E., Trubetskoj, O. A., Richard, C., Vervald, A. M., Burikov, S. A., Marchenkov, V. V., Shenderova, O. A., Patsaeva, S. V., & Dolenko, T. A. (2021). High-performance size exclusion chromatography with online fluorescence and multi-wavelength absorbance detection for isolation of high-purity carbon dots fractions, free of non-fluorescent material. *Journal of Chromatography A*, *1650*, 462251. https://doi.org/10.1016/j.chroma.2021.462251
145. Tuchin, V. S., Stepanidenko, E. A., Vedernikova, A. A., Cherevkov, S. A., Li, D., Li, L., Döring, A., Otyepka, M., Ushakova, E. V., & Rogach, A. L. (2024). Optical Properties Prediction for Red and Near-Infrared Emitting Carbon Dots Using Machine Learning. *Small*, *20*(29), 2310402. https://doi.org/10.1002/smll.202310402
146. Vinci, J. C., & Colon, L. A. (2012). Fractionation of Carbon-Based Nanomaterials by Anion-Exchange HPLC. *Analytical Chemistry*, *84*(2), 1178–1183. https://doi.org/10.1021/ac202667x
147. Wang, H., Su, W., & Tan, M. (2020). Endogenous Fluorescence Carbon Dots Derived from Food Items. *The Innovation*, *1*(1), 100009. https://doi.org/10.1016/j.xinn.2020.04.009
148. Wang, H., Xie, Y., Na, X., Bi, J., Liu, S., Zhang, L., & Tan, M. (2019). Fluorescent carbon dots in baked lamb: Formation, cytotoxicity and scavenging capability to free radicals. *Food Chemistry*, *286*, 405–412. https://doi.org/10.1016/j.foodchem.2019.02.034
149. Wang, X., Qu, K., Xu, B., Ren, J., & Qu, X. (2011). Microwave assisted one-step green synthesis of cell-permeable multicolor photoluminescent carbon dots without surface passivation reagents. *Journal of Materials Chemistry*, *21*(8), 2445. https://doi.org/10.1039/c0jm02963g
150. Wang, Z., Liao, H., Wu, H., Wang, B., Zhao, H., & Tan, M. (2015). Fluorescent carbon dots from beer for breast cancer cell imaging and drug delivery. *Analytical Methods*, *7*(20), 8911–8917. https://doi.org/10.1039/C5AY01978H
151. Wang, Z., Wang, Z., & Wu, F. (2022). Carbon Dots as Drug Delivery Vehicles for Antimicrobial Applications: A Minireview. *ChemMedChem*, *17*(13), e202200003. https://doi.org/10.1002/cmdc.202200003
152. Wu, T., Bai, X., Zhang, Y., Dai, E., Ma, J., Yu, C., He, C., Li, Q., Yang, Y., Kong, H., Qu, H., & Zhao, Y. (2024). Natural medicines-derived carbon dots as novel oral antioxidant administration strategy for ulcerative colitis therapy. *Journal of Nanobiotechnology*, *22*(1), 511. https://doi.org/10.1186/s12951-024-02702-2
153. Xavier, S. S. J., Siva, G., Annaraj, J., Kim, A. R., Yoo, D. J., & Kumar, G. G. (2018). Sensitive and selective turn-off-on fluorescence detection of Hg2+ and cysteine using nitrogen doped carbon nanodots derived from citron and urine. *Sensors and Actuators B: Chemical*, *259*, 1133–1143. https://doi.org/10.1016/j.snb.2017.12.046
154. Xu, X., Ray, R., Gu, Y., Ploehn, H. J., Gearheart, L., Raker, K., & Scrivens, W. A. (2004). Electrophoretic Analysis and Purification of Fluorescent Single-Walled Carbon Nanotube Fragments. *Journal of the American Chemical Society*, *126*(40), 12736–12737. https://doi.org/10.1021/ja040082h

155. Yan, F., Jiang, Y., Sun, X., Bai, Z., Zhang, Y., & Zhou, X. (2018). Surface modification and chemical functionalization of carbon dots: A review. *Microchimica Acta*, *185*(9), 424. https://doi.org/10.1007/s00604-018-2953-9
156. Yang, S.-T., Wang, X., Wang, H., Lu, F., Luo, P. G., Cao, L., Meziani, M. J., Liu, J.-H., Liu, Y., Chen, M., Huang, Y., & Sun, Y.-P. (2009). Carbon Dots as Nontoxic and High-Performance Fluorescence Imaging Agents. *The Journal of Physical Chemistry C*, *113*(42), 18110–18114. https://doi.org/10.1021/jp9085969
157. Yin, J., Yuan, S., Guo, Y., Yu, H., Cheng, Y., Xie, Y., Qian, H., & Yao, W. (2024). Carbon dots in fried breadcrumbs: In vitro toxicity to normal rat kidney cells and its control method. *Process Biochemistry*, *139*, 125–136. https://doi.org/10.1016/j.procbio.2024.01.026
158. Yorozuya, H., Ashrafi, N. E., Sato, K., Islam, A., Fukae, R., Tagashira, Y., & Iimori, T. (2025). Synthesis and Fluorescence Mechanism of Nitrogen-Doped Carbon Dots Utilizing Biopolymer and Urea. *Molecules*, *30*(9), 2068. https://doi.org/10.3390/molecules30092068
159. Yu, H., Shi, R., Zhao, Y., Waterhouse, G. I. N., Wu, L., Tung, C., & Zhang, T. (2016). Smart Utilization of Carbon Dots in Semiconductor Photocatalysis. *Advanced Materials*, *28*(43), 9454–9477. https://doi.org/10.1002/adma.201602581
160. Zhao, C., Wang, X., Wu, L., Wu, W., Zheng, Y., Lin, L., Weng, S., & Lin, X. (2019). Nitrogen-doped carbon quantum dots as an antimicrobial agent against Staphylococcus for the treatment of infected wounds. *Colloids and Surfaces B: Biointerfaces*, *179*, 17–27. https://doi.org/10.1016/j.colsurfb.2019.03.042
161. Zhao, L., Zhang, M., Mujumdar, A. S., & Wang, H. (2023). Application of carbon dots in food preservation: A critical review for packaging enhancers and food preservatives. *Critical Reviews in Food Science and Nutrition*, *63*(24), 6738–6756. https://doi.org/10.1080/10408398.2022.2039896
162. Zhao, P., Jin, B., Zhang, Q., & Peng, R. (2021). High-Quality Carbon Nitride Quantum Dots on Photoluminescence: Effect of Carbon Sources. *Langmuir*, *37*(5), 1760–1767. https://doi.org/10.1021/acs.langmuir.0c02966
163. Zhao, Q., Song, W., Zhao, B., & Yang, B. (2020). Spectroscopic studies of the optical properties of carbon dots: Recent advances and future prospects. *Materials Chemistry Frontiers*, *4*(2), 472–488. https://doi.org/10.1039/C9QM00592G
164. Zhao, W., Lu, Z., Song, F., Han, J., Zhang, Q., Cong, Y., Lu, A., & Gao, T. (2025). One-step electrolytic synthesis of nitrogen-doped carbon dots using graphite electrode in ionic liquid and their LED applications. *Colloids and Surfaces A: Physicochemical and Engineering Aspects*, *712*, 136459. https://doi.org/10.1016/j.colsurfa.2025.136459
165. Zhao, Y., Liu, X., Yang, Y., Kang, L., Yang, Z., Liu, W., & Chen, L. (2015). Carbon Dots: From Intense Absorption in Visible Range to Excitation-Independent and Excitation-Dependent Photoluminescence. *Fullerenes, Nanotubes and Carbon Nanostructures*, *23*(11), 922–929. https://doi.org/10.1080/1536383X.2015.1018413
166. Zhou, Y., Mintz, K. J., Sharma, S. K., & Leblanc, R. M. (2019). Carbon Dots: Diverse Preparation, Application, and Perspective in Surface Chemistry. *Langmuir*, *35*(28), 9115–9132. https://doi.org/10.1021/acs.langmuir.9b00595

167. Zhu, S., Song, Y., Zhao, X., Shao, J., Zhang, J., & Yang, B. (2015). The photoluminescence mechanism in carbon dots (graphene quantum dots, carbon nanodots, and polymer dots): Current state and future perspective. *Nano Research*, *8*(2), 355–381. https://doi.org/10.1007/s12274-014-0644-3
168. Zu, F., Yan, F., Bai, Z., Xu, J., Wang, Y., Huang, Y., & Zhou, X. (2017). The quenching of the fluorescence of carbon dots: A review on mechanisms and applications. *Microchimica Acta*, *184*(7), 1899–1914. https://doi.org/10.1007/s00604-017-2318-9

PUBLICATIONS IN THE FIELD OF RESEARCH

UNIVERSITY AND NATIONAL LIBRARY
UNIVERSITY OF DEBRECEN
H-4002 Egyetem tér 1, Debrecen
Phone: +3652/410-443, email: publikaciok@lib.unideb.hu

Registry number: DEENK/97/2026.PL
Subject: PhD Publication List

Candidate: Huu Huong Duyen Nguyen
Doctoral School: Doctoral School of Nutrition and Food Sciences, Doctoral Programme of Food Sciences
MTMT ID: 10093013

List of publications related to the dissertation

Foreign language international book chapters (2)

1. **Nguyen, H. H. D.**, Muthu, A., Béni, Á., Prokisch, J.: Analytical Techniques for Characterization of Carbon Dots.
   In: Carbon Nanodots - Synthesis and Applications in Health, Food and Agriculture / (eds.) Mahendra Rai, Sushama Talegaonkar, József Prokisch, Springer Nature, Philadelphia, 121-147, 2026. ISBN: 9789819547050

2. **Nguyen, H. H. D.**, Prokisch, J.: Carbon Dots in Food and Beverages: Formation, Benefits, Risks, and Toxicity.
   In: Carbon Nanodots - Synthesis and Applications in Health, Food and Agriculture. Ed.: Mahendra Rai, Sushama Talegaonkar, József Prokisch, Springer Nature, Singapore, 277-300, 2026. ISBN: 9789819547050

Foreign language scientific articles in international journals (13)

3. Semsey, D., **Nguyen, H. H. D.**, Seresné Törős, G., Papp, V. A., Pénzes, J., Vida, T., Béni, Á., Rai, M., Prokisch, J.: Analysis of fluorescent carbon nanodots synthesized from spices through thermal processes treatment.
   Nanomaterials. 15 (8), 1-16, 2025. ISSN: 2079-4991.
   DOI: https://doi.org/10.3390/nano15080625
   IF: 4.3 (2024)

4. **Nguyen, H. H. D.**, Muthu, A., Elsakhawy, T., Sheta, M., Abdalla, N., El-Ramady, H., Prokisch, J.: Carbon Nanodots-Based Sensors: A Promising Tool for Detecting and Monitoring Toxic Compounds.
   Nanomaterials. 15 (10), 1-27, 2025. ISSN: 2079-4991.
   DOI: http://dx.doi.org/10.3390/nano15100725
   IF: 4.3 (2024)

DEBRECENI EGYETEM * Egyetemi és Nemzeti Könyvtár *

UNIVERSITY of DEBRECEN

UNIVERSITY AND NATIONAL LIBRARY
UNIVERSITY OF DEBRECEN
H-4002 Egyetem tér 1, Debrecen
Phone: +3652/410-443, email: publikaciok@lib.unideb.hu

5. **Nguyen, H. H. D.**, El-Ramady, H., Prokisch, J.: Carbon nanodots derived from glycine for rapid detection of caffeine in beverages.
J. Food Compos. Anal. 145, 1-10, 2025. ISSN: 0889-1575.
DOI: http://dx.doi.org/10.1016/j.jfca.2025.107784
IF: 4.6 (2024)

6. **Nguyen, H. H. D.**, El-Ramady, H., Seresné Törős, G., Muthu, A., Elsakhawy, T., Abdalla, N., Alibrahem, W., Kharrat Helu, N., Prokisch, J.: Food-Derived Carbon Dots: Formation, Detection, and Impact on Gut Microbiota.
Foods. 14 (17), 1-21, 2025. EISSN: 2304-8158.
DOI: http://dx.doi.org/10.3390/foods14172980
IF: 5.1 (2024)

7. **Nguyen, H. H. D.**, El-Ramady, H., Prokisch, J.: Food safety aspects of carbon dots: a review.
Environ. Chem. Lett. 23 (1), 337-360, 2025. ISSN: 1610-3653.
DOI: http://dx.doi.org/10.1007/s10311-024-01779-3
IF: 20.4 (2024)

8. Muthu, A., **Nguyen, H. H. D.**, Ferroudj, A., Prokisch, J., El-Ramady, H., Neji, C., Béni, Á.: Green Synthesised Carbon Nanodots Using the Maillard Reaction for the Rapid Detection of Elemental Selenium in Water and Carbonated Beverages.
Nanomaterials. 15 (15), 1-16, 2025. ISSN: 2079-4991.
DOI: http://dx.doi.org/10.3390/nano15151161
IF: 4.3 (2024)

9. Muthu, A., **Nguyen, H. H. D.**, Neji, C., Seresné Törős, G., Ferroudj, A., Atieh, R., Prokisch, J., El-Ramady, H., Béni, Á.: Nanomaterials for Smart and Sustainable Food Packaging: Nano-Sensing Mechanisms, and Regulatory Perspectives.
Foods. 14 (15), 2-29, 2025. EISSN: 2304-8158.
DOI: https://doi.org/10.3390/foods14152657
IF: 5.1 (2024)

10. Prokisch, J., Seresné Törős, G., **Nguyen, H. H. D.**, Muthu, A., Labidi, S., Sheta, M., El-Ramady, H.: Sustainable Approach of Carbon Nanodots: Agro-Applications for Soil Health.
Egypt. J. Soil Sci. 65 (1), 639-657, 2025. ISSN: 0302-6701.
DOI: http://dx.doi.org/10.21608/ejss.2025.353791.1969
IF: 3.4 (2024)

11. Semsey, D., **Nguyen, H. H. D.**, Seresné Törős, G., Muthu, A., Labidi, S., El-Ramady, H., Béni, Á., Rai, M., Prokisch, J.: Analysis of Fluorescent Carbon Nanodot Formation during Pretzel Production.
Nanomaterials. 14 (13), 1-11, 2024. ISSN: 2079-4991.
DOI: http://dx.doi.org/10.3390/nano14131142
IF: 4.3

DEBRECENI EGYETEM Egyetemi és Nemzeti Könyvtár

12. Prokisch, J., **Nguyen, H. H. D.**, Muthu, A., Ferroudj, A., Singh, A., Agrawal, S., Rajput, V. D., Ghazaryan, K., El-Ramady, H., Rai, M.: Carbon Nanodot-Microbe-Plant Nexus in Agroecosystem and Antimicrobial Applications.
Nanomaterials. 14 (15), 1-37, 2024. ISSN: 2079-4991.
DOI: http://dx.doi.org/10.3390/nano14151249
IF: 4.3

13. **Nguyen, H. H. D.**, Muthu, A., El-Ramady, H., Béni, Á., Prokisch, J.: Detection and formation of fluorescent carbon nanodots in coffee brews and its relationship with other compositions.
J. Food Compos. Anal. 132, 1-10, 2024. ISSN: 0889-1575.
DOI: http://dx.doi.org/10.1016/j.jfca.2024.106347
IF: 4.6

14. **Nguyen, H. H. D.**, Muthu, A., El-Ramady, H., Daróczi, L., Nagy, L., Kéki, S., Béni, Á., Csarnovics, I., Prokisch, J.: Optimization of Extraction Conditions to Synthesize Green Carbon Nanodots from Maillard Reaction.
Mater. Adv. 5, 3499-3505, 2024. EISSN: 2633-5409.
DOI: http://dx.doi.org/10.1039/D4MA00037D
IF: 4.7

15. **Nguyen, H. H. D.**, El-Ramady, H., Llanaj, X., Seresné Törős, G., Hajdú, P., Prokisch, J.: Chemical Composition and Health Attributes of Agri-Foods: A Scientific Overview on Black Foods.
Sustainability. 15 (4), 1-32, 2023. ISSN: 2071-1050.
DOI: http://dx.doi.org/10.3390/su15043852
IF: 3.3

Foreign language abstracts (6)

16. **Nguyen, H. H. D.**, Prokisch, J.: Coffee brew-derived carbon dots for rapid caffeine detection in foods.
In: 4th Food Chemistry Conference: Reshaping Global Food Systems: Abstract Book, Elsevier, Glasgow, 352, 2025.

17. **Nguyen, H. H. D.**, Prokisch, J.: Exploring the formation and applications of carbon dots in food matrices.
In: 4th Food Chemistry Conference: Reshaping Global Food Systems: Abstract Book, Elsevier, Glasgow, 141-141, 2025.

18. **Nguyen, H. H. D.**, Prokisch, J.: Optimizing Banana Peel-Derived Carbon Nanodots for Intelligent Food Packaging Solutions: a Machine Learning Approach.
In: Fostering Transition to Sustainable Food Systems: Embracing Novelty and Overcome Challenges : Abtract book, [S.n.], [S.l.], [52], 2025.

DEBRECENI EGYETEM Egyetemi és Nemzeti Könyvtár

19. **Nguyen, H. H. D.**, Prokisch, J.: Upcycling Food Waste into Carbon Dots: a sustainable approach for green nanotechnology.
In: 1st International Congress on Sustainable Food, Green Chemistry and Human Nutrition: Book of Abstracts. Ed.: Filip Dujmić, Sven Karlović, Antonela Ninčević Grassino, University of Zagreb, Faculty of Food Technology and Biotechnology, Srebreno, Dubrovnik, 91, 2025.
ISBN: 9789536893225

20. **Nguyen, H. H. D.**: Sustainable production of carbon nanodots with controlled properties via a green Maillard reaction approach.
FEBS Open Bio. 14 (S2), 38, 2024. ISSN: 2211-5463.

21. **Nguyen, H. H. D.**, Muthu, A., El-Ramady, H., Prokisch, J.: Detection of Carbon nanodots in black foods.
In: Táplálkozástudományi Kutatások : XI. PhD konferencia programja és az előadások összefoglalói. Szerk.: Bíró Lajos, Gelencsér Éva, Lugasi Andrea, Rurik Imre, Simonné Sarkadi Livia, Magyar Táplálkozástudományi Társaság, Budapest, 16, 2023. ISBN: 9786155606144

List of other publications

Foreign language scientific articles in international journals (13)

22. Seresné Törős, G., El-Ramady, H., **Nguyen, H. H. D.**, Alibrahem, W., Helu, N. K., Atieh, R., Muthu, A., Jevcsák, S., Semsey, D., Abdalla, N., Elsakhawy, T., Tóth, F. A., Nagy, P. T., Prokisch, J.: Green-Synthesized Nanomaterials from Edible and Medicinal Mushrooms: A Sustainable Strategy Against Antimicrobial Resistance.
Pharmaceutics. 17 (11), 1-26, 2025. EISSN: 1999-4923.
DOI: https://doi.org/10.3390/pharmaceutics17111388
IF: 5.5 (2024)

23. Alibrahem, W., **Nguyen, H. H. D.**, Kharrat Helu, N., Tóth, F. A., Nagy, P. T., Posta, J., Prokisch, J., Oláh, C.: Health Benefits, Applications, and Analytical Methods of Freshly Produced Allyl Isothiocyanate.
Foods. 14 (4), 1-24, 2025. EISSN: 2304-8158.
DOI: http://dx.doi.org/10.3390/foods14040579
IF: 5.1 (2024)

DEBRECENI EGYETEM Egyetemi és Nemzeti Könyvtár

24. Muthu, A., **Nguyen, H. H. D.**, Neji, C., El-Ramady, H., Prokisch, J., Béni, Á.: Nanohybrid-based fluorescent "turn-on" system for selective detection of mercury (II) in aqueous solution.
J. Food Compos. Anal. 148, 1-10, 2025. ISSN: 0889-1575.
DOI: http://dx.doi.org/10.1016/j.jfca.2025.108653
IF: 4.6 (2024)

25. Prokisch, J., Seresné Törős, G., **Nguyen, H. H. D.**, Neji, C., Ferroudj, A., Sári, D., Muthu, A., Brevik, E. C., El-Ramady, H.: Nano-Food Farming: Toward Sustainable Applications of Proteins, Mushrooms, Nano-Nutrients, and Nanofibers.
Agron. J. 14, 1-30, 2024. ISSN: 0002-1962.
DOI: http://dx.doi.org/https://doi.org/10.3390/agronomy14030606
IF: 2

26. Van, H. P., **Nguyen, H. H. D.**, Nguyen, T. T. H., Hanh, T. T. N., Nguyen, T. D. T., Nguyen, H. T. P.: Flavonoid Glycosides from the Leaves of Magnolia lamdongensis.
Chem. Nat. Compd. 59 (4), 773-775, 2023. ISSN: 0009-3130.
DOI: http://dx.doi.org/10.1007/s10600-023-04108-2
IF: 0.8

27. Seresné Törős, G., El-Ramady, H., Prokisch, J., Velasco, F., Llanaj, X., **Nguyen, H. H. D.**, Peles, F.: Modulation of the Gut Microbiota with Prebiotics and Antimicrobial Agents from Pleurotus ostreatus Mushroom.
Foods. 12 (10), 1-23, 2023. EISSN: 2304-8158.
DOI: http://dx.doi.org/https://doi.org/10.3390/foods12102010
IF: 4.7

28. Nguyen, T. T. H., **Nguyen, H. H. D.**, Nguyen, T. D. T., Hanh, T. T. N., Pham, V. H., Hoang, T. N. A., Nguyen, X. H., Pham, N. K., Nguyen, M. C., Nguyen, H. T. P.: In vitro and in silico cytotoxic activities of triterpenoids from the leaves of Aralia dasyphylla Miq. and the assessment of their ADMET properties.
J. Biomol. Struct. Dyn. 41 (12), 5863-5871, 2022. ISSN: 0739-1102.
DOI: http://dx.doi.org/10.1080/07391102.2022.2098822
IF: 4.4

29. **Nguyen, H. H. D.**, Nguyen, H. V. H.: Effects of storage temperature on postharvest physico-chemical attributes of nano-chitosan coated strawberry (Fragaria x ananassa Duch.).
J Horticult Postharvest Res. 4, 101-114, 2021. ISSN: 2588-4883.
DOI: https://doi.org10.22077/JHPR.2020.3317.1139

30. Nguyen, H. T. P., Nguyen, T. D. T., **Nguyen, H. H. D.**, Tran, T. H. H., Tran, H. Q., Nguyen, X. C., Nguyen, H. N.: Chemical Constituents from the Branches and Leaves of Alchornea trewioides.
Chem. pharm. bull. 69, 150-154, 2020. ISSN: 0009-2363.
DOI: http://dx.doi.org/10.1248/cpb.c20-00628
IF: 1.645

31. Nguyen, H. T. P., Nguyen, T. D. T., Nguyen, T. T. H., Pham, V. H., **Nguyen, H. H. D.**, Tran, T. H. H., Nguyen, X. C., Tran, H. Q., Nguyen, H. N., Chau, V. M.: Codojavanosides A-C, three new sesquiterpenoid glycosides from the roots of Codonopsis javanica.
Phytochem. Lett. 40, 166-170, 2020. ISSN: 1874-3900.
DOI: https://doi.org/10.1016/j.phytol.2020.10.002
IF: 1.679

DEBRECENI EGYETEM Egyetemi és Nemzeti Könyvtár

32. Nguyen, V. T. B., **Nguyen, H. H. D.**, Nguyen, H. V. H.: Combination effects of calcium chloride and nano-chitosan on the postharvest quality of strawberry (Fragaria x ananassa Duch.).
Postharvest Biol. Technol. 162, 1-8, 2020. ISSN: 0925-5214.
DOI: https://doi.org/10.1016/j.postharvbio.2019.111103
IF: 5.537

33. **Nguyen, H. H. D.**, Nguyen, H. V. H.: Effects of nano-chitosan and chitosan coating on the postharvest quality, polyphenol oxidase activity and malondialdehyde content of strawberry (Fragaria x ananassa Duch.).
J Horticult Postharvest Res. 3 (6), 11-24, 2020. ISSN: 2588-4883.
DOI: https://doi.org/10.22077/jhpr.2019.2698.1082

34. Nguyen, H. T. P., Nguyen, T. D. T., Nguyen, T. T. H., Pham, V. H., **Nguyen, H. H. D.**, Tran, T. H. H., Nguyen, X. C., Tran, H. Q., Nguyen, H. N., Chau, V. M.: Polyacetylene and phenolic constituents from the roots of Codonopsis javanica.
Nat. Prod. Res. 36 (9), 2314-2320, 2020. ISSN: 1478-6419.
DOI: https://doi.org/10.1080/14786419.2020.1833200
IF: 2.861

Foreign language abstracts (3)

35. Muthu, A., Neji, C., **Nguyen, H. H. D.**, Prokisch, J., Béni, Á.: Application of Machine learning for predicting survival outcomes of nano selenium dosage in different in-vivo and in-vitro models.
In: Reshaping Global Food Systems / (eds.) Dongxiao Sun-Waterhouse, Paul Finglas, Sian Astley, Nandika Bandara, Elsevier, Glasgow, 21, 2025.

36. Muthu, A., **Nguyen, H. H. D.**, Prokisch, J., Béni, Á.: Biosynthesis of Selenium and Tellurium nanoparticles and their alloys using Lactobacillus casei: a sustainable approach to functional nutraceuticals.
In: 1st International Congress on Sustainable Food, Green Chemistry and Human Nutrition : GreenNutrifood2025 : Book of abstracts. Eds.: Filip Dujmić, Sven Karlović, Antonela Ninčević Grassino, University of Zagreb, Zagreb, 38-38, 2025. ISBN: 9789536893225

37. Muthu, A., **Nguyen, H. H. D.**, Prokisch, J., Béni, Á.: Rapid estimation of elemental selenium (Se0) using carbon nanodots.
In: Abstract Book / s.n, Elsevier, Glasgow, 102-102, 2025.

Total IF of journals (all publications): 111,522
Total IF of journals (publications related to the dissertation): 72,7

DEBRECENI EGYETEM * Egyetemi és Nemzeti Könyvtár *

The Candidate's publication data submitted to the Tudóstér have been validated by DEENK on the basis of the Journal Citation Report (Impact Factor) database.

03 March, 2026

STATEMENT

I wrote this thesis in the framework of the University of Debrecen, Doctoral School of Food Science for the purpose of obtaining a doctoral degree (Ph.D.) at the University of Debrecen.

Debrecen, 11st November 2025

…….

Signature of the candidate

STATEMENT

I hereby certify that the doctoral candidate NGUYEN HUU HUONG DUYEN has carried out her work under my supervision within the framework of the above-mentioned Doctoral School between 2022 – 2026. The candidate has made a decisive contribution to the results of the thesis through her independent creative work, and the thesis is the candidate's independent work. I recommend that the thesis be accepted.

Debrecen, 11st November 2025

…….

Signature of the supervisor

ACKNOWLEGMENT

First, I want to thank the University of Debrecen for giving me a home for this work and the environment to grow as a researcher.

I gratefully acknowledge support from the Stipendium Hungaricum Scholarship, the Debrecen Publication Support Fund, and the Pannonian Scholarship. Your support made this journey possible.

I'm deeply grateful to my supervisor, Prof. Dr. Joszef Prokisch. He backed every plan and idea I brought, encouraged my creativity every day, and kept his door open for discussion. Our talks about science and new directions shaped this dissertation more than anything else.

I'm thankful to the Nanofood Laboratory and the Institute of Agricultural Chemistry and Soil Science, and to the Department of Solid State Physics, Department of Applied Chemistry, and Department of Experimental Physics for the facilities, instruments, and day-to-day help that made these experiments possible.

My sincere thanks to Prof. Hassan El-Ramady, Prof. Lajos Daróczi, Dr. Lajos Nagy, Dr. Áron Béni, and Dr. István Csarnovics for your advice, feedback, and practical help along the way.

To my friends and colleagues at the Nanofood Laboratory: thank you for your kindness, teamwork, and the many inspiring conversations. You made the hard days lighter and the good days even better.

To my family and my partner: thank you for standing by me. Your patience, love, and steady belief in my choices gave me the strength to keep going.

And finally, a note to myself. There were many times I felt like stopping. I'm proud that I stayed with it and saw this journey through to the end. Finally, I would like to thank myself. There were many moments when I considered stopping, but I chose to persevere and complete this journey. This dissertation is a testament to that persistent.